US ARMY
MATERIEL
COMMAND

CONTRACT REPORT BRL-CR-542

CLOSED-BOMB COMBUSTION OF HIVELITE-BASED VERY HIGH BURN RATE (VHBR) PROPELLANT

Calspan Corporation
P.O. Box 400
Buffalo, New York 14225

April 1985

US ARMY BALLISTIC RESEARCH LABORATORY
ABERDEEN PROVING GROUND, MARYLAND

Destroy this report when it is no longer needed.
Do not return it to the originator.

Additional copies of this report may be obtained from the National Technical Information Service, U. S. Department of Commerce, Springfield, Virginia 22161.

The findings in this report are not to be construed as an official Department of the Army position, unless so designated by other authorized documents.

The use of trade names or manufacturers' names in this report does not constitute indorsement of any commercial product.

UNCLASSIFIED

SECURITY CLASSIFICATION OF THIS PAGE (When Data Entered)

REPORT DOCUMENTATION PAGE		READ INSTRUCTIONS BEFORE COMPLETING FORM
1. REPORT NUMBER Contract Report BRL-CR-542	2. GOVT ACCESSION NO.	3. RECIPIENT'S CATALOG NUMBER
4. TITLE (and Subtitle) CLOSED-BOMB COMBUSTION OF HIVELITE-BASED, VERY HIGH BURN RATE (VHBR) PROPELLANT		5. TYPE OF REPORT & PERIOD COVERED 6. PERFORMING ORG. REPORT NUMBER
7. AUTHOR(s) E.B. Fisher C.C. Morphy		8. CONTRACT OR GRANT NUMBER(s) DAAK11-80-C-0062
9. PERFORMING ORGANIZATION NAME AND ADDRESS Calspan Corporation P.O. Box 400 Buffalo, New York 14225		10. PROGRAM ELEMENT, PROJECT, TASK AREA & WORK UNIT NUMBERS
11. CONTROLLING OFFICE NAME AND ADDRESS US Army Ballistic Research Laboratory ATTN: AMXBR-OD-ST Aberdeen Proving Ground, MD 21005-5066		12. REPORT DATE April 1985 13. NUMBER OF PAGES 117
14. MONITORING AGENCY NAME & ADDRESS(if different from Controlling Office)		15. SECURITY CLASS. (of this report) Unclassified 15a. DECLASSIFICATION/DOWNGRADING SCHEDULE

16. DISTRIBUTION STATEMENT (of this Report)

Approved for public release; distribution unlimited.

17. DISTRIBUTION STATEMENT (of the abstract entered in Block 20, if different from Report)

18. SUPPLEMENTARY NOTES

19. KEY WORDS (Continue on reverse side if necessary and identify by block number)

Very High Burn Rate (VHBR) Propellant
Hivelite
Propellant combustion
Closed bomb testing

20. ABSTRACT (Continue on reverse side if necessary and identify by block number)

An experimental investigation of the combustion characteristics of a Hivelite-based, very-high-burn-rate (VHBR) propellant was conducted. The experiments were performed in a closed chamber, called the VHBR bomb, that was specially designed and constructed for these experiments. The device was designed with the same diameter as the propellant samples in order to maintain one dimensional combustion processes and transient wave phenomena to simplify subsequent interpretation and analysis.

DD FORM 1 JAN 73 1473 EDITION OF 1 NOV 65 IS OBSOLETE

UNCLASSIFIED

SECURITY CLASSIFICATION OF THIS PAGE (When Data Entered)

20. continued

In addition to pressures at several important locations in the vicinity of the propellant sample and the center of the combustion chamber, the device contained a long rod, gaged to measure unsteady stress. This provided a means for measuring the total force (gas pressure plus solid stress) exerted against the end of the rod which represents the projectile base. This unique measurement provided the means for determining the thrust generated by propellant combustion which is an important factor in realizing the full benefits of the traveling charge concept. Quasi-steady and unsteady combustion characteristics were determined during this program.

The overall program conducted at Calspan Corporation involved eight propellant formulations. A few of these formulations were also compacted at two densities. The results of the tests conducted previously are given in Reference 10. The current program, described in this report, consisted of tests of a single formulation, designated 1086-7B, compacted to 88% of theoretical maximum density. The test parameters included propellant loading density, sample weight for a given loading density, surface coating, and sample mounting material.

Propellant combustion was characterized by a low burn rate (about 1 m/s) until a pressure in the vicinity of 15-20 MPa is reached. After this pressure, which may represent the propellant crushing or break pressure, the combustion rate accelerated to levels from 10 to 180 m/s, depending on other test parameters. Tests conducted at different loading densities indicated that combustion rate was a strong function of pressure. Variation of sample weight at constant loading density demonstrated that increasing the amount of unburned propellant at the time the break pressure was reached also causes burn rate and thrust to increase. A coating that makes the outside surface of the sample slippery tended to reduce the apparent burn rate but use of a coating which retarded transmission of gas pressure along the periphery of the sample increased the apparent burn rate as well as thrust. Change of mounting interface properties caused significant differences in the dynamic characteristics leading to increased thrust.

TABLE OF CONTENTS

LIST OF ILLUSTRATIONS

LIST OF ILLUSTRATIONS (continued)

LIST OF TABLES

I. INTRODUCTION

The traveling charge concept has been under consideration for many years as a means to achieve muzzle velocities higher than those possible in conventional gun systems. This concept is one where propellant combustion is tailored in a way to generate thrust in addition to the quasi-steady pressure force that normally provides projectile acceleration. Thrust is a reaction due to the momentum of the combustion products leaving the burning surface and becomes significant when the burn rate exceeds 100 meters per second. The main limitation in traveling charges has been the failure to formulate propellants with a sufficiently high burn rate. With the advent of Hivelite-based propellants, burn rates upward of 500 meters per second can be achieved which are in the range of interest for traveling-charge ammunition.

A test fixture with a long slender combustion chamber in the configuration of a gun barrel was designed and fabricated by Calspan Corporation for the purpose of characterizing the thrust generated by various formulations of Hivelite-based propellants in support of BRL Project No. 1L162l8AH80, "Development of Improved VHBR (Very High Burn Rate) Propellants."[1,2,3] The fixture was instrumented with several pressure ports in order to help characterize the overall rate, pressure dependence, and dynamic aspects of VHBR propellant combustion. Special instrumentation in the form of a steel rod with strain gages was incorporated to measure the total force applied to the projectile base. The total force and pressure measurements in conjunction with a model of the combustion process made it possible to determine the thrust component resulting from the combustion process.[2]

The objectives of the tests described in this report are to generate additional combustion data and investigate the effects of several test parameters on the combustion characteristics of one VHBR formulation. The test fixture, test program, results and conclusions of this program together with previous results of the VHBR program are discussed in this report.

II. BACKGROUND

A. Overview

VHBR propellants are a relatively new class of propellant formulations that exhibit burn rates from 1 to 500 meters per second. Propellants with this range of combustion rates have been sought for many years for use in traveling charge development and Ballistic Research Laboratory (BRL) has now begun a systematic program to investigate the use of these propellants for this purpose. The program began with deliberate analysis and careful selection of formulations that were believed to generate propellants with the right thermodynamic and combustion characteristics.

The first article of the Background section is devoted to propellant formulation, chemistry, thermodynamic properties, and theoretical combustion considerations. The next article presents experimental combustion results that have been obtained for a series of 8 formulations that span the desired combustion range. Finally, previously reported results and conclusions from the project just concluded at Calspan Corporation are presented as a prelude to the testing described in the remainder of the report. Much of the background information was found in BRL references 1, 2 and 3.

B. Propellant Characteristics

The propellants incorporated in this investigation are boron-hydride based propellants that were initially part of ignition ordnance formulations based on the decahydrodecaborate anion.[1,2] These formulations appear to propagate at velocities intermediate between the deflagration and detonation, which is the range of one to 500 meters per second. In order to achieve the right properties for traveling charge application, it is necessary to tailor the propagation velocities to those that match interior ballistics requirements. In addition, the propellants that are developed need to adhere to conventional propellant requirements for safety and ease of handling. Of over 200 different propellant formulations that were thermochemically examined by computer analysis, eight were selected as being of potential interest. The formulation of these propellants is shown in Table 1.

Table 1. VHBR Propellant Formulations Studies

Sample Code	Fuel	(%)	Oxidizer	(%)	Binder	(%)
1086-ID	498	10.2	HMX	74.8	CTPB	15.0
1086-2C	466	17.1	AN	70.9	CTPB	12.0
1086-3	466	25.7	AN	59.1	NC/DNT	15.2
1086-4B	466	10.6	TAGN	74.2	NC/DNT	15.2
1086-5A	498	8.8	TAGN	76.0	NC/DNT	15.2
1086-6B	466	27.0	AN	67.1	C4000	5.0
1086-7B	466	10.5	TAGN	84.5	C4000	5.0
1086-8A	498	8.6	TAGN	86.4	C4000	5.0

The oxidizers chosen to mix with the Boron Hydride element were cyclotetramethylenetetranitramine (HMX), ammonium nitrate (AN), and triaminoguanidinium nitrate (TAGN). Binders included carboxyterminated polybutadiene/nitrocellulose and a polyethylene glycol, carbowax 4000. The fuels used in the composition are coded according to a numerical scheme. The identity of the fuels is proprietary to Teledyne McCormick-Selph.

The performance parameters needed for gun interior ballistics were computed with the Blake thermochemical code and are given in Table 2. The pressure computed for closed vessel experiments on several of these propellants were significantly higher than measured

Table 2. Comparison of Selected Thermochemical Properties of VHBR Propellants with M30A1

Propellant	Impetus (J/g)	Temperature (K)	Gas Molecular Weight (AMU)	Covolume (cm^3/g)	Specific Heat Ratio
M30A1	1064.7	3000	23.430	1.044	1.2406
1086-2C	976.0	2170	14.454	1.246	1.2679
1086-3	1094.6	2538	13.085	1.221	1.2670
1086-4B	1090.4	2402	15.926	1.301	1.2719
1086-5A	1124.7	2647	17.500	1.198	1.2662
1086-6B	1094.1	2488	12.245	1.240	1.2650
1086-7B	1084.4	2329	15.335	1.328	1.2710
1086-8A	1119.1	2539	16.815	1.229	1.2692

values.[4] The discrepancy probably derives from the complex nature of the combustion of these materials.

The BLAKE code was also used to compute the major combustion products of a typical VHBR propellant. The results of this calculation are shown in Table 3 and compared with those of a conventional high energy military propellant, M30A1. Note the significant differences of hydrogen and the liquid precipitate of the boron-containing compound.

Table 3. Comparison of Major Combustion Products Of VHBR 1086-4B with M30A1

Species	M30A1 (moles/kg)	1086-4B (moles/kg)
H_2	3.42	24.03
N_2	11.77	16.17
CO	11.72	10.01
H_2O	10.49	1.89
CO_2	2.99	0.12
NH_3	0.02	0.40
HCN	0.007	0.33
CH_4	0.0005	1.36
B_2O_3 (Liquid)	---------	1.88

The combustion mechanism of VHBR propellants is not well understood at the present time. What is agreed upon is that the laminar burning rate used to characterize normal solid propellant is not appropriate for use with VHBR propellants because VHBR propellants are porous and it is believed that the combustion zone is propagated by infiltration of hot combustion products through pores in the sample ahead of the flame front.[5] Thus, the term "apparent burning rate" was developed because a closed-bomb data-reduction procedure used to extract burn rates from the measured pressure history for conventional propellants has been applied to VHBR propellants. This procedure assumes that the propellant surface recedes according to a function defined by surface geometry. While this technique is not necessarily an accurate method describing VHBR propellant combustion for ballistic design, it is a means by which different propellants can be compared and the overall combustion rate mechanism quantified in terms that ballisticians understand.

In a convective burning environment, there are many variables that may play a role in determining the combustion rate. These include the sample porosity, constituent particle size, mechanical strength, lateral confinement and whether or not the pores of a sample are prepressurized with an inert gas. In addition, quantities such as burning surface temperature, flame temperature and the energy release profiles in the condensed phase at the burning surface and in the flame zone are also important factors. Gough has prepared a one-dimensional traveling charge code.[6] In this code, a thin flame zone was assumed. However, work by Baer[7] in trying to apply the code to closed vessel combustion data discovered that combustion results could not be correlated with that code. At present, Kooker is developing a code[8] that assumes a different mechanism for the burning rate of these high density, porous, energetic materials. In this work Kooker suggests that the deflagration of a confined, end-burning column of high-density, compacted-granular, energetic material does not accelerate from a surface burning mode by convective combustion through a rigid, stationary, porous matrix. Instead, it is proposed that porous material upstream of the burning interface collapses to form a plug of high-percent TMD material. Proper confinement leads to an increase in the stress field beyond an allowable rate of shear which is then responsible for local ignition in shear bands and fracture of the collapsed plug. The fragments are entrained into the flame zone creating a two phase flow combustion process which is capable of supporting rapid increases in pressure. Thus the combustion mechanisms of the VHBR propellants appear to be quite complex. In this context, apparent burn rates cited in the ensuing text can only be used as a relative means for quantifying the combustion process.

C. Experimental Results

The eight propellant formulations cited in the previous section were fabricated into test samples 12.7 cm in diameter and 40.8 mm long (small) and 36.6 mm in diameter and 25.4 mm long (large). These samples were compacted to various densities in confined and unconfined configurations as indicated in Table 4. The confined samples were

Table 4. VHBR Propellants and Densities

Sample Type	Small Confined		Small Unconfined		Large Diameter	
	Density (g/cm^3)	% Theoretical Density	Density (g/cm^3)	% Theoretical Density	Density (g/cm^3)	% Theoretical Density
1086-ID	1.385	92	1.480	86		
1086-26	1.340	90	1.280	86		
1086-3	1.238	83	1.367	91		
1086-4B	1.277	88	1.404	97		
1086-5A	1.280	85	1.305	86	1.486	98
			1.486	98		
1086-6B	1.240	84	1.254	85		
			1.297	88		
1086-7B	1.250	88	1.399	98	1.399	98
1086-8A	1.250	84	1.443	97	1.443	97

encased in steel sleeves 1.57 mm thick. The significant difference between the confined and unconfined samples was that, during conventional closed vessel tests, the confined samples experienced no pressurization along the side but only from the end. Whereas, unconfined samples experienced the gas pressure of the closed bomb over the entire surface except the mounting end. Thus, the forces and the restraint during the combustion process are the primary difference in these two sample configurations.

Two kinds of tests were conducted. The propellant samples were tested in conventional closed bombs at BRL[3] and Calspan Corporation.[9] The chambers of this bomb configuration are typically not much longer than the sample length and the diameter of the chamber is somewhat larger than the diameter of the sample. Pressure rise rates at one or more locations in the bombs were obtained. A force gage was used in Reference 9 to measure thrust but the frequency response was found to be unacceptable.

The second kind of test that was conducted was in what is termed the VHBR bomb,[10] a combustion device specially designed for VHBR propellant testing. This device features a unique piece of instrumentation that measures the total force on the end of the bomb that is created by combustion of the sample. That is, both the pressure force pushing on the sample and the momentum exchange

are measured. While confined and unconfined samples were tested in the conventional closed bomb, only unconfined samples were tested in the VHBR bomb but the combustion process was somewhat constrained by the tight-fitting diameter of the VHBR bomb which was essentially the same as the diameter of the propellant samples. The length of the combustion chamber was approximately 10 times as long as the propellant samples. Thus, pressure waves in the VHBR bomb are much more severe than in the conventional bomb. Instrumentation includes the device to measure thrust at one end in addition to several pressure transducers along the length of the propellant sample and in the middle of the bomb.

Because combustion rates of the magnitude exhibited by VHBR propellants are of the same order of magnitude as the speed of sound of the combustion products for the faster-burning formulations, strong pressure waves dominate the combustion process for these high-rate formulations in both conventional and VHBR closed combustion vessels. BRL personnel have used a Fourier analysis technique to extract the quasi-steady response from the dynamic pressure data generated in conventional closed bombs.[3] From this data apparent burn rates were computed based on techniques used for conventional propellants. It is cautioned that use of these techniques may have some hidden errors because the combustion rates of some of the propellants tested are of the same order of magnitude as pressure wave propagation rates and instantaneous combustion of the propellant can be significantly influenced by the peaks and valleys of the pressure waves. These influences are not addressed by the conventional data reduction techniques. However, as stated previously, this approach does provide a method by which the combustion behavior of the various propellants can be compared.

Apparent burning rates of confined (cased 12.7 mm diameter) VHBR samples as tested in a conventional closed bomb are shown in Table 5.[3] Similar results for unconfined (bare 12.7 mm diameter) samples are shown in Table 6.[3] Burn rate data for larger unconfined (bare 36.6 mm diameter) samples are shown in Table 7.[3] Apparent

Table 5. Apparent Burning Rates of Confined VHBR Samples

	Burning Rate (m/s)		
Sample	50 MPa	100 MPa	150 MPa
1086-ID	0.596 ± 0.005	1.117 ± 0.003	1.37 ± 0.04
1086-2C	2.200 ± 0.300	3.010 ± 0.020	2.72 ± 0.08
1086-3	242.0 ± 4.000	256.0 ± 7.000	181 ± 11
1086-4B	230.0 ± 20	235.0 ± 11	153 ± 15
1086-5A	451.0 ± 113	505.0 ± 137	442 ± 140
1086-6B	214.0 ± 3	231.0 ± 1	169 ± 3
1086-7B	304.0 ± 8	249.0 ± 1	318 ± 15
1086-8A	247.0 ± 19	272.0 ± 15	220 ± 11

Table 6. Apparent Burning Rates of Unconfined Samples

		Burning Rates (m/s)		
Sample	TMD (%)	50 MPa	100 MPa	150 MPa
1086-ID	86	0.36 ± 0.03	0.82 ± 0.03	1.12 ± 0.07
1086-2C	86	1.50 ± 0.20	2.00 ± 0.20	1.80 ± 0.20
1086-3	91	96 ± 40	145 ± 61	114 ± 71
1086-4B	97	47 ± 8	101 ± 14	101 ± 3
1086-5A	86	368 ± 176	455 ± 195	463 ± 195
	98	256 ± 116	315 ± 133	332 ± 113
1086-6B	85	39 ± 26	57 ± 23	39 ± 15
	88	22 ± 5	18.6 ± 0.6	17 ± 1
1086-7B	98	2.3 ± 0.1	4.22 ± 0.08	9.4 ± 0.9
1086-8A	97	11.6 ± 0.1	26.0 ± 0.4	102 ± 2

Table 7. Apparent Burning Rates of Large Diameter Samples

	Burning Rates (m/s)		
Sample	50 MPa	100 MPa	150 MPa
1086-5A	86.4	95.1	91.5
1086-7B (Lot 4)	2.4	5.0	13.2
1086-7B (Lot 5)	1.4	3.3	10.7
1086-8A	1.1	57.3	146.1

burning rates for confined VHBR propellants and M30A1 propellant are shown in Figure 1 to illustrate both the pressure influence on combustion and to demonstrate the tremendous range of combustion that is exhibited by these propellants. It is of interest to note that the repeatability based on a few firings is fair for propellants in the low to intermediate burn rate. The high-burn rate propellants experience greater variability, perhaps as a result of the inadequate treatment of dynamic phenomena cited above. Also of interest is the fact that when propellants of the same formulation but different compaction densities are tested, propellants with the lowest percent TMD (Theoretical Maximum Density) always exhibit higher burning rates. It is also of interest to note that confined VHBR samples experienced a greater degree of consistency than unconfined samples. Data from propellant sample 7B is shown in Figure 2. Here the confined 88% TMD burn rate is at a high level while the higher percent TMD burns at a lower rate.

D. Previous Results and Conclusions from the Current Project

The VHBR bomb was designed by Calspan to provide a measurement of the thrust produced by the combustion process. The bomb contained a force gage in the form of strain patches on a long steel rod that formed a closure on one end of the bomb. The propellant sample was installed adjacent to the rod so that, as gas and solid products spalled off the burning surface, the impulse, in addition to the pressure force transmitted through the propellant sample, could be measured simultaneously.

All propellant formulations and compaction densities were tested in the VHBR bomb. Apparent burning rate data based on the time required for the pressure to rise from 10 to 90% of the peak value is shown in Table 8 in comparison with similarly calculated apparent burn rate data obtained from a conventional closed bomb. The faster burning-rate propellants exhibited such strong dynamic tendencies that it was virtually impossible to generate burn rate information by this technique. Pressure data

Table 8. Comparison of Current With Previous Burn Rate Measurements

Sample	Density (gm/cm^3)	Average Burn Rate (m/s)				
		VHBR Bomb Current Program and Ref. 10	Calspan Tests (Ref. 9)		BRL Tests (Ref. 2,3)	
			Bare	Confined	Bare	Confined
1D	1.585	---	---	---	---	1.0
1D	1.480	0.4	---	---	0.6	---
2C	1.340	---	---	2.4	---	2.6
2C	1.280	1.3	---	---	1.5	---
3	1.367	50	35	---	89	---
3	1.238	---	---	89	---	104
4B	1.404	80-100	---	---	82	---
4B	1.277	---	---	---	---	161
5A	1.486	---	113	418	238	---
5A	1.305	---	245	---	357	---
5A	1.299	---	---	476	---	385
6B	1.254	22	22	90	24	45
6B	1.297	21	---	69	16	---
7B	1.399	2.5	6.1	---	4.5	---
7B	1.268	180	---	102	---	250
8A	1.443	21	42	---	32	---
8A	1.274	---	---	294	---	192

were completely dominated by the dynamics and it was impossible to obtain the quasi-steady pressurization rate to obtain the apparent burn rate.

The combined pressure and thrust information allows the apparent rates of VHBR propellants to be extracted without the restrictive space mean pressure assumptions required in the standard closed bomb analysis. Based on the fundamental balances of mass, momentum, and energy, Gough derived a relationship between propellant regression rate and the solid and gas phase stresses on either side of the propellant surface. The resultant equation appears below. A full exposition of the theory appears elsewhere.[2]

$$r = \left(\frac{g_o}{2\rho_p^2} \; \frac{(\sigma - P)\left(\sigma + \frac{\gamma+1}{\gamma-1} P\right)}{e_p + \frac{P}{\gamma-1}\left(b - \frac{1}{\rho_p}\right)} \right)^{1/2} \qquad (1)$$

where r = regression rate
g_o = gravitational constant
ρ_p = solid propellant density
σ = stress at propellant surface
P = pressure at propellant surface
γ = specific heat ratio
b = covolume
e_p = propellant energy

It should be emphasized that the values of σ and P used in the equation are for the gas-solid interface, rather than the experimentally measured values. The experimental values were actually measured at some small distance from the gas-solid interface (see Figure 11 for location of sensors relative to the propellant), hence, there is a phase difference between the measured values and the values at the interface at any given instant. The appropriate corrections to the experimental values were done using the characteristic forms of the equations of motion for each of the media. Values of e_p, γ, and b for specific formulations were obtained from thermodynamic equilibrium calculations. Propellant density is a measured quantity. The analysis assumes a reaction zone sufficiently thin to be quasi-steady, and one dimensional, in order to describe the linear-elastic behavior of the propellant.

1. Fast Burning Case

A propellant sample of composition 1086-5A at a TMD of 98% resulted in the most dramatic demonstration of a substantial thrust contribution due to very high burning rates. Figure 3 shows derived pressure and stress at the gas-propellant interface as a function of time. The data are quite similar to the measured values, but offset in time. The maximum value of stress to pressure $(\sigma/P)_{max}$ is greater than two. The force produced by thrust alone, therefore, exceeded the force produced by the gas pressure.

Regression rates up to 300 m/s were computed for this case by means of Equation (1). Considering the widely different assumptions in the two analysis methods, this value matches the high burning rate value from the standard closed bomb analysis remarkably well. A correlation of the computed regression rates as a function of pressure as plotted in Figure 4. The rise and decay times of this event are on the order of 100 microseconds. In this highly transient environment, it is perhaps, not surprising that the regression rates are not the same in both the pressurization and the depressurization region, an indication of a hysteresis. Figure 5 correlates burning rate with stress. The hysteresis is greatly reduced which leads to the conjecture that a solid phase stress-induced mechanism such as surface breakup is a strong factor in the burning mechanism.

2. Moderate Burning Case

A sample of 1086-3 (91.5% TMD), although a significantly slower-burning material, also exhibited substantial thrust. The reduced pressure and stress at the combustion gas-propellant interface is depicted in Figure 6. The analysis is terminated at about 350 microseconds after rapid pressurization occurs to eliminate complexities due to wave reflections in the stress rod. Regression rates are shown in Figures 7 and 8. Again, a better correlation is obtained for stress than for pressure. The agreement with the

standard closed bomb results of the unconfined samples of the same density is satisfactory in the peak values obtained. In the lower pressure region the agreement is poor, however.

3. Anomalous Cases

In two tests of 1086-6B at both 86.6% and 84.7% TMD unusual results were obtained. Detailed examination of the pressure and real stress gages indicated that both the stress and the pressure (p1) near the stress rod begin to rise almost simultaneously. The pressure gages, p2, p3, and p4 begin to rise sequentially later in time as shown in Figure 9. It is our conjecture that in these cases the fast burning process started at the endwall and then propagated towards the front end of the sample where initial ignition due to the igniter first occurred. It is also likely that high pressures at the sample base caused it to be accelerated toward the igniter end of the chamber. Flashing down the sidewall or compaction-induced accelerated burning at the end wall are possible mechanisms for such an event. Friction induced heating and ignition, however, cannot be ruled out. No thrust production was observed for these cases. This would be expected if the sample were no longer in contact with the stress rod.

E. Current Program

While thrust and burn rate measurements of many samples were made, the parameters that govern the combustion mechanism have not yet been investigated. The primary objective of the program discussed subsequently in this report is to vary test parameters and determine what influences the rate of combustion and what the causes of the anomalous cases may be. For this, a single propellant was chosen, 1086-7B, compacted to 88% TMD. While the conclusions drawn from these tests may not apply to all formulations and compaction densities, greater insight into VHBR propellant combustion is expected to be achieved.

III. TEST EQUIPMENT AND PROCEDURES

A. Test Fixture

The test fixture used in this program was designed and fabricated by Calspan Corporation for the expressed purpose of investigating combustion phenomena of very high burn rate (VHBR) propellants. The fixture, called the VHBR bomb, was machined from 4340 steel and is shown completely assembled in Figure 10. The bomb combustion chamber has a volume of approximately 53.1 cubic centimeters and was statically pressure checked at 410 MPa prior to use.

The main body of the bomb consists of a combustion chamber, an end cover, a seal plug and an electrode, as shown schematically in Figure 11. The electrode was made from heavy thermocouple wire, which was silver soldered into an Armco steel fitting. When the bomb was pressurized, the end cover maintained the position of the electrode assembly. The thermocouple wire concept provided two electrodes insulated from the combustion chamber so that when electrical power was applied to initiate an electric match, no pulse was evident on any of the instrumentation. The seal plug is a 1.9-cm long Armco steel unit that is used to back up the test sample. It contains the sealing elements for the end of the bomb opposite the electrode. The seal on both ends consists of an O-ring backed by a triangular-shaped beryllium-copper ring which provides a metal-to-metal seal at high pressures.

The seal plug is supported by a unique piece of instrumentation called a stress rod. This stress rod, which will be discussed in more detail in the next subsection, is an Armco steel bar 1.27 cm in diameter and 91.4-cm long. The bar, in turn, is butted against a steel brace with an adjustable screw attachment in order to provide axial adjustment. A 5-cm thick steel plate with a slot milled in the top and covered by a 1.5-cm thick plate, bolted to the bottom plate, is used as a stiffening mechanism for the stress

rod. This means of stiffening prevents the stress rod from buckling when it is subjected to very high pressures or stress levels. The relationship of the stress rod to the VHBR bomb and the means for supporting and stiffening it are illustrated in Figure 12.

B. Instrumentation

The VHBR bomb was instrumented with four pressure transducers and a stress rod. The test samples were up to 5.08 cm long with the base of the test sample resting against the face of the seal plug. The centerline of the transducer, identified as p1, was located 0.48 cm from the seal plug. Transducer p2 was located 2.70 cm from the seal plug and transducer p3 was located 5.56 cm from the seal plug. For reference, the seal plug face was located 3.33 cm from the end face of the closed bomb. Therefore, these three transducers measured pressure essentially at the base end of the test sample, which corresponds to the projectile base, the center of the test sample, and at the front end of a 5.08-cm long sample. A fourth transducer, p4, was located approximately in the center of the closed bomb. Pressure p2 or p3, whichever was located at the front end of the propellant sample, is considered to represent the end-of-grain pressure developed by a propellant charge in a gun chamber and is the pressure which is subtracted from the total force acting on the projectile to determine the thrust. All pressure transducers were PCB type-118A transducers.

The transducers were flush mounted to the inside surface of the combustion chamber in order to optimize response time. The front surface of the transducers was covered with porous ceramic to minimize temperature effects on the pressure readings. The transducers have a capability of recording pressures over 700 MPa at 500 khz response. Transducer output was converted to a voltage signal by means of charge amplifiers which have a frequency response of 150 kilohertz.

The stress rod consisted of a 91.4-cm long Armco steel bar that was heat treated to approximately 200,000 psi yield stress.

Strain gages were bonded to the bar with the gage centerline located 3 cm from the end of the bar adjacent to the seal plug. Including the length of the plug, the total distance of the strain gages from the base of the test sample was 4.9 cm. The speed of sound in steel is 4,900 meters per second. Therefore, the time required for a stress wave to travel from the base of the sample to the location of the strain patches is approximately 10 μsec. A diagram showing the physical and electrical hookup of the strain gages is shown in Figure 13.

The pressure transducers and the stress rod were calibrated simultaneously by installing them in the VHBR bomb and pressurizing it to a pressure in excess of 200 MPa. In this way, all instrumentation was calibrated in its installed configuration and used the test data acquisition setup to assure the relative accuracy of the data.

The theory of the stress rod is illustrated in Figure 14. Here it is shown that an elastic stress wave initiated at time zero requires approximately 185 μsec to traverse the length of the rod. At that time the wave is reflected by the steel support at the far end and traverses the rod again towards the origin. The time between the initiation of the wave and the arrival of the reflected wave at the origin is approximately 370 μsec. When the rod is used to provide data in this time "window" it is being used in the unsteady mode. When used in this mode, the stress rod response is limited only by that of its amplifier, which, for this program was a specially constructed DC amplifier with a frequency response in excess of 1 Mhz. After this time, the reflected waves complicate the signal and the actual stress level at the base of the sample can no longer be deciphered. The rod can also respond in the quasi-steady mode and behave as a medium-response pressure transducer. This mode of operation applies when the pressure rise rate is slow with respect to the stress wave transit time. This rate of pressurization makes the magnitude of reflected waves small in comparison to the ambient pressure level.

The VHBR bomb also has the capability to signify the presence of heat due to ignition or flame front arrival at the base of the propellant sample. For this measurement, a thermocouple is mounted in the seal plug and run through a hole, angled so the thermocouple enters the end, and passes through the side of the stress rod. In theory, the thermocouple signifies the time when the flame front or an ignition stimulus reaches the base of the test sample. The configuration consists of a chromel alumel thermocouple, made out of 0.076-mm wire, mounted over a cone-shaped steel plug with epoxy to provide a seal. An amplifier similar to that used with the stress rod is required for the thermocouple so that the electrical response of the thermocouple system is sufficient to resolve the intended events.

All data were recorded on Nicolet Explorer III digital oscilloscopes. These oscilloscopes have a wrap-around memory feature that allows pre-trigger information to be recorded. Permanent records of the data were obtained on floppy discs with the disc attachment of the oscilloscope. Data reduction and hard copies were obtained with a Hewlett-Packard desk-top computer and plotter. The trigger signal for all oscilloscopes was created by a specially fabricated electronic device that generated a 5-volt pulse when the pressure p3 reached a predetermined level during the first twelve tests conducted with the VHBR bomb. Time zero for these runs was the time the pulse was generated. Because it was not possible to cause the trigger to occur at the same voltage for each oscilloscope, small differences in time zero were present. To eliminate this problem, pressure p3 was recorded on each oscilloscope for all subsequent runs. The trigger signals during this period were generated internally when pressure p3 reached a predetermined level. Time zero, the time the oscilloscope was triggered, was different for each oscilloscope for this latter group of runs, but the presence of common data on all oscilloscopes made it possible to provide exact relative timing for all data.

IV. TEST PROGRAM

The tests described in this section represent the third in a series of three test phases that were conducted during this program. The details of the previous tests, numbered 1 through 23, are described in detail in Reference 8. Some of the pertinent results from those tests are described in the Background Section of this report. While the objective of the first two phases was to generate combustion and thrust data for a variety of VHBR propellants under the same test conditions, the objective of the third phase described here is to generate combustion data for a single sample formulation under a variety of test conditions.

Material formulation, density, and the basic sample configuration were the same for all tests. The samples were made by Teledyne McCormick-Selph of Hollister, California and were all of the 1086-7B formulation, pressed to a density of 1.69 gm/cc, which is 88% TMD. Because 88% TMD 1086-7B propellant was not tested previously in the VHBR bomb an additional objective of this phase was to generate basic combustion data for comparison with data generated previously from samples of different formulations and, in particular, samples with the same formulation but with a different compaction density.

The samples were 2.54-cm long and 1.27 cm in diameter. All samples were weighed, measured and examined with an optical microscope prior to testing. In each case at least one end of a propellant sample was almost completely smooth and free of defects. This end was placed next to the stress rod. In most cases the other end had some type of defect such as surface spallation that must have occurred when the sample was being molded, or being removed from the mold.

Pitted or spalled surfaces looked like granular snow under a microscope. Propellant particles were clearly visible and appeared to be loose or loosely bonded to the surface. Some spall marks were quite abrupt and edges and sharp valleys were apparent. Cracks did not appear to extend into the base material from the valleys.

Table 9. Physical Characteristics of the Samples

Sample No.	Run Tested	Length (cm)	Weight (gm)	Results of Examination
1	24	2.520	3.9942	Side: Evidence of grain layer, no discernible cracks End o Relatively rough, craters about 0.1mm diameter, evidence of flaking, deconsolidation (igniter end End oo Single very small crater (stress rod end)
2	25	2.520	3.9755	Side: Spots and general contamination on oo end - 1/2 of sample End o Generally pock-marked, rough surface; look as if material stuck to press (igniter end) End oo Small chip off edge, nearly perfect end; spots of stain (stress rod end)
3	28	2.522	3.9782	Side: Tiny microcracks evident, evidence of strain beneath surface End o Essentially perfect end (stress rod end) End oo Large chip from edge (igniter end)
4	26	2.527	3.9867	Side: Some strain or contamination exists at o end, a tiny microcrack structure is evident but no cracks are open End o Good surface, small chunk out of edge - 1mm x 1/2mm (stress rod end) End oo Rough surface, characteristic pit size is 0.3mm dia (igniter end)
5	26	2.540	3.9815	Side: Some contamination at oo end End o Very rough surface, depth of pits 0.2-0.3mm (igniter end) End oo Very nearly perfect end (interface of second sample)
6	25	2.525	3.9805	Side: Slight stain at o end, a few microseconds noticeable End o One pit approximately 0.05mm x 0.05mm (stress rod end) End oo Four minor pits and chips out of edge (interface of second sample)

Table 9. Physical Characteristics of the Samples (Cont.)

Sample No.	Run Tested	Length (cm)	Weight (gm)		Results of Examination
7	27	2.527	3.9824	Side:	Slight gouge on o end, stain on oo end, tiny microcracks observed
8	29	2.512	3.9720	Side:	Tiny microcracks, stain at o end
				End o	Essentially perfect end, some indication of stain, which may be mold lubrication (stress rod end)
				End oo	Severe pitting, spall (igniter end)
9	30	2.515	3.9800	Side:	Stain at o end, tiny microcracks
				End o	Nearly perfect end (stress rod end)
				End oo	Surface very rough, large spall (igniter end)
10	31	2.512	3.9893	Side:	Stain at o end, tiny microcracks
				End o	Very smooth surface (stress rod end)
				End oo	Generally distributed spall marks (igniter end)

No samples had any major cracks in either the sidewall or the ends. The length, weight and observations of the test samples are contained in Table 9.

Test variables for this phase of the program included the number of samples tested, the surface deterrent configuration, the chamber volume of the VHBR bomb and the interface between the sample and the stress rod. The number of samples tested was either one or two at one time. The standard deterrent configuration was to coat the entire surface of the propellant sample with the Calspan ablator, which is dimethyl silicone thickened with Cabosil. Only the surface adjacent to the igniter and, when two samples were tested simultaneously, the interface between the samples, were not deterred. During the program one sample was tested without deterrent of any kind while two samples were coated with a deterrent of glycol-based organic grease. The chamber volume was reduced by approximately 1/2 through the addition of a brass rod at the igniter end of the chamber. In this way propellant loading density was altered independently of the propellant weight. Finally, a piece of rubber approximately 0.5 cm thick was used to form the interface between a propellant sample and the stress rod during one test to alter the effective wave reflection characteristics.

The test technique was to mount a sample in the test chamber, install the stress rod and then install the igniter. The igniter consisted of an electric match with a 0.5-gram charge of 4X black powder tied in a Kimwipe sack around the end of the electric match. The electric match was located at the end of a substantial length of wire. The wire was coiled and extended so that the electric match and the black powder charge were adjacent to the test sample when the igniter was installed in the closed bomb. A six-volt battery was used to fire the match and begin the test.

A total of 8 tests were conducted during this phase and the main parameters and pertinent data are listed in Table 10. In this table the run number signifies the order in which the tests were conducted. The Sample I.D. is an identifier used by BRL and Teledyne McCormick-Selph to signify the propellant formulation. The last

Table 10. Test Summary

Run	Sample I.D.	Loading Density (gm/cc)	Data Frequency (μsec/pt)	Pressure I.D.	Time 10%-90% (msec)	1st Peak Pmax (MPa)	Overall Pmax (MPa)	Δp-1st peak to min (MPa)	Test Variable
24	1086-7B-1	0.075	20	p1	5.6	59	70	NA	Single sample-standard preparation-Silicone ablator on all surfaces except adjacent to igniter
				p2	6.8	59	68.5	NA	
				p3	6.8	59	68	NA	
				p4	6.8	58.5	60	NA	
				SR		No Data	NA	NA	
25	1086-7B-2 1086-7B-6	0.150	10	p1	0.4	150	325	275	Two samples-standard preparation-Generate 88% TMD data to compare with previous tests
				p2	0.4	125	160,200	120	
				p3	0.4	125	130,225	NA	
				p4	0.3	150	260	190	
				SR	0.3	140	280	240	
26	1086-7B-4 1086-7B-5	0.150	2	p1	NA	NA	190-250	145	Repeat of Run 25
				p2	NA	NA	165,250	125	
				p3	NA	NA	120,250	90	
				p4	NA	NA	55,130	NA	
				SR	NA	NA	200,250	150	
27	1086-7B-7	0.147	5	p1	0.30	120	110,275	NA	Use brass filler bar to obtain same loading density as Runs 26 and 27- Ablator as in Run 24
				p2	0.30	120	100,215	NA	
				p3	0.15	120	100,185	NA	
				p4	NA	NA	NA	NA	
				SR	0.20	120	95,275	NA	
28	1086-7B-3	0.147	5	p1	0.15	130	345	200	Repeat Run 27 without ablator-Use brass filler bar
				p2	0.18	130	260	100	
				p3	.20	130	260	65	
				p4	NA	NA	NA	NA	
				SR	NA	NA	NA	NA	
29	1086-7B-8	0.149	5	p1	0.20	150	340, 500	300	Repeat Run 27 with 0.5 cm rubber cushion between seal plug and sample
				p2	0.20	150	490	440	
				p3	0.18	155	120,400	50	
				p4	NA	NA	NA	NA	
				SR	NA	NA	NA	NA	
30	1086-7B-9	0.147	5	p1	0.9	105	155	75	Repeat Run 27 with rod, seal plug and sample coated with glycol-base Battenfeld grease
				p2	0.9	105	140	55	
				p3	0.9	105	135	50	
				p4	NA	NA	NA	NA	
				SR		No Data			
31	1086-7B-10	0.147	5	p1	1.0	110	215	135	Repeat Run 30 to obtain stress rod data
				p2	1.0	110	185	105	
				p3	1.0	110	170	85	
				p4	NA	NA	NA	NA	
				SR	NA	NA	310	190	

digit is a number assigned during the test which identifies each individual sample and is used to correlate with the observations and weights presented in Table 9. The loading density is simply the total weight of the test sample or samples divided by the volume of the VHBR bomb for a specific test. It is noted that the brass rod incorporated during several tests reduced the volume of the bomb from 53.1 cc to 27.2 cc. This change in volume is figured into the loading density of Table 10.

The Data Frequency column signifies the time interval between the data points as recorded by the Nicolet oscilloscopes. Pressure identification number signifies the pressure transducer location. P1 is the pressure transducer mounted in the wall of the test chamber at the approximate location of the seal plug closure which corresponds to the projectile base in a gun. P2 is located in the wall of the test chamber at the location of the surface to be ignited when a single propellant sample is tested or at the break line when two propellant samples are tested at the same time. Pressure p3 is located adjacent to the ignition surface when two propellant samples are tested simultaneously. The centerlines of pressure transducers p2 and p3 are separated by 2.86 cm. This region is one where combustion of spall particles takes place and ought to be of great interest to help define the combustion process. P4 is a transducer located at the midpoint of the test chamber and SR signifies the stress rod which contains a strain gage and is used to measure the total force felt by a projectile in a gun barrel.

The next two columns in the table signify quasi-steady performance measurements that were made during the tests. These quasi-steady values represent averages that are functions only of time and not position in the test chamber. Thus, excursions or pressure levels caused by waves are not included in these columns. While all pressure data contained some pressure waves, the quasi-steady values were estimated by manually drawing a curve through the unsteady pressure data. The time for the pressure to rise from 10 to 90% of its peak value is a measure of the overall burning rate while the peak pressure signifies the force of the propellant.

Dynamic characteristics of the combustion process are presented in the next two columns. In these columns, p_{max}, indicates the peak value of pressure reached by the first pressure wave and then the maximum reached by any pressure wave during the test. When only one value is presented, this signifies that the first pressure wave did, in fact, reach the maximum value of any pressure wave during the test. Finally, the Δp from the first peak to the minimum value following that peak signifies the overall strength of the pressure wave and the rarefaction process that occurs after the maximum peak pressure is reached.

NA was placed in columns in both quasi-steady and dynamic values to signify that the data were not available, not appropriate, or not applicable for the case involved. When pressure traces that were characterized by severe dynamics to the extent that the quasi-steady values could not even be approximated without sophisticated Fourier analyses, an NA was placed under the quasi-steady column. This occurred for the data obtained during Run 26. Because the curves drawn through the dynamic data to approximate the quasi-steady values were drawn manually, the accuracy of these estimates diminish as the dynamic character of the pressure becomes more severe.

The last entry in Table 10 is entitled Test Variable. In this column the primary test variable or individual test objective is identified.

Before the individual tests are described it is useful to discuss the theory behind the experiment in order for the reader to appreciate the significance of some of the observations contained in the following text. The experiment was designed to promote cigarette-type combustion; that is, ignition at the exposed surface followed by uniform progression of the combustion zone along the length of the sample. The samples were normally deterred with Calspan ablator on all surfaces except the free surface to be ignited. Gas flow along the length of the sample was restricted by the tight fit of the sample in the combustion chamber and the deterrent coating, which also inhibited flamespread along the exterior surface.

Combustion characterized as slow to moderate in comparison to pressure wave transit times in either gas or solid phases should create pressure histories that are nearly identical at each of the pressure gage locations and the stress rod. The quasi-steady response of gages covered by the sample can be due to gas flow around the sample or transmission of pressure through the solid phase and/or the viscous inhibitor/ablator. Gas flow around the sample can be prevented due to the stress-strain behavior of the sample. When the pressures are below a certain minimum value the solid is expected to undergo elastic deformation which could restrict gas flow around the sample and delay gage pressurization. The deterrent coating applied to the sample can also help prevent gas flow along the exterior and delay pressurization. At higher pressures the ultimate strength of the solid matrix is exceeded and the propellant is expected to behave as a fluid. Thus, some deviations from uniform quasi-steady response may occur during the period of plastic deformation when pressures are relatively low.

When the combustion rate is very high, pressure response is no longer quasi-steady but is characterized by strong waves both in the solid and gas media. The momentum of the gas and particles leaving the propellant surface creates a reaction force that is transmitted through the propellant along with the static pressure force of the gas medium. This force is transmitted to the stress rod at the base of the sample. Until the propellant exhibits substantial plastic deformation or the gas has pressurized the peripheral volume, the side pressure transducers may not indicate a reading. For very fast-burning propellant, the force is sufficient to exceed the propellant ultimate stress immediately so that a pressure response is recorded at the side of the chamber. When the exposed surface is ignited it is expected that the pressure transducer adjacent to the surface, which is p2 or p3, whichever is at the front edge of the sample, would respond initially and be followed in sequence by the pressure at the center of the sample and then by the last pressure pl and the stress rod as the stress wave propagates through the sample. The transit time of the stress wave through the rod to the strain gage is about 10 μsec. This must be factored into the data analysis. Thrust is nominally the positive difference between the stress rod

data, corrected for timing delay, and p2 and p3. When the pressures respond in the proper sequence the data can be interpreted with the aid of a computer model of the combustion process as discussed in the background.

During some experiments the pressures did not respond in the expected sequence. For example, in some tests conducted during the first and second phases of the test program, pressure p2 responded initially, while in others pressure p1 or the stress rod preceded the other pressures. This posed questions pertaining to the location where ignition occurred, the mechanism for in-depth ignition and the shape and extent of the combustion zone. The following paragraphs discuss the data and events concerning the individual tests conducted during the third phase of the VHBR thrust test program.

A single propellant sample was tested during Run 24. The VHBR bomb loading density was 0.075 g/cc. Data obtained from the four pressure transducers are presented in Figure 15. A malfunction in the stress rod circuitry caused its data to be lost. The pressures p1, p2 and p3 were nearly identical in their overall response and in the shape and character of the dynamic features. Pressure p4 was different only in the dynamic features, which is a result of being located in the center of the combustion chamber rather than at the end where the combustion was taking place. The pressures appeared to exhibit two distinct combustion regions. From time zero until the time the pressure reached approximately 15 MPa, at a time of 18.2 msec, the pressure traces exhibited a slight upward curving trend that appears to resemble cigarette-type burning combustion. At 15 MPa the pressure curve accelerated its upward trend and at that point the dynamic features became readily apparent. It appears as if the combustion changed from the cigarette-type to a different type of convective combustion that is characteristic of fast burning VHBR propellants. Conceivably the value of 15 mPa represented the point at which the propellant failed structurally or began to crush. Because pressures p1, p2 and p3 were all very nearly identical, it is believed that very little if any thrust was exhibited during this particular test.

Two samples, loaded end-to-end, were tested during Run 25 so that the bomb loading density was 0.15 g/cm^3. Data obtained from all 4 pressure transducers and the stress rod are presented in Figure 16. For this run, the pressure p3 was located adjacent to the surface exposed to the igniter. P3 began a gradual rise until a pressure of 17 MPa was reached (a). At that time, it rose abruptly to a level in the vicinity of 150 MPa. The pressure p2 was very similar to p3 in all respects (b). Transducer p1, however, experienced little, if any, pressure buildup until p3 reached the 17 MPa level, at which time p1 rose abruptly to a level in excess of 250 MPa (a). The stress rod data corresponded to pressure p3 prior to the time p3 reached the 17 MPa pressure level (d). After p3 reached 17 MPa, the stress rod data appeared to follow the rise rate of pressure p1. The difference between the rod stress at the first peak and p3, 180 MPa (g), is representative of the maximum thrust that was generated during the test. The pressure levels indicated by p1, p4, and the stress rod were nearly identical at the end of the data set (about 145 MPa at a time of 15 ms), while the pressures indicated by p2 and p3 were equal but at a lower level than the others (b) (about 115 MPa at 15 ms). The difference in pressure levels is a mystery at this point and there is no satisfactory explanation for the differences. The fact that the stress rod tracked the progress of pressure p3 in the early times is evidence that the propellant sample was accurately transmitting the pressure force to the stress rod. It is also evident that at 17 MPa pressure the propellant sample experienced a structural breakup as indicated by the time that the pressure was sensed by p1. The fact that the combustion rate accelerated drastically at that time is evidence that breakup is a strong factor that influences VHBR combustion.

Test 26 also incorporated two propellant samples with a VHBR bomb loading density of 0.15 g/cm^3. The objective of this test was to repeat the test of Run 25 but with a higher data collection frequency to obtain better definition of the rapid pressure rise regions. As indicated by the data shown in Figure 17, these results were somewhat different than those of Run 25. Pressures p2 and p3 as well as the stress rod rose together during the early times until a pressure of approximately 6 MPa was reached. During this early time, as in the previous test, p1 indicated no pressure.

When pressure p3 had reached about 5 MPa, pressure p1 gradually began to rise at an accelerating rate so that when pressure p3 had reached 6 MPa, p1 had already exceeded a pressure of 100 MPa. The relationship between p1 and p3 was very similar to that of Run 25 but p1 responded much more rapidly than p3. The response of the stress rod was initially negative which corresponded to the very beginning of the rise of p1. This may signify a localized ignition in the base region. At the time Run 26 was being conducted, the presence of a negative output from the stress rod was not understood. However, it is now believed that the presence of a negative pulse may have been in response to cocking of the seal plug which then may have caused a bending stress in the rod which created the negative signal. A localized ignition may have provided unsymmetrical loading which may have been the source of seal plug cocking. The runs with large oscillations in stress were not used to evaluate propellant thrust. The unusual response of p4 also suggests that ignition may have occurred at the base end of the propellant sample because its response is totally unlike the others and unlike the one that was observed during Run 25. It appears as if p4 were not experiencing the total dynamics of the combustion column of the same type that the other pressures experienced as if there were a piece of solid propellant separating p4 from the other pressures. Although the physical setup of Run 25 and 26 was identical, the combustion phenomena were somewhat different.

During Run 27, a single propellant sample was tested at approximately the same VHBR bomb loading density as the previous two runs where two propellant samples were tested. A brass bar was inserted in the bomb to occupy volume and thus reduce the volume of the combustion chamber. The bar was approximately 30-cm long and also altered the dynamics of the cavity which may also have had a bearing on the subsequent results. Because p4 was covered by the bar, its response to gas flow is expected to be altered somewhat and the readings from it were likely affected by the presence of the bar. The data from this test, as shown in Figure 18, indicate that all pressures, including p1 and the stress rod, responded uniformly until a pressure of about 8 MPa was reached. This, of course, was during the early cigarette-type burning of combustion. At that time pressure p1 began to rise more rapidly than p2, p3 and the stress rod.

Slightly later in time, when a pressure of 15 MPa had been reached, pressure p2 began to depart from the level of p3. It must be remembered that during this test pressure p2 corresponded to the forward end of the propellant sample. The stress rod data rose in accordance with p3 until a pressure of 35 MPa had been reached. Thus, the stress rod lagged behind both p2 and p1 for some unknown reason. The early rise of pressure p1 seems to indicate that ignition may have occurred at the time of the pressure rise near the base of the propellant sample. However, this is difficult to conclude from the observed data.

During Run 28, a single sample was tested in the same configuration as Run 27. This time the sample contained no flame retardant coating whatsoever and represented the first test in the VHBR bomb of an uncoated sample. The early-time response indicates that there may have been flamespread around the exterior of the sample because the pressure buildup shown in Figure 19 appears to be substantially more rapid than that of Run 27 and earlier tests. During this test, there does not appear to be an abrupt knee in the curve signifying a transition from cigarette burning to a rapid convective type burning but a gradual change that might be indicative of a gradual envelopment of the sample in flame. Pressure p1 and the stress rod show some rather unusual hitches in steps that may be indicative of sample hangup rather than easy sliding in the chamber. The stress rod in particular shows a rather severe hitch at a pressure from 15 to 20 MPa which is about the pressure level when sample breakup might be expected. The lack of a grease-type flame retardant may have made frictional restraint more severe in this case and cocking may have been a problem. Otherwise, the overall behavior of the curve after the rapid rise in pressure was very similar to that of Run 27.

During Run 29, a 1/2-cm thick section of rubber was bonded to the seal plug to form the interface between the propellant sample and the plug. Again, a brass bar was used to create a VHBR bomb loading density of 0.149 g/cm^3. The sample was covered with ablator on the sides and at the base end. Because pressure gage p1 was

covered by the rubber, it responded to the compression forces exerted by the rubber. As shown in Figure 20, p1, p2 and p3 and the stress rod all responded in a similar manner in the early time. However, pressure p1 exhibited a larger early time pressure rise while pressure p3 seemed to be suppressed from those of the earlier tests. The dynamics and effects of the rubber are quite complex and a rather detailed analysis of the pressure data and the effect of modifying the boundary condition is going to be required in order to truly assess the impact of this parameter.

During Runs 30 and 31 a different kind of flame retardant was used on the propellant sample. A grease made by the Battenfeld Company of Buffalo, New York, which is a glycol-based organic grease, was used to coat the propellant samples in place of the Calspan ablator. In addition, the grease was used to coat the seal plug, rings, and the stress rod in order to prevent uneven movements that were believed to be responsible for negative signals from the stress rod data. During Run 30 a malfunction prevented taking of stress rod data. However, pressures p1, p2 and p3 all responded in a similar fashion throughout the Runs 30 and 31 with very little deviation and virtually none of the excessive dynamics that had been observed during the previous runs. It is noted that these runs are duplicates of Runs 27 and 28 with the exception of the grease. The positive difference between the rod stress and the pressure p2 reached a peak value of 125 MPa, which indicates that thrust was generated by the combustion process. However, the rod stress level at the end of the data set was about 150 MPa, while the pressures measured by p1, p2, and p3 were only 90 MPa. This unexplained difference in stress and pressure levels casts some doubt on the indicated thrust level.

V. DISCUSSION

A. Overview

The primary objectives of the tests described in this report were to generate basic combustion data for 88% TMD 1086-7B propellant with the VHBR bomb and to identify important parameters and to quantify their impact on the combustion process. The various parametric variations and test objectives of the current program are listed in Table 11. Here the parametric comparisons that were made are also listed. The first item in the table is the loading density which was investigated during Runs 24 and 27. A single sample was tested in the VHBR bomb during Runs 24 and 27, but in Run 27 a brass filler bar was incorporated to reduce the chamber volume so that the effective loading density of the bomb was doubled. All other aspects of the tests were the same.

The second item listed in Table 11 is the number of samples tested at constant loading density. In Runs 25 and 26, two samples were tested in the VHBR bomb using full chamber volume, but in Run 27 a single sample was tested using the brass bar so that loading density was the same as for Runs 25 and 26. Flamespread deterrent on the outside surface was investigated during Runs 27, 28, 30 and 31. During these tests a single sample was tested in the bomb with the brass bar. In Run 27 the sample was coated with Calspan ablator while the sample tested during Run 28 had no deterrent coating at all. In runs 30 and 31 the sample was covered with an organic-based grease.

The stress rod interface was investigated during Runs 27 and 29. In Run 27 the sample butted up against the seal plug but for Run 29, a 0.5 cm piece of rubber was inserted between the propellant sample and the seal plug. Combustion repeatability was investigated during Runs 25 and 26 when two samples were used in the full chamber and also during Runs 30 and 31 where a single sample was tested in the chamber with the brass bar inserted.

Table 11. Parametric Variations

	Parameter	Runs Where Evaluated
1.	Loading Density	24,27
2.	Number of samples at constant loading density	25,26,27
3.	Flame deterrent	27,28,30,31
4.	Stress rod interface	27,29
5.	Event Repeatability	
	- 2 samples, full chamber	25,25
	- 1 sample, half chamber	30,31
6.	Combustion data for 88% TMD 7B propellant to complete the previous set of data generated in the VHBR Bomb	25,26

Finally, basic combustion data for the 88% TMD 1086-7B propellant under conditions similar to those tested in the previous 2 phases of the program was generated during Runs 25 and 26 when two samples were tested in the full VHBR bomb.

The data of interest during this program are the apparent burn rate, the peak pressure, thrust generated and the dynamic characteristics of the combustion process. In addition, a factor that appears to govern the apparent burn rate is the pressure break point, which is the pressure at which the combustion process appears to change from a slow cigarette-type burning to one involving high-rate convective combustion. The burn rate, the pressure break point, and the peak pressure are addressed in the next section entitled Combustion Data. Thrust and dynamic characteristics are discussed together in the following section.

B. Combustion Data

A summary of combustion data is presented in Table 12. In this table the apparent burn rate is computed for three different periods, entitled "Early Time, After Pressure Break, and 10% to 90% Pressure." The early time apparent burn rate includes that part of the pressure curve from the first indication of pressure until the point on the curve when the rate of pressure rise changes dramatically. This is the region in the combustion process that is believed to be cigarette-type burning. The data were obtained by forming the ratio of the break pressure with the maximum quasi-steady pressure. The assumption is made that the ratio represents the fraction of the sample that was burned during the early-time period. This quantity of the sample that was burned was then divided by the time from when pressure was first perceived to the break pressure. The burn rate after the break pressure is determined in a similar manner by using the segment of the quasi-steady pressure rise curve from the break pressure to about 90% of the peak pressure. Again it was assumed that the fraction of the sample combustion that occurred during this period was directly proportional to the fraction of pressure rise. The 10 to 90% pressure represents that time period

Table 12. Summary of Combustion Data

Run	Apparent Burn Rate-m/s: Early Time	Apparent Burn Rate-m/s: After Pressure Break	Apparent Burn Rate-m/s: 10%-90% Pressure	Break Pressure (MPa)	Max. Pressure (Quasi-Steady) (MPa)	Parameters
24	0.4	8.9	3.4	15	59	Single sample, L.D. = 0.075 ablator deterrent
25	0.8	180	102	17	125	Two samples, L.D. = 0.150 ablator deterrent
26	1.6	NA	NA	7	NA	Same as run 25
27	0.7	127	81	15	120	Single sample, L.D. = 0.147 ablator deterrent
28	1.1	49	41	15	130	Single sample, L.D. = 0.147 no deterrent
29	0.7	100	100	17	150	Single sample, L.D. = 0.149, rubber interface, ablator deterrent
30	1.1	42	23	17	105	Single sample, L.D. = 0.147, organic grease deterrent
31	0.9	43	20	20	110	Same as run 30

when 80% of the sample burned and includes part of the early-time combustion and all of after-pressure-break data. Therefore, in most cases the burn rate based on the 10 to 90% pressures is somewhat intermediate to the other burn rates. The quasi-steady state pressure curve was estimated and the burn rates based on these estimates are only approximate values.

According to the data that has been presented, loading density has a large effect on the combustion process, there being nearly an order of magnitude of difference in the burn rates that occurred between Runs 24 and 27. It is apparent that during Run 24, when a single sample was tested with a full VHBR chamber, that at the time of break pressure at 15 mPa, a higher percentage of the sample had been consumed in comparison with Run 27. Thus, after the break, when the combustion has a tendency to accelerate, more material was available to burn at the high rate and pressure was also higher, both of which tended to increase the combustion rate during Run 27.

The significance of quantity of material remaining after the pressure break is confirmed by comparing results of tests conducted at the same loading density, Runs 25, 26 and 27. Two propellant samples were tested during Runs 25 and 26, while a single sample was tested during Run 27, when the brass bar was used to occupy volume to maintain the same loading density. Thus, the quasi-steady pressure as a function of percent burned was nearly the same in both instances and only the absolute propellant weight and chamber dynamics were different. The tests that consumed two samples compared quite favorably with the single sample test although it is noted that during Run 25 the burn rate is somewhat higher than that of Run 27. This is attributed to the fact that once the break pressure was reached, more material in the configuration of a longer segment was left to burn during the runs where two samples were tested.

The influence of flame deterrent coating on the surface of the propellant samples provided a dramatic change in the combustion process. The samples coated with the Calspan ablator achieved

the highest burn rate of the three variations. Because ablator consists of dimethyl silicone thickened with Cabosil, it is believed to be a rather poor lubricant and this may have influenced the combustion rate. During the time of pressure loading and immediately after the break pressure, friction along the side of the chamber may result in sources of ignition of the sample, thus enhancing what is termed the apparent burn rate. In contrast, the organic-based lubricant used during Runs 30 and 31 created a relatively low burn rate while the sample tested without a deterrent was intermediate between the two. While the eventual burn rate during Run 28 (no deterrent) may have been equal to the level achieved during Run 27 when ablator was used, the pressure break was much less abrupt than that of Run 27. Because of that, the calculated burning rate was lower. Pressure was equilibrated along the length of the samples tested during Runs 28, 30 and 31. If gas pressure is felt along the length of the sample, axial loads which result from the axial pressure difference, are greatly reduced. Therefore, breakup resulting from an end-to-end pressure difference of 15 to 20 MPa may be delayed or eliminated. In addition, flame may spread over the outside surface so that a large surface area, burning in cigarette manner, may result. The nearly simultaneous pressure rise over the exterior surface creates an inward, radial pressure gradient that could cause the porous matrix to collapse. However, the slower pressure rise indicates that radial collapse has a much smaller effect on combustion than axial breakup. It is noted that this occurs during tests of unconfined samples in conventional closed bombs when the apparent burn rate is reduced.

Insertion of a rubber interface between the propellant and the stress rod may have had some influence on the combustion process during Run 29. While dynamic behavior was somewhat different, as cited in the next section, the estimated quasi-steady data were quite close to those from Run 27. Thus, differences in the boundary did not appear to have a significant effect on the quasi-steady representation of combustion. The quasi-steady peak pressure appeared to be higher than that of Run 27 but the uncertainty of estimated value in light of the dynamics involved does not make that difference significant at this time.

The combustion processes of Runs 25 and 26 were somewhat different, as mentioned previously. This conclusion is based on the different response characteristics exhibited by the pressure which seems to indicate that ignition may have occurred at the base end of the sample tested early during Run 26 while a more normal progression of combustion likely occurred during Run 25. This, however, is only conjecture at this time and additional analyses are required before a true conclusion can be made. During Run 26 the data window was shortened and it was not possible to estimate the quasi-steady pressure history. Thus, burn rates could not be estimated for that run in comparison to Run 25.

Based on the characteristics of the pressure curves, the combustion process of Runs 30 and 31 was reasonably repeatable. The pressure traces of Runs 30 and 31 were quite similar, although the dynamic character of Run 31 was more pronounced. The apparent burn rate data were within 10%.

The calculated burn rate of the low density 7B propellant is generally in excess of 100 meters per second, placing it in a relatively high rate combustion category in contrast to that of 97% TMD 7B propellant. This clearly demonstrates the importance of propellant compaction density on the combustion process. The apparent burn rate data from Run 25 is also presented in Table 8 where all other burn rate data obtained during this program for 5.08 cm long sample tested at a loading density of 0.15 g/cc are also presented.

An item of interest and also of great significance is the break pressure. In all cases except one, the break pressure, which is essentially the point on the pressure curve where the rate of pressure rise accelerates markedly, is between 15 and 20 MPa. From the data generated during this program, it appears that when the pressure pushing on low density 1086-7B propellant exceeds 15 to 20 MPa, the mode of combustion is likely to change from what we believe to be a slow cigarette-type burning, into the rapid convective mode. Once the change occurs, it accelerates rapidly to a level that is governed by the pressure level and the amount of material present. As discussed previously, the governing mechanism of the combustion acceleration may be stress and, as the combustion accelerates, thrust is added to the pressure which serves to enhance the stress so that runaway combustion mechanism, much the same as that due to end ignition in a bed of granular propellant, may exist.

It is also noted that tests where pressure at the interface between the sample and the stress rod rose suddenly at the break pressure were more likely to experience a high burn rate than those where the pressure at that location rose gradually along with the pressure at the ignition end of the sample. For example, during Run 25, p1 did not experience pressure until the break pressure had been

reached (Figure 16a). Its subsequent rise rate signified both the highest burn rate and also the highest rate of burn rate acceleration after the break pressure. In contrast, during Run 28, the test of a sample without flamespread deterrent, pressure p1 rose quite consistently with pressure p3 (Figure 19a) and, in that case, the acceleration to a higher burn rate was more gradual, even though, by the time the propellant was consumed, the end rate may have been similar. This difference in combustion is believed to be due to differences in propellant loading and subsequent breakup and convective phenomena.

C. Thrust and Dynamic Data

The dynamic data of Run 24 (Figure 15) consisted entirely of pulsating pressure waves in the gas space of the VHBR chamber. The combustion process was so slow that even though the stress rod data were not obtained it is certain that no thrust was generated.

During Runs 25 and 26 (Figures 16 and 17), the dynamic character of the run began at the instant the break pressure was reached. At that time combustion became extremely rapid and the dynamics dominated the character of the pressure data. Once the break pressure was reached, both the stress rod and pressure p1 accelerated rapidly and reached a high level before that of p3. This leads one to believe that combustion was initiated at some point within the sample, probably at a location close to the base where pressure p1 and the stress rod would be the first to sense such a pressure rise. The stress rod data greatly exceeded the level obtained by p3 and this, in essence, may be considered some form of thrust where thrust is the total momentum exchange of the gas and solid phases at the burning surface.

During Run 27, pressure p1 rose continually with p2 and p3 during the early time, but when a pressure of approximately 8 MPa was reached the rate of rise of p1 accelerated from that of p3 and reached a higher level sooner (Figure 18a). Once p3 began to accelerate it rose much more rapidly than p1 so that the high pressure level was reached at about the same time. The pressure curves intertwine and are so poorly defined that it is difficult to deter-

mine whether or not thrust was measured during this test. It does not appear to be a clearly defined property because it is lost in the dynamics at the end of the combustion process.

During Run 28, the test without flamespread deterrent, the pressures all appeared to rise unformly during the early time and also well into the rapid rise portion of the pressure history (Figure 19). Thus, the gas was able to flow past the sample so that pressure was sensed even at the base of the sample. During this test, the stress rod data were erratic and was comprised of steps and bumps (Figure 19a). This may be due to the fact that the outside of the propellant sample was not lubricated and that the stress rod did not feel the entire force that was exerted by the sample. In other words, friction along the bomb sidewalls might have absorbed some of the force that was normally sensed by the stress rod. In addition it was believed that cocking of the seal plug, located between the stress rod and the propellant sample, may have been a problem during this test and may have been the reason why the stress rod indicated a large negative spike just before it rose to a high level. At the time it reached the high level the value of the stress exceeded the pressures indicated by p2 and p3 and this may signify thrust. Otherwise the combustion dynamics are very strong during this period and appear to be dominated by a combination of waves within the sample and the chamber.

The effect of the rubber interface between the propellant sample and the stress rod during Run 29 was most prominent in the dynamic characteristics of pressure p1, and the subsequent effects of p1 on p2. The only difference between Runs 27 and 29 was the rubber interface used during Run 29. However, p1 responded more abruptly, and reached a higher level, during Run 29 than during Run 27. This change in the dynamics caused the level of p1 to exceed that of p3 by nearly 300 MPa for a brief period, which may be interpreted as thrust. However, the pressure p3 seems to behave differently in that the initial pressure pulse is less than that generated during other runs. Conceivably, this may be due to reduced spallation at the free surface resulting from a weaker wave reflection at the interface. Therefore, the rubber interface did appear to alter the dynamic behavior of the combustion process. The true significance of this is going to require more sophisticated analyses of the data to truly assess what the effect was.

The burn rates during Runs 30 and 31 were somewhat reduced from those of the previous samples and the dynamic character of the traces was correspondingly subdued (Figures 21 and 22). Pressures p1, p2 and p3 all rose and fell in unison with the exception that p1 either rose higher or fell lower than the others which is due to the proximity to the wall where wave reflections occur. The stress rod data appear to be substantially higher than p1 or p2 which is indicative of thrust. However, the value of the stress data toward the end of the data window is substantially higher than p2. Thus, it is not known whether or not the large value of thrust is a real value or a data shift or calibration error. It is noted that during the early-time rise the stress rod data is about 50% higher than that of p3 where one might expect the two to correspond quite closely. If this were the case the level of thrust would be much less than that indicated by the excess of the stress rod pressure over that of p2. On the basis of the burn rate, a reduced level of thrust would be anticipated.

VI. CONCLUSIONS

Much new information and insight into the combustion mechanisms of VHBR propellant were obtained during this program. To date, only approximate analyses have been performed. Conclusions presented in this report are based on those analyses and observations made as a result of examining the pressure and stress histories. Therefore, some of these conclusions must be considered tentative until more sophisticated data analysis techniques have been used. With this in mind, the following conclusions are stated:

1. Comparison of results from tests of 97% TMD 1086-7B samples tested previously [10] with the 88% TMD samples tested during the current program (Runs 25 and 26) indicated that the lower density material burns more than 10 times faster.

2. Tests of a single sample at two loading densities show that pressure has a large effect on combustion rate.

3. Tests of one and two samples at the same loading density show similar combustion characteristics but that the amount of material also has an influence on the eventual apparent burn rate magnitude.

4. Tests of samples with different coatings or no coatings indicate that this is an important parameter; a slippery coating tends to suppress the combustion rate.

5. The combustion of 88% TMD 1086-7B propellant appears to be characterized by slow, cigarette-type combustion until a "break" pressure in the vicinity of 15-20 MPa is reached, followed by an accelerating, high-rate mode of convective combustion.

6. Pressure at the propellant sample base and rod stress exceeded the pressure at the front end of the sample by more than 50%, during several tests. This indicates that thrust is generated by combustion of 88% TMD 1086-7B propellant.

7. Results from the test involving the rubber disc between the stress rod and the propellant indicate a relatively minor influence on the quasi-steady combustion characteristics. However, a large influence on the dynamic characteristics and thrust was observed as indicated by the pressure difference from one end of the propellant sample to the other. This finding indicates that the interface altered the dynamic combustion mechanism.

8. When pressure was felt by the transducer adjacent to the stress rod prior to the "break pressure," the combustion rate was normally reduced from the rate attained when pressure at that location was experienced at or following the break pressure. This may be part of the difference between confined and bare samples tested in conventional closed bombs.

9. Negative pulses from the stress rod appear to be caused by cocking of the seal plug. Lubrication of the seal plug with high-quality grease may prevent this phenomenon from occurring in the future.

VII. REFERENCES

1. Juhasz, A.A., and May, I.W., "Advanced Propellants for Hypervelocity Gun Applications," Sixth International Symposium on Ballistics, Battelle, Columbus Laboratories, 505 King Avenue, Columbus, Ohio, October 1981.

2. May, I., Lynn, F., Gough, P., Juhasz, A., and Fisher, E., "Thrust Characterization of Very High Burning Rate Propellants," 18th JANNAF Combustion Meeting, CPIA Publication 347, October 1981.

3. Juhasz, A., May, I., Aungst, W., and Lynn, F., "Combustion Studies of Very High Burning Rate (VHBR) Propellants," Ballistic Research Laboratory Memorandum Report ARBRL-MR-03152, February 1982. (AD A113 029)

4. Freedman, E., "The Thermodynamics of VHBR Propellants," 18th JANNAF Combustion Meeting, CPIA Publication 347, October 1981.

5. Fifer, R., "Workshop Report: Combustion of Very High Burning Rate (VHBR) Propellants," 18th JANNAF Combustion Meeting, CPIA Publication 347, October 1981.

6. Gough, P., "A Model of the Traveling Charge," USA ARRADCOM, Ballistic Research Laboratory Contract Report, ARBRL-CR-00432, July 1980. (AD B053 309L)

7. Baer, P., "Simulation of Closed Chamber Burning of Very-High Burning Rate Propellant," 18th JANNAF Combustion Meeting, CPIA Publication 347, October 1981.

8. Kooker, D., and Anderson, R., "A Mechanism for the Burning Rate of High Density, Porous, Energetic Materials," 18th JANNAF Combustion Meeting, CPIA Publication 347, October 1981.

9. Fisher, E., "Closed Bomb Tests of Hivelite-Based VHBR Propellants," Ballistic Research Laboratory Contract Report ARBRL-CR-00449, March 1981. (AD B057 344L)

10. Fisher, E., "One-Dimensional Closed-Bomb Tests of Very High Burn Rate (VHBR) Propellants," BRL Contract No. DAAK11-80-C-0062, Calspan Report No. 6744-D-1, June 1982.

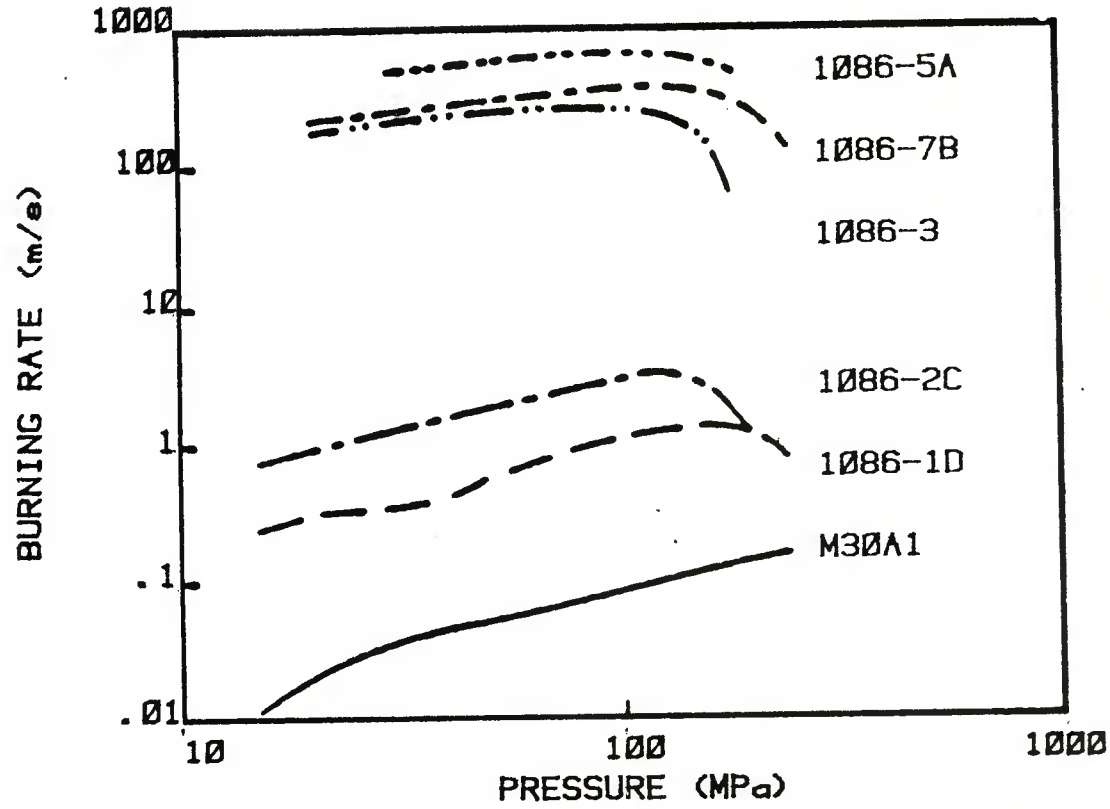

Fig. 1. Apparent Closed Chamber Burning Rates for Confined VHBR Propellants and M30A1

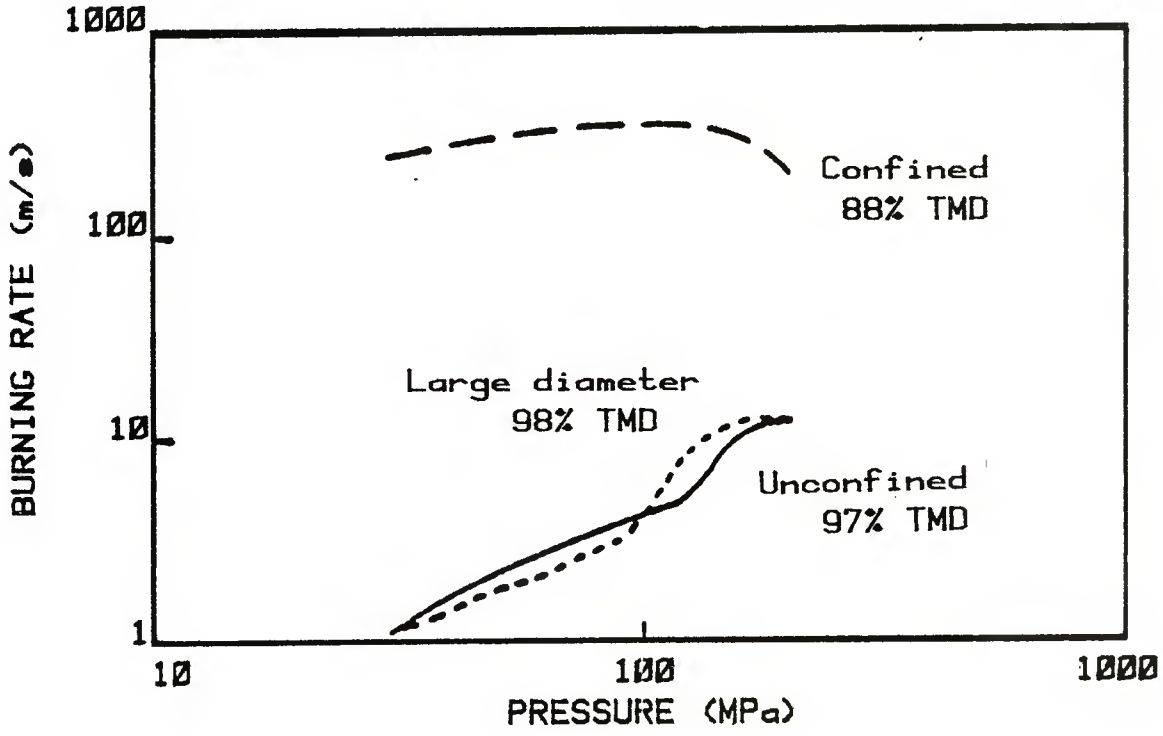

Figure 2. Apparent Burning Rates of VHBR 1086-7B

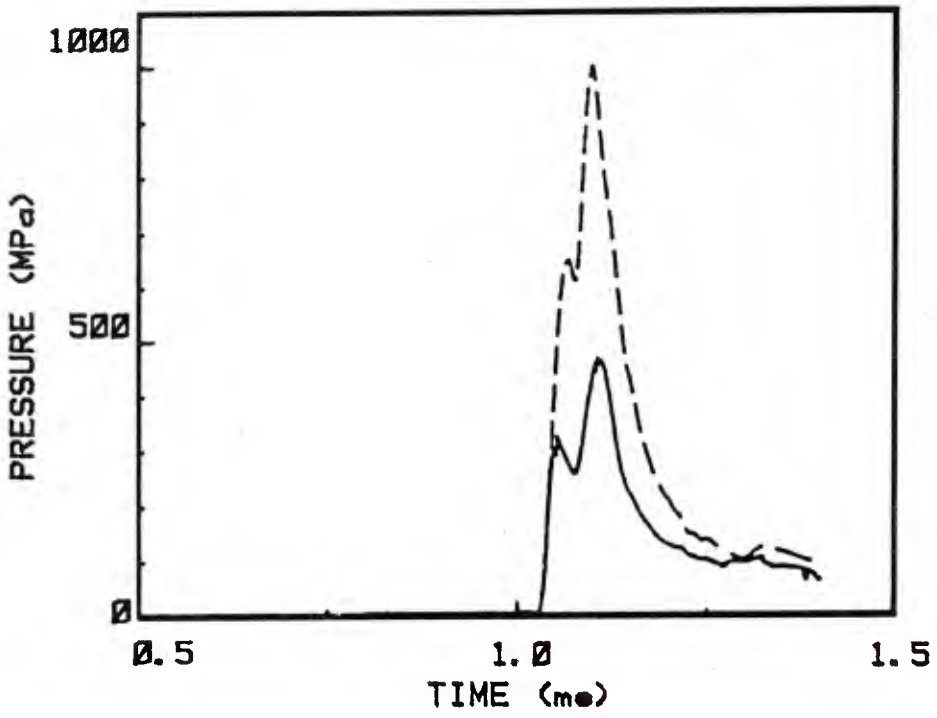

Figure 3. Interface Pressure (-) and Stress (---) for 1086-5A

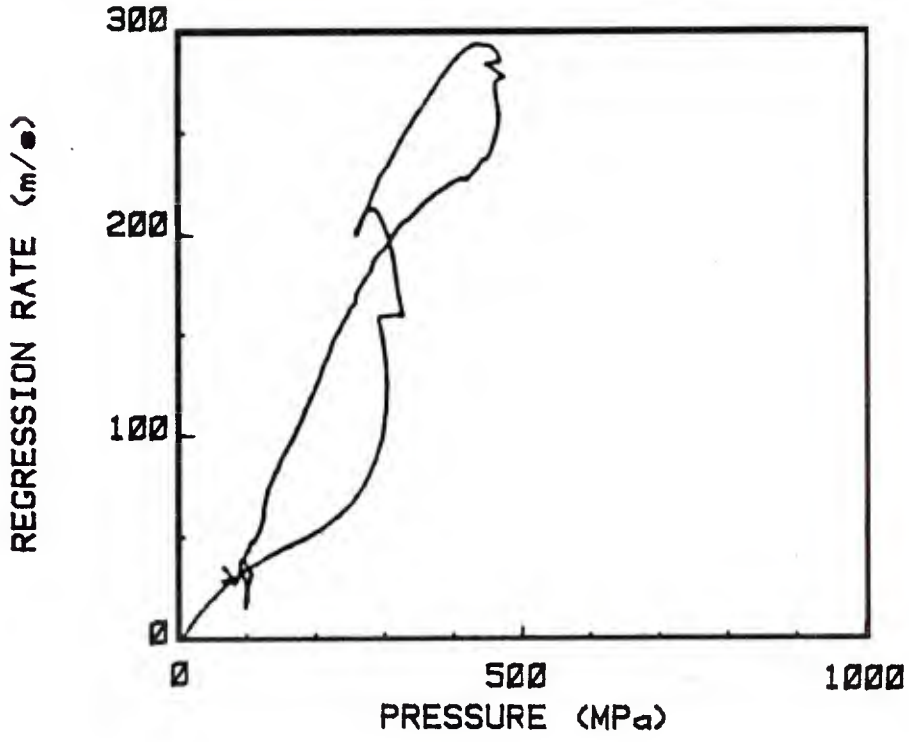

Figure 4. Regression Rate Versus Pressure for 1086-5A

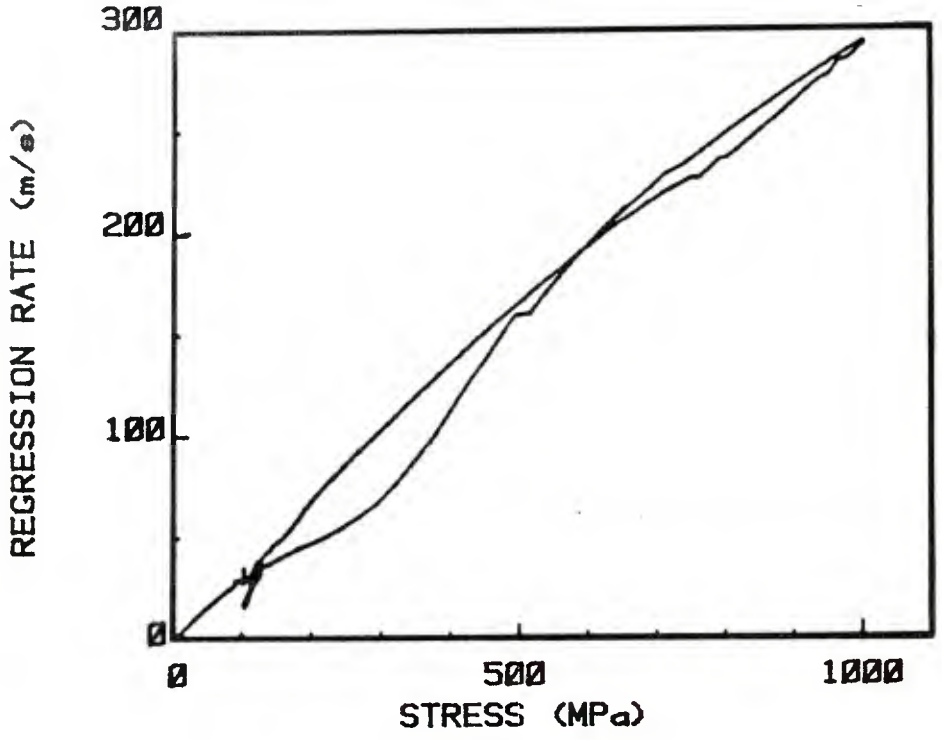

Figure 5. Regression Rate Versus Interface Stress for 1086-5A

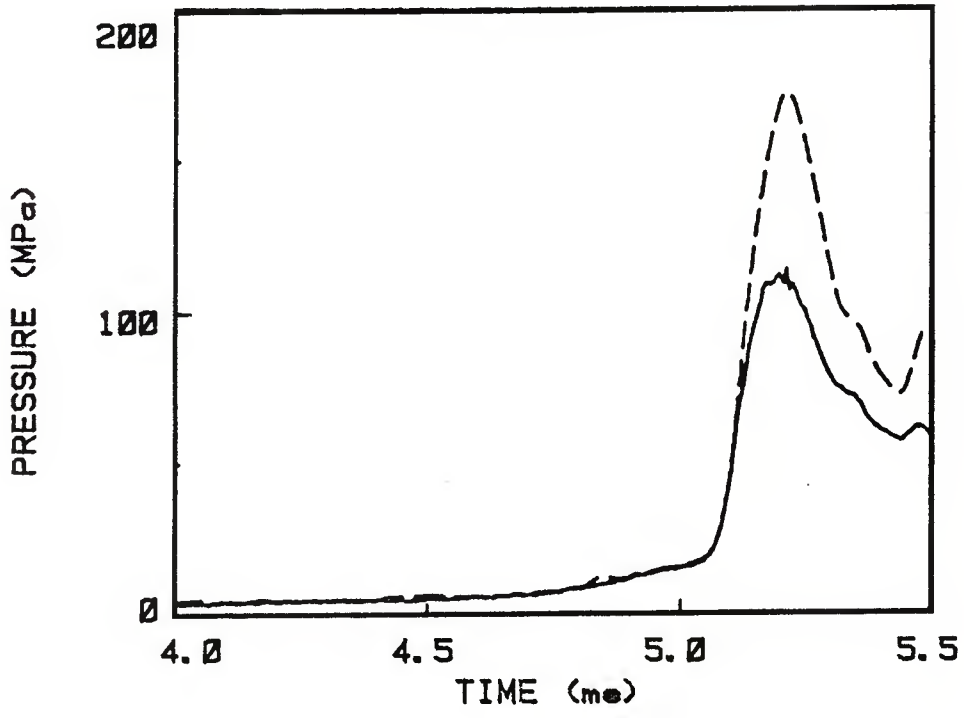

Figure 6. Interface Pressure (-) and Stress (---) for 1086-3

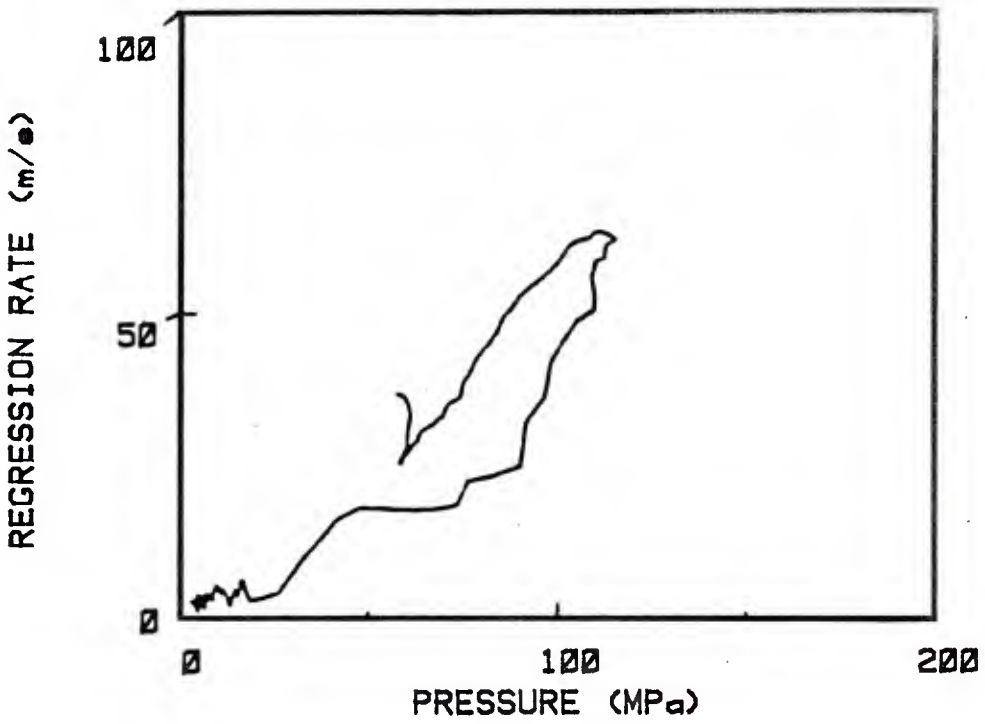

Figure 7. Regression Rate Versus Interface Pressure for 1086-3

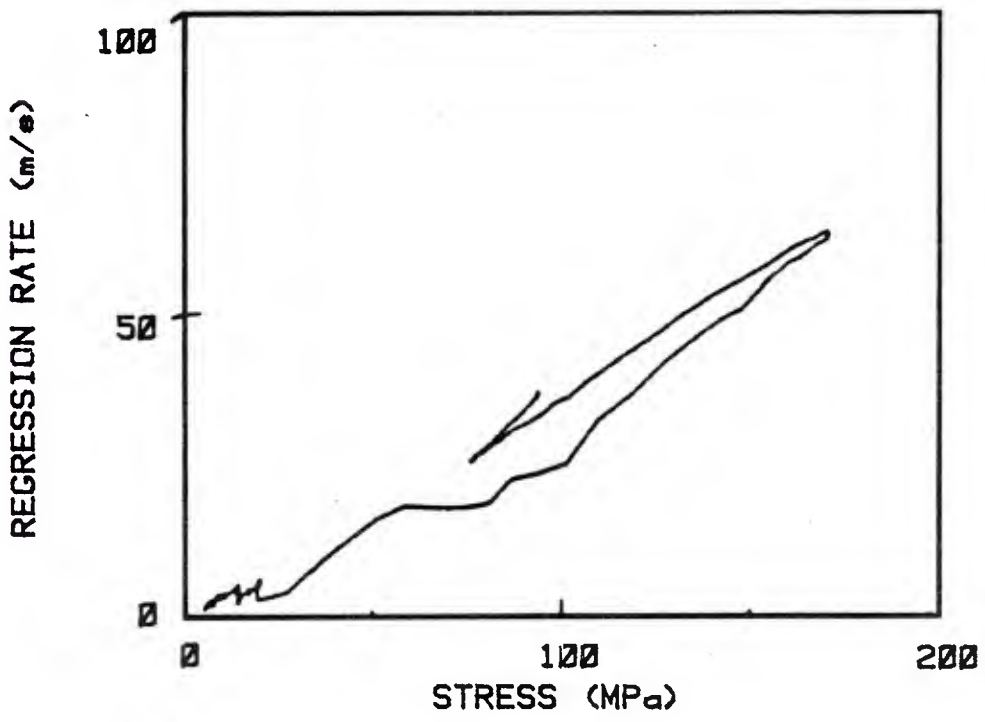

Figure 8. Regression Rate Versus Interface Stress for 1086-3

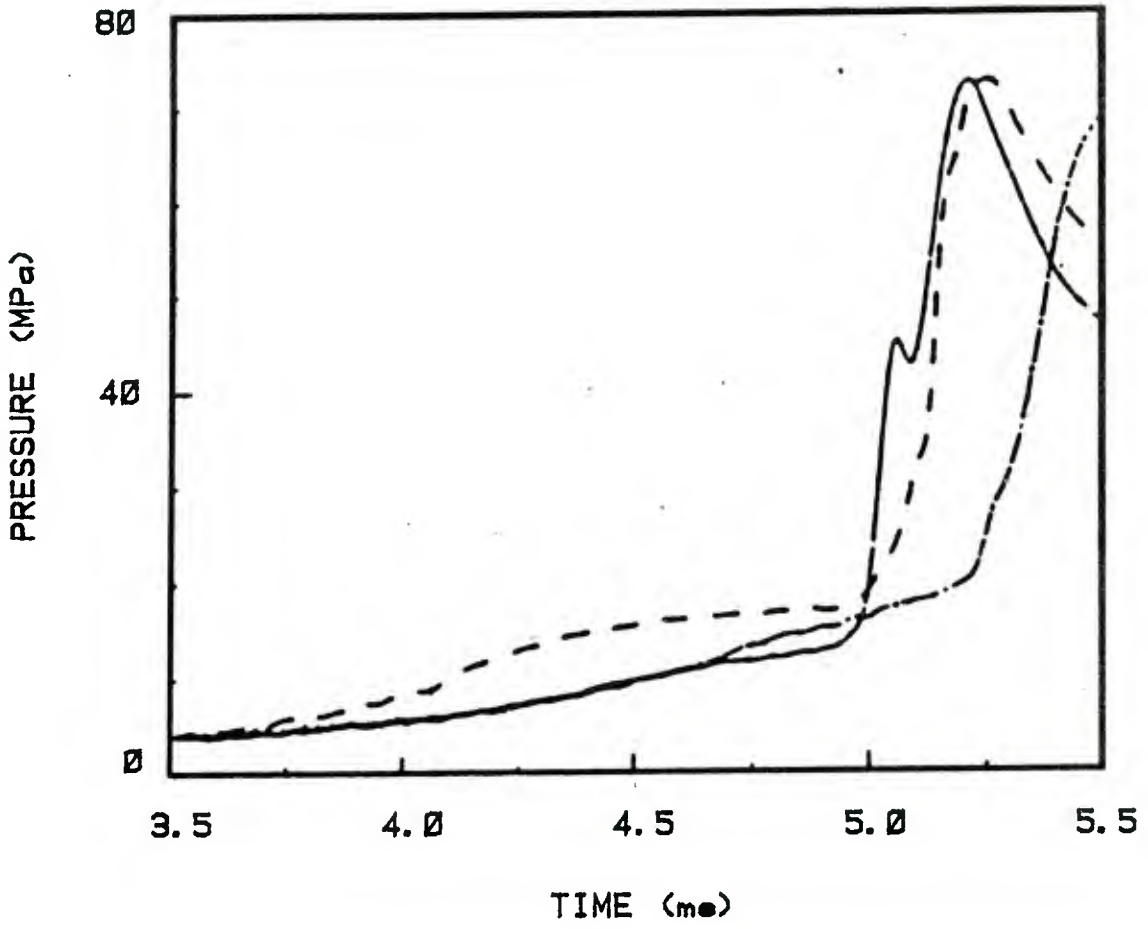

Figure 9. Sequence of Events for 1086-6B. P1 (——), P2 (----), P4 (-·-·)

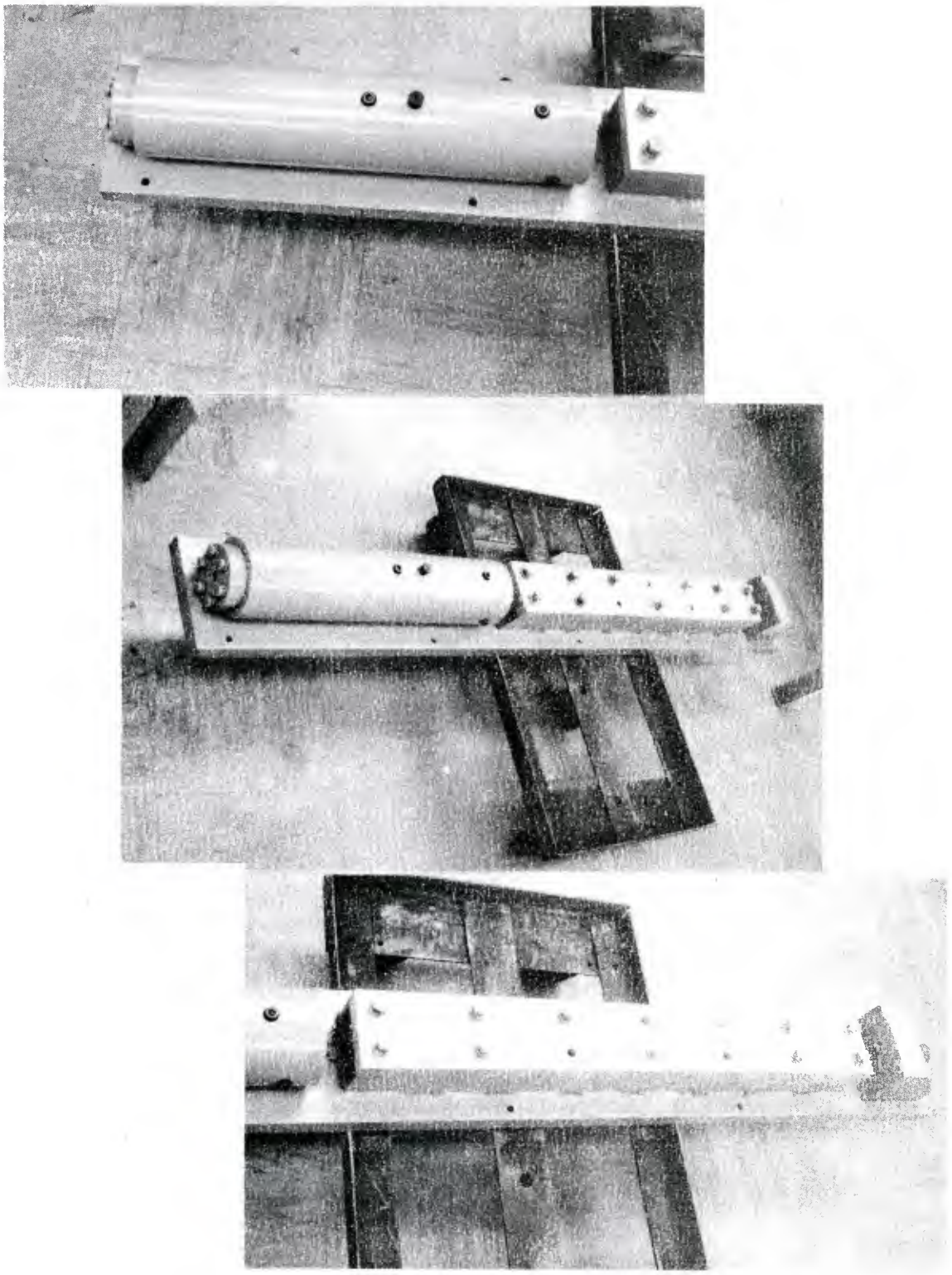

Figure 10. Photo of VHBR Bomb

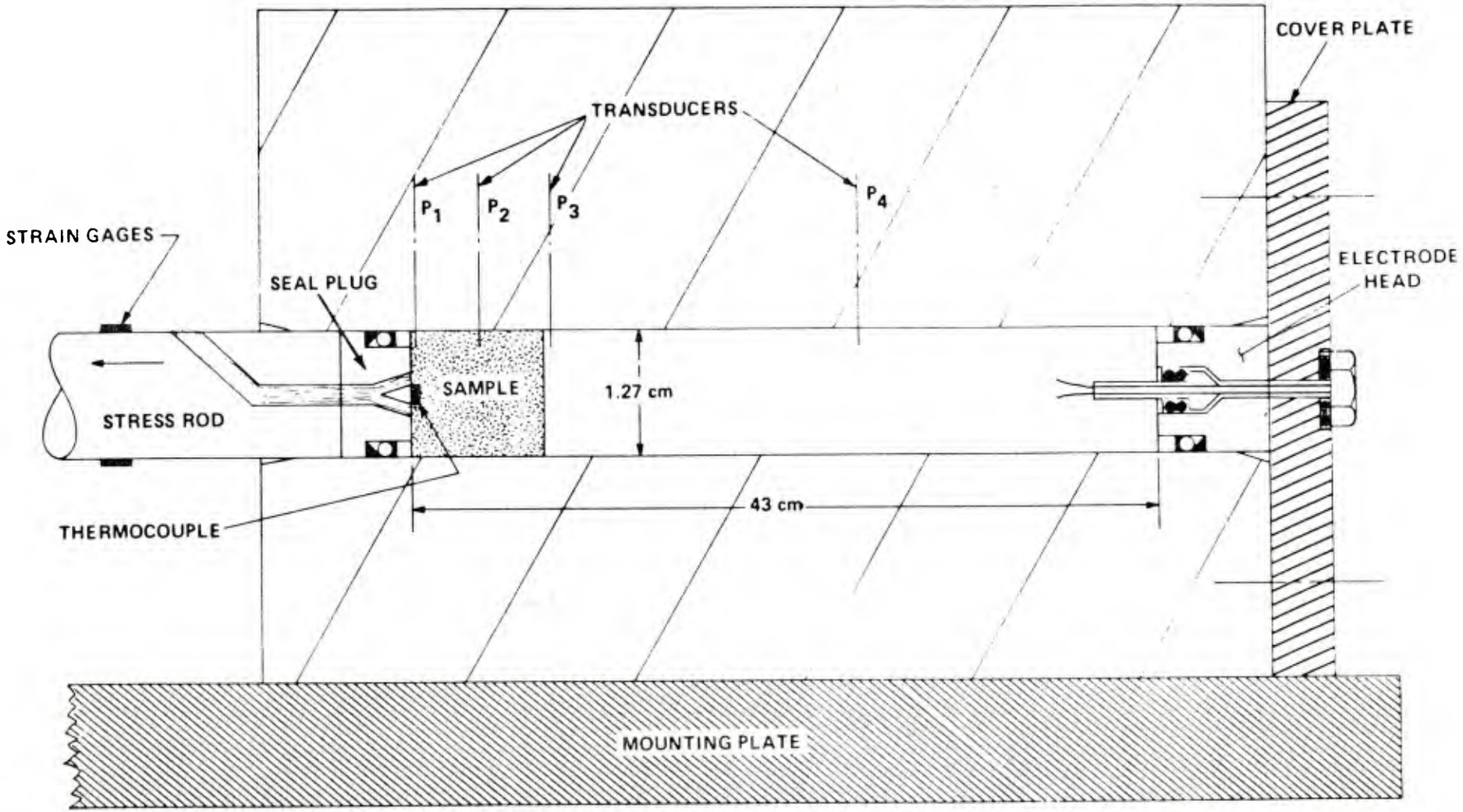

Figure 11. VHBR Combustion Chamber Schematic

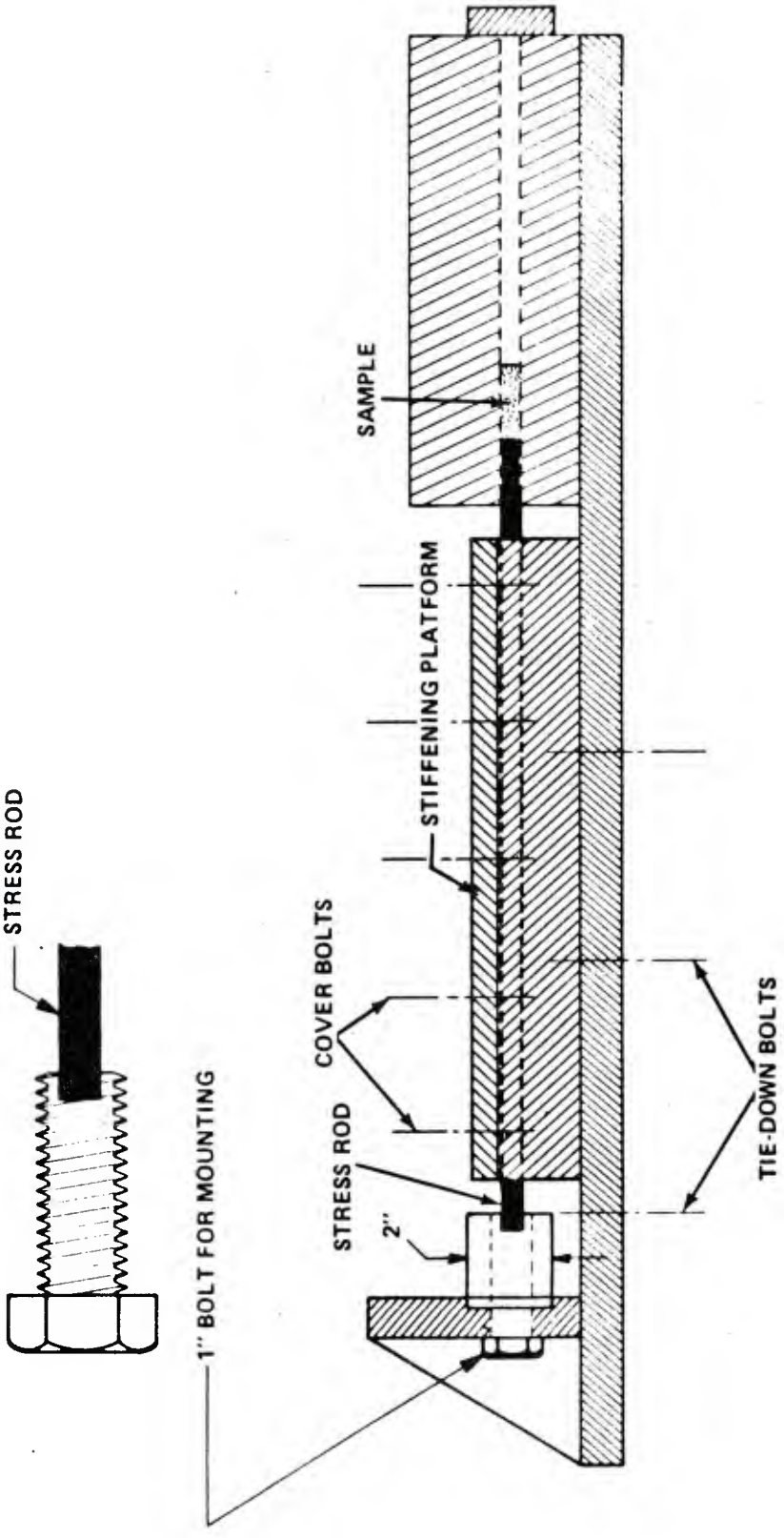

Figure 12. VHBR Test Fixture Schematic Showing Stress Rod Mount

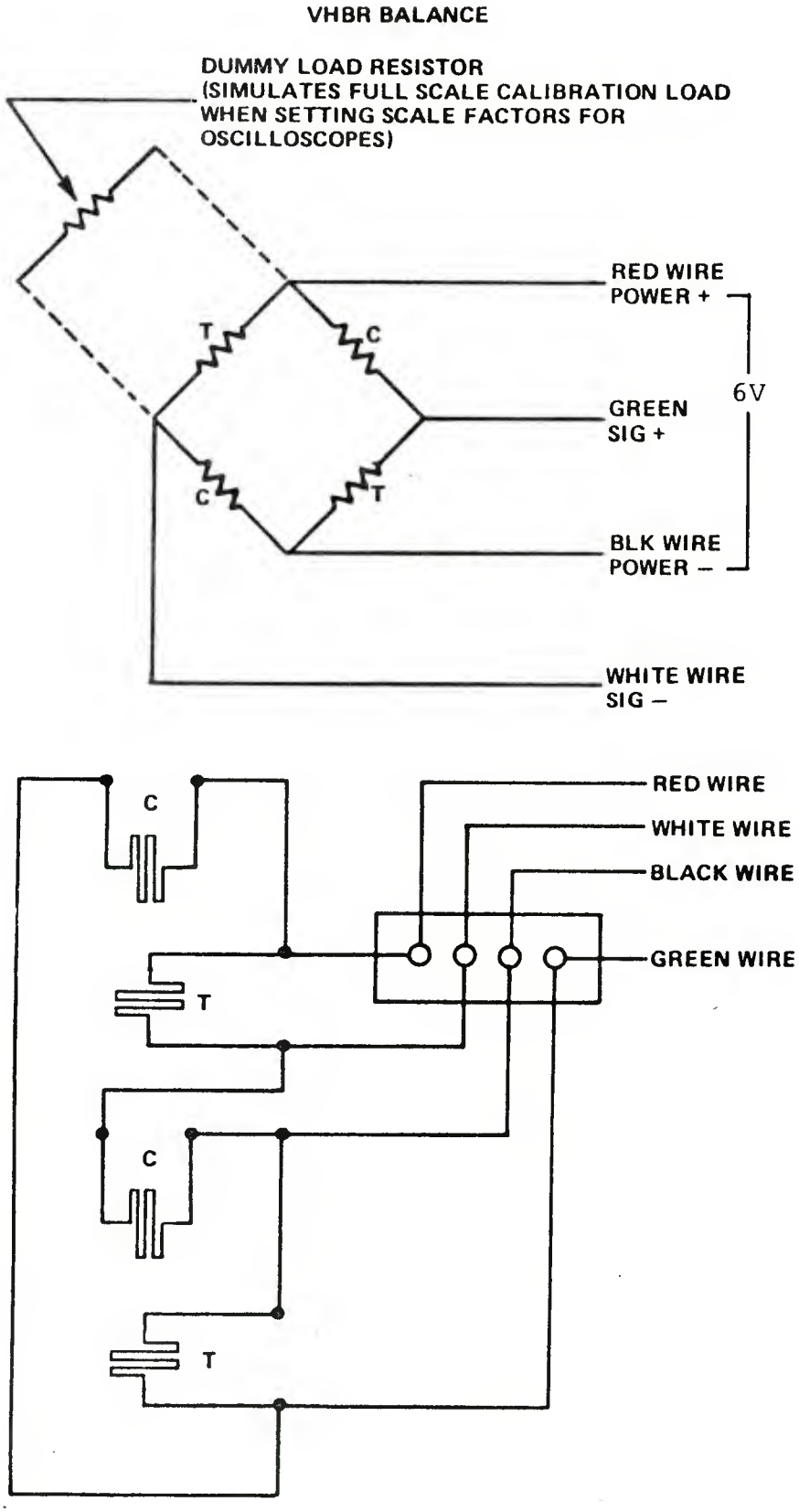

Figure 13. Strain Gage Diagram for Stress Rod

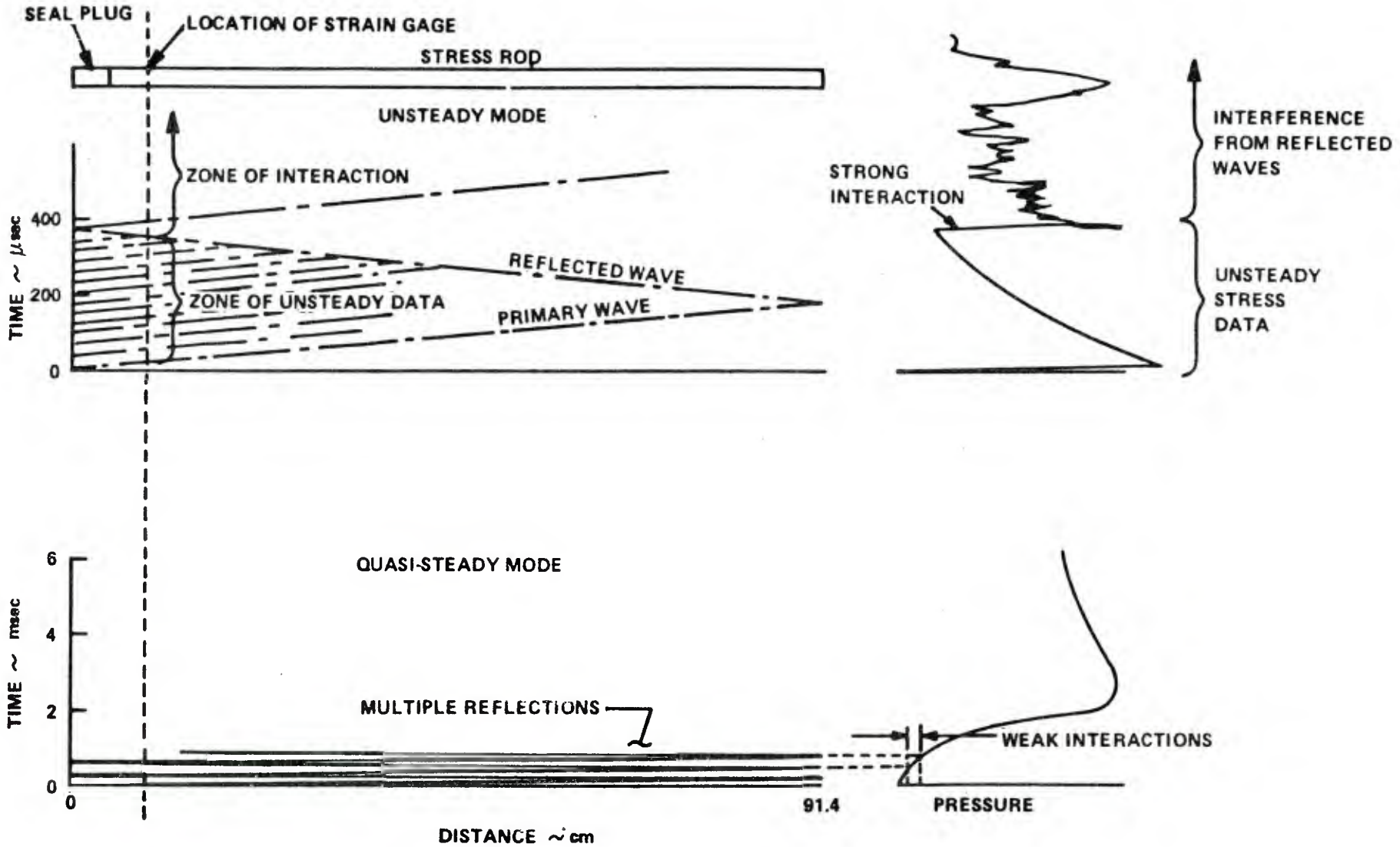

Figure 14. Illustration of the Unsteady and Quasi-Steady Modes of Stress Rod Operations

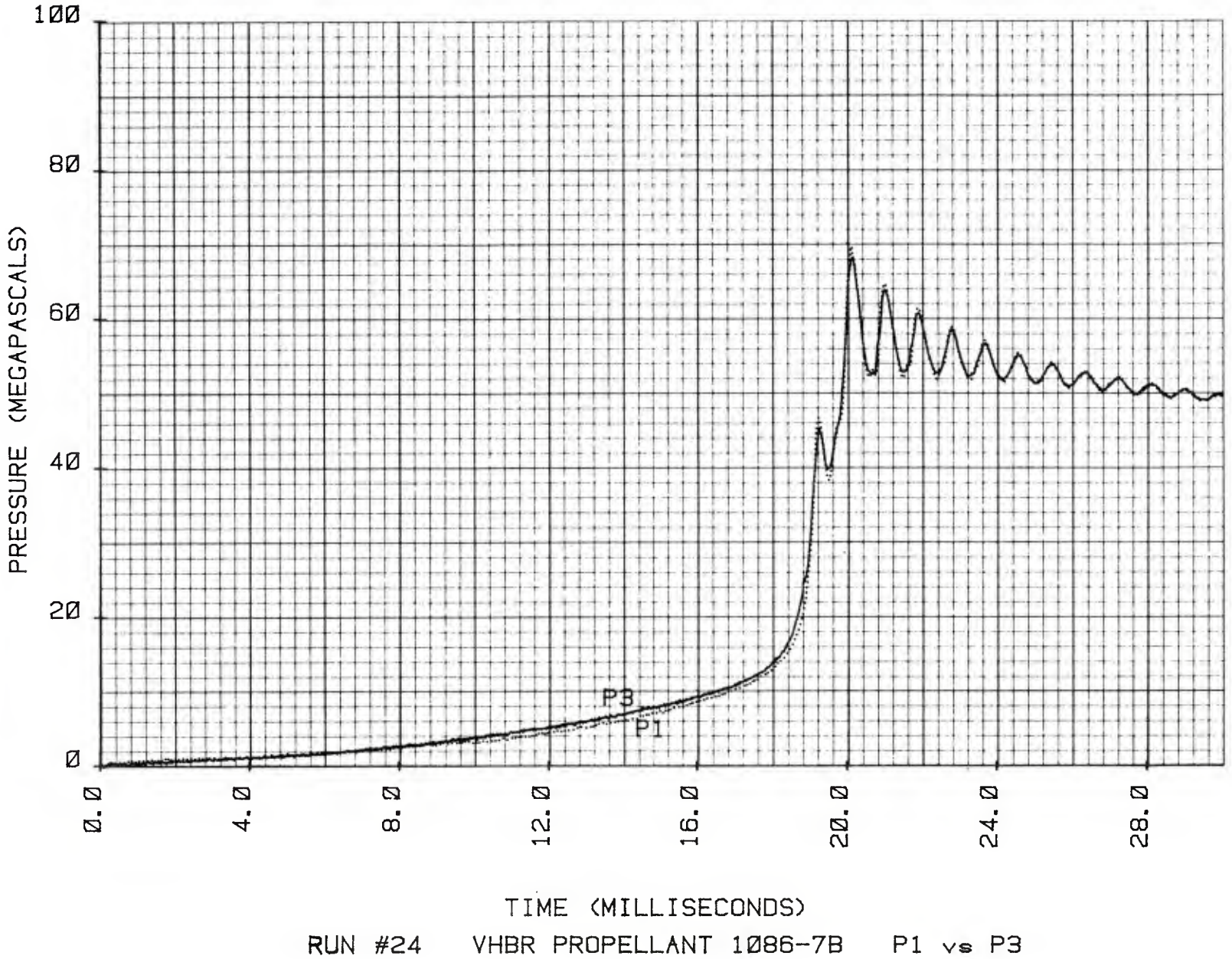

Figure 15a. Pressure History for a Single Propellant Sample Coated with Silicone Ablator and Tested at a Loading Density of 0.075 g/cc

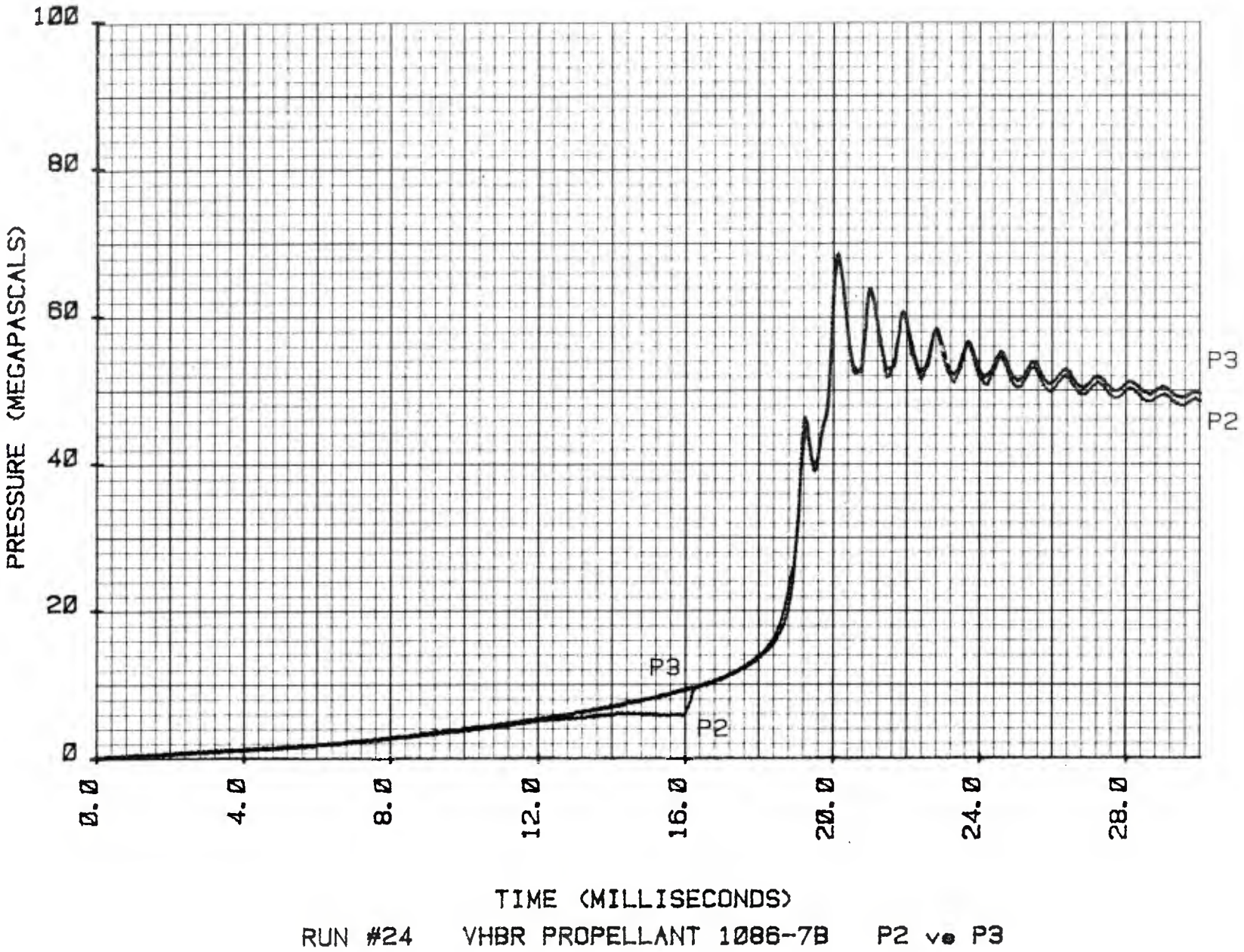

Figure 15b. Pressure History for a Single Propellant Sample Coated with Silicone Ablator and Tested at a Loading Density of 0.075 g/cc

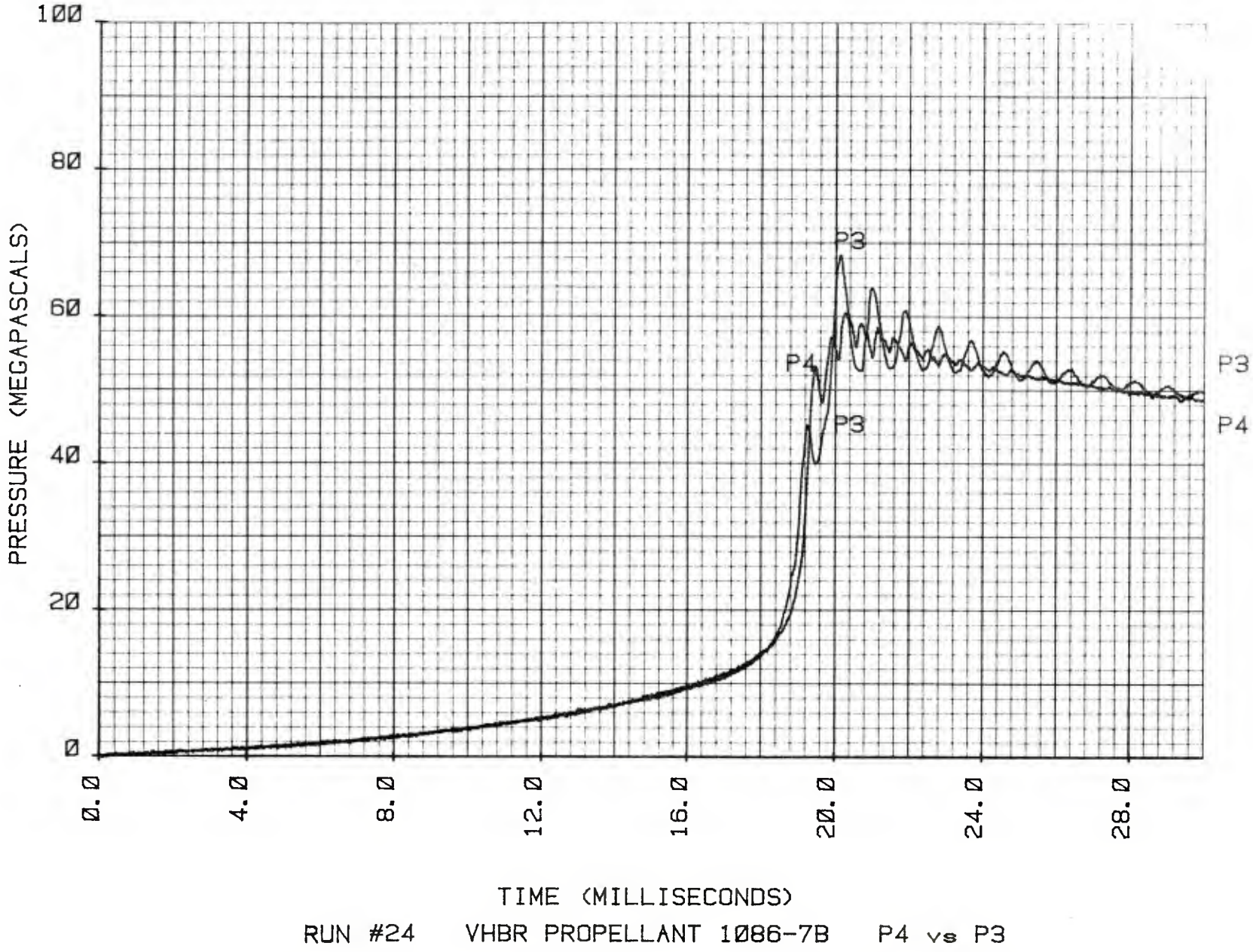

Figure 15c. Pressure History for a Single Propellant Sample Coated with Silicone Ablator and Tested at a Loading Density of 0.075 g/cc

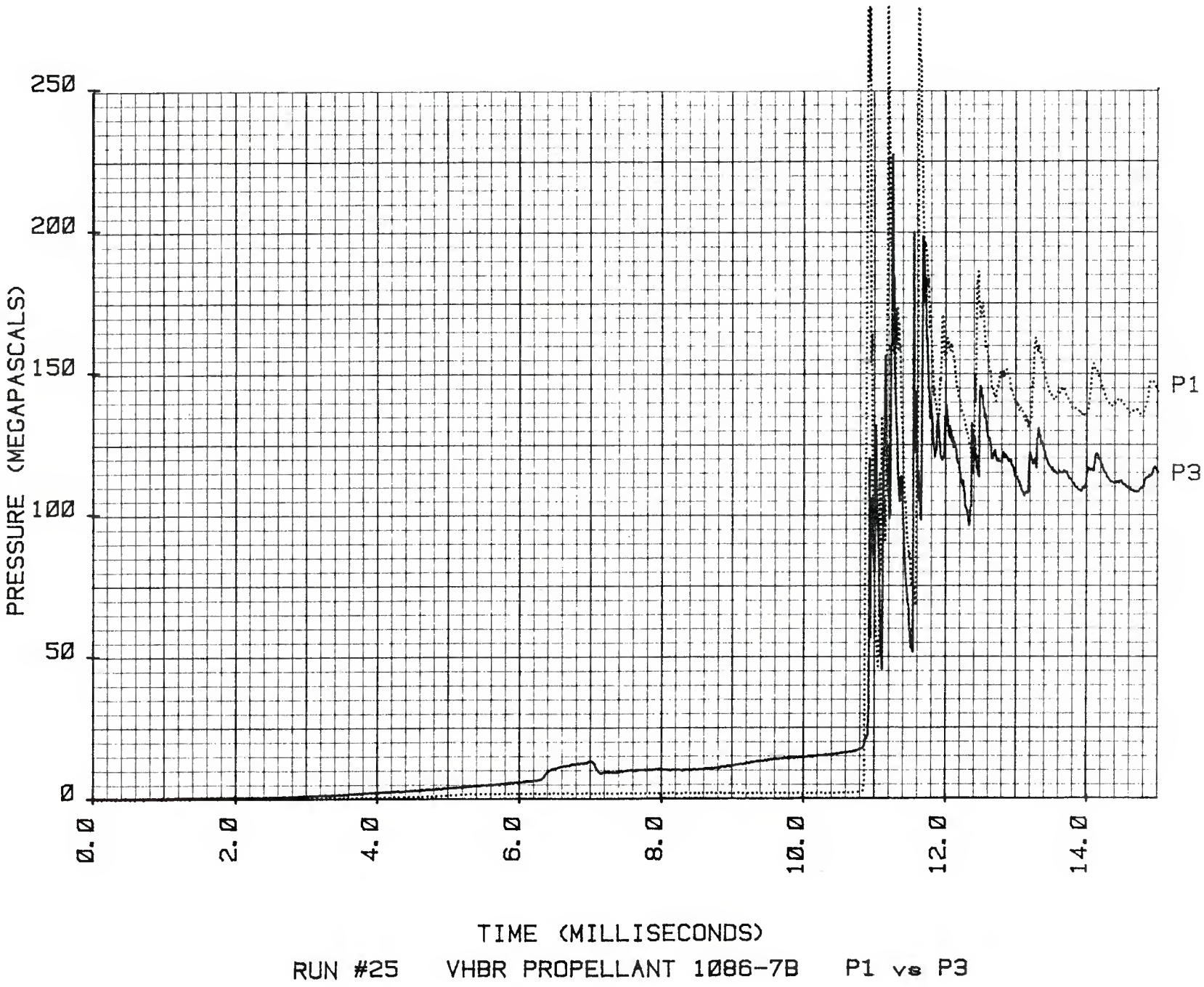

Figure 16a. Pressure History for Two Propellant Samples Coated with Silicone Ablator and Tested at a Loading Density of 0.15 g/cc

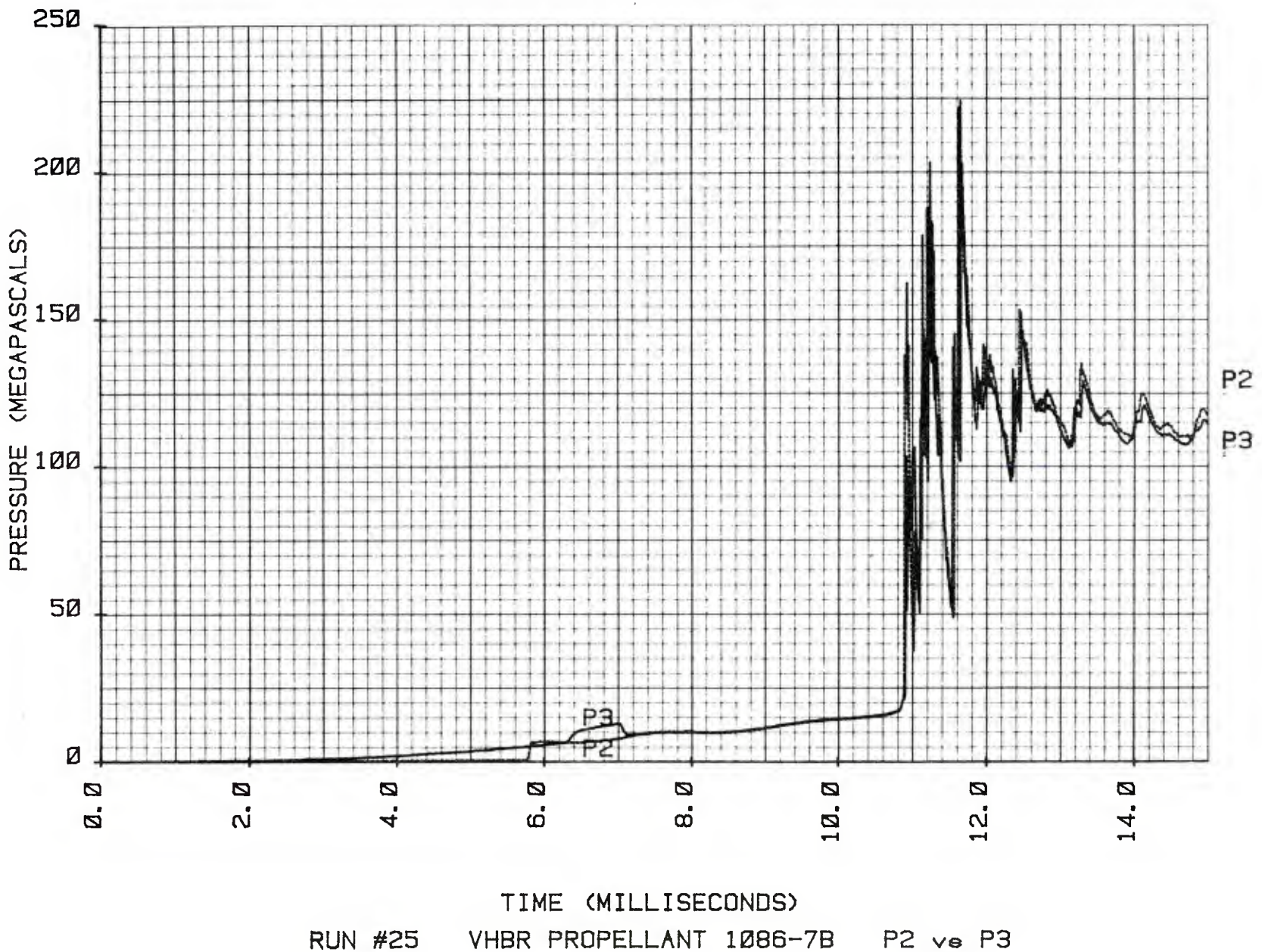

Figure 16b. Pressure History for Two Propellant Samples Coated with Silicone Ablator and Tested at a Loading Density of 0.15 g/cc

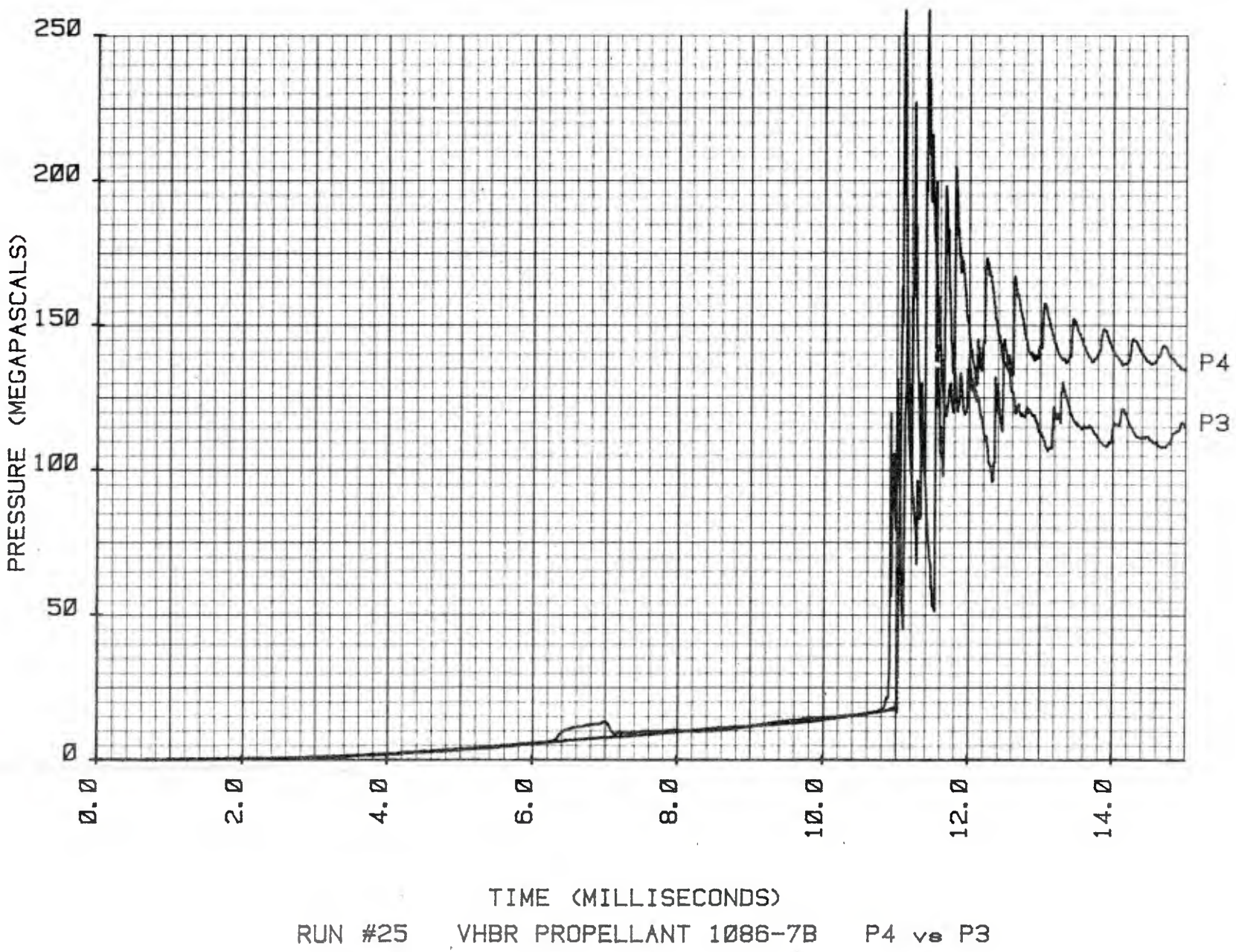

Figure 16c. Pressure History for Two Propellant Samples Coated with Silicone Ablator and Tested at a Loading Density of 0.15 g/cc

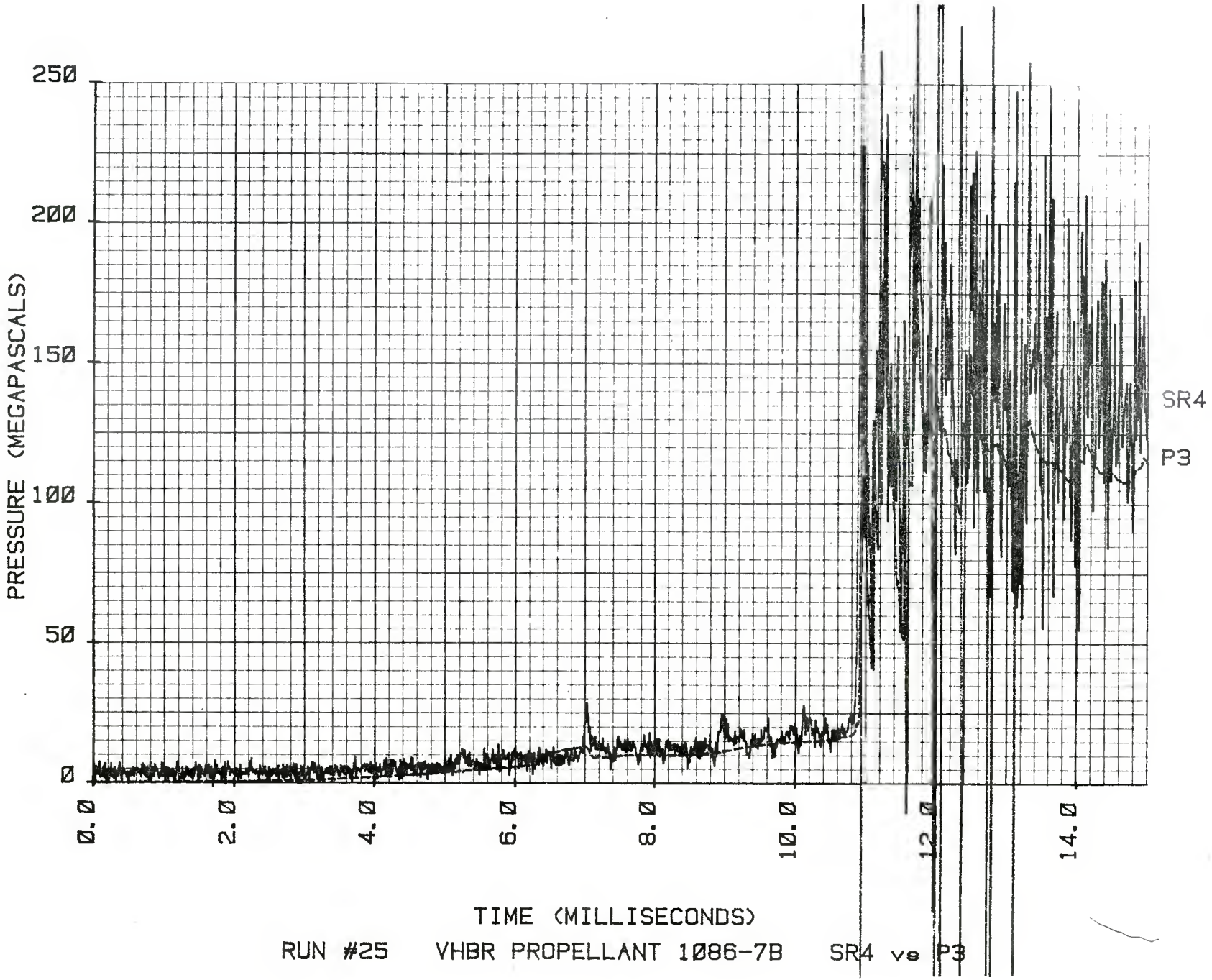

Figure 16d. Pressure History for Two Propellant Samples Coated with Silicone Ablator and Tested at a Loading Density of 0.15 g/cc

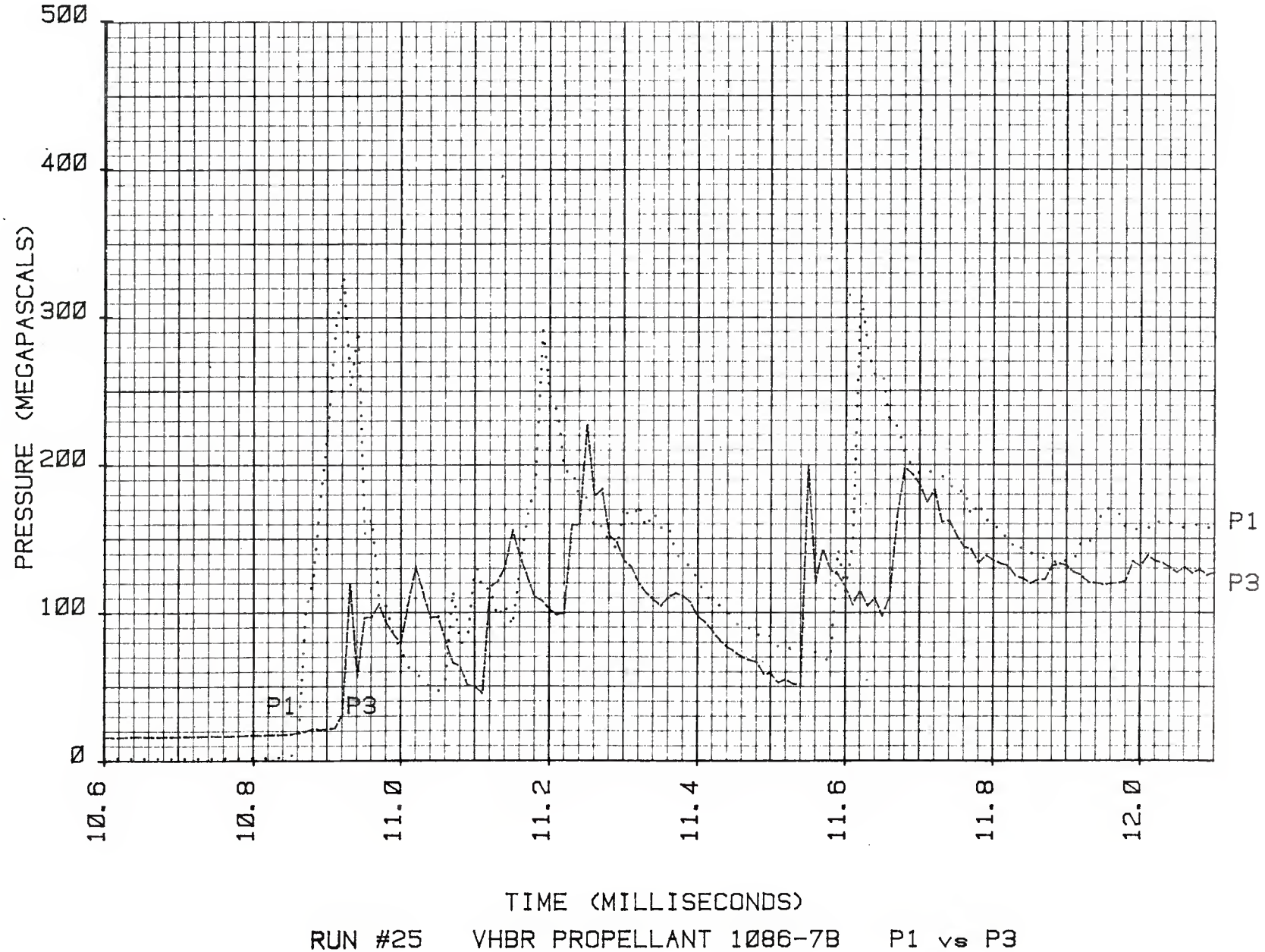

Figure 16e. Pressure History for Two Propellant Samples Coated with Silicone Ablator and Tested at a Loading Density of 0.15 g/cc

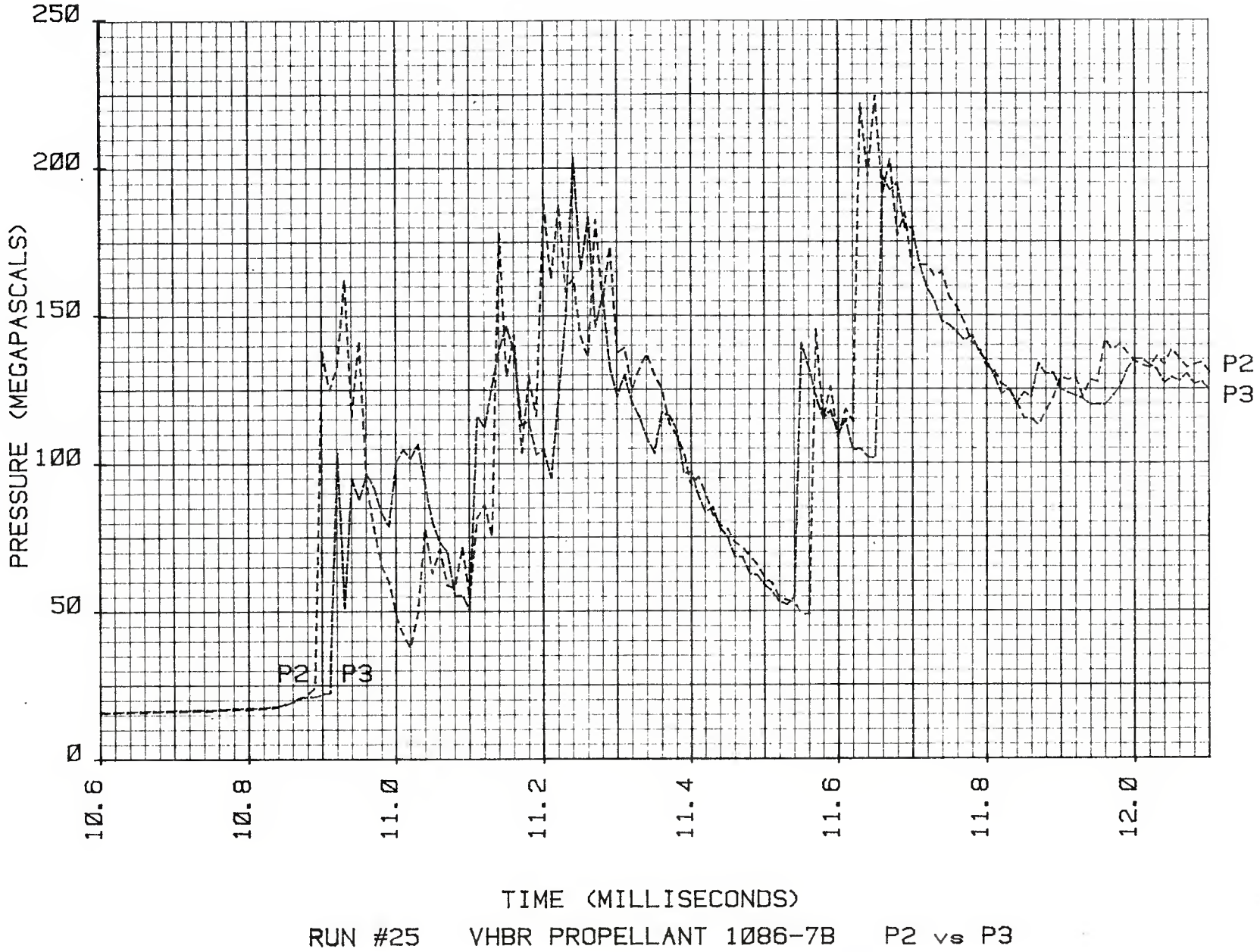

Figure 16f. Pressure History for Two Propellant Samples Coated with Silicone Ablator and Tested at a Loading Density of 0.15 g/cc

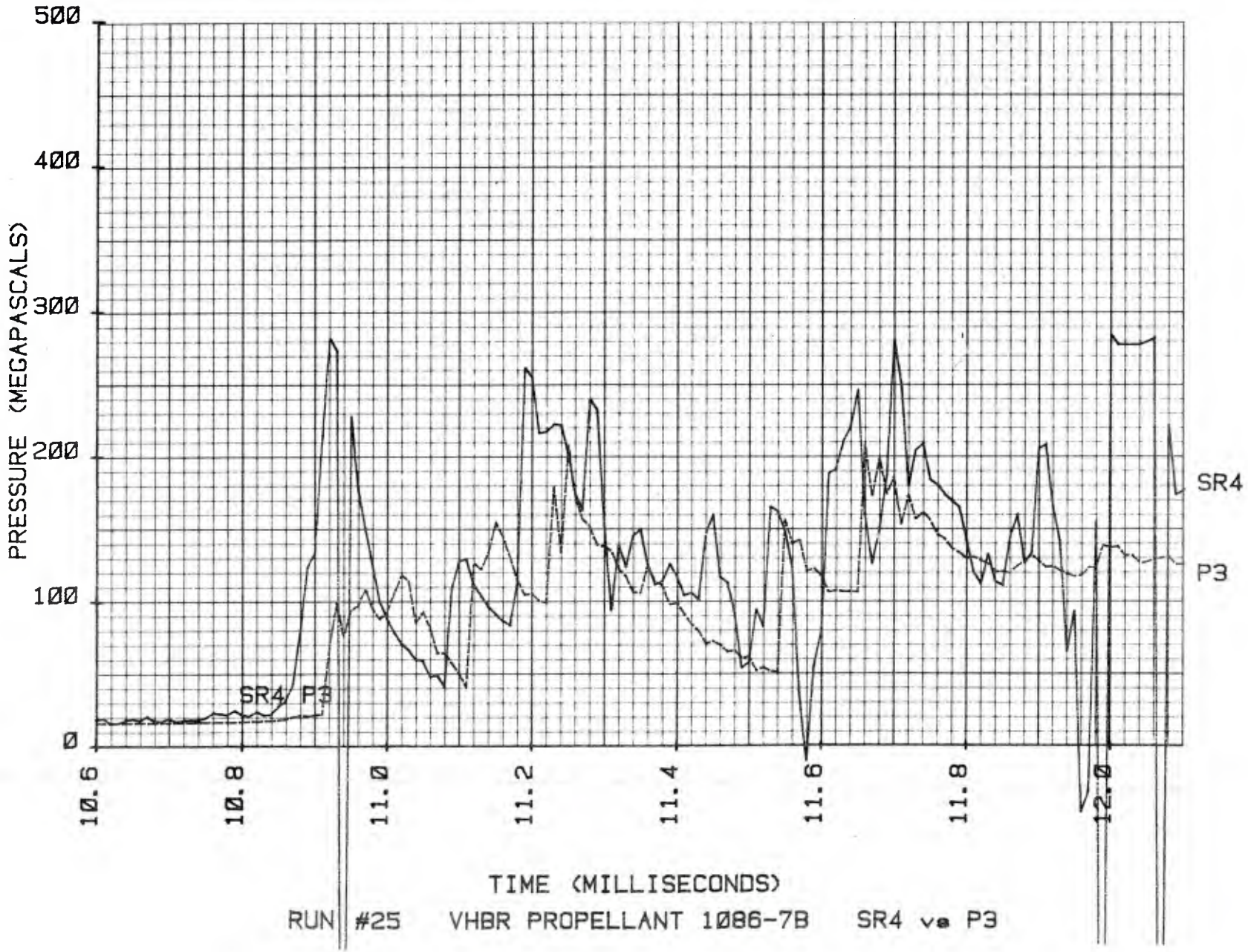

Figure 16g. Pressure History for Two Propellant Samples Coated with Silicone Ablator and Tested at a Loading Density of 0.15 g/cc

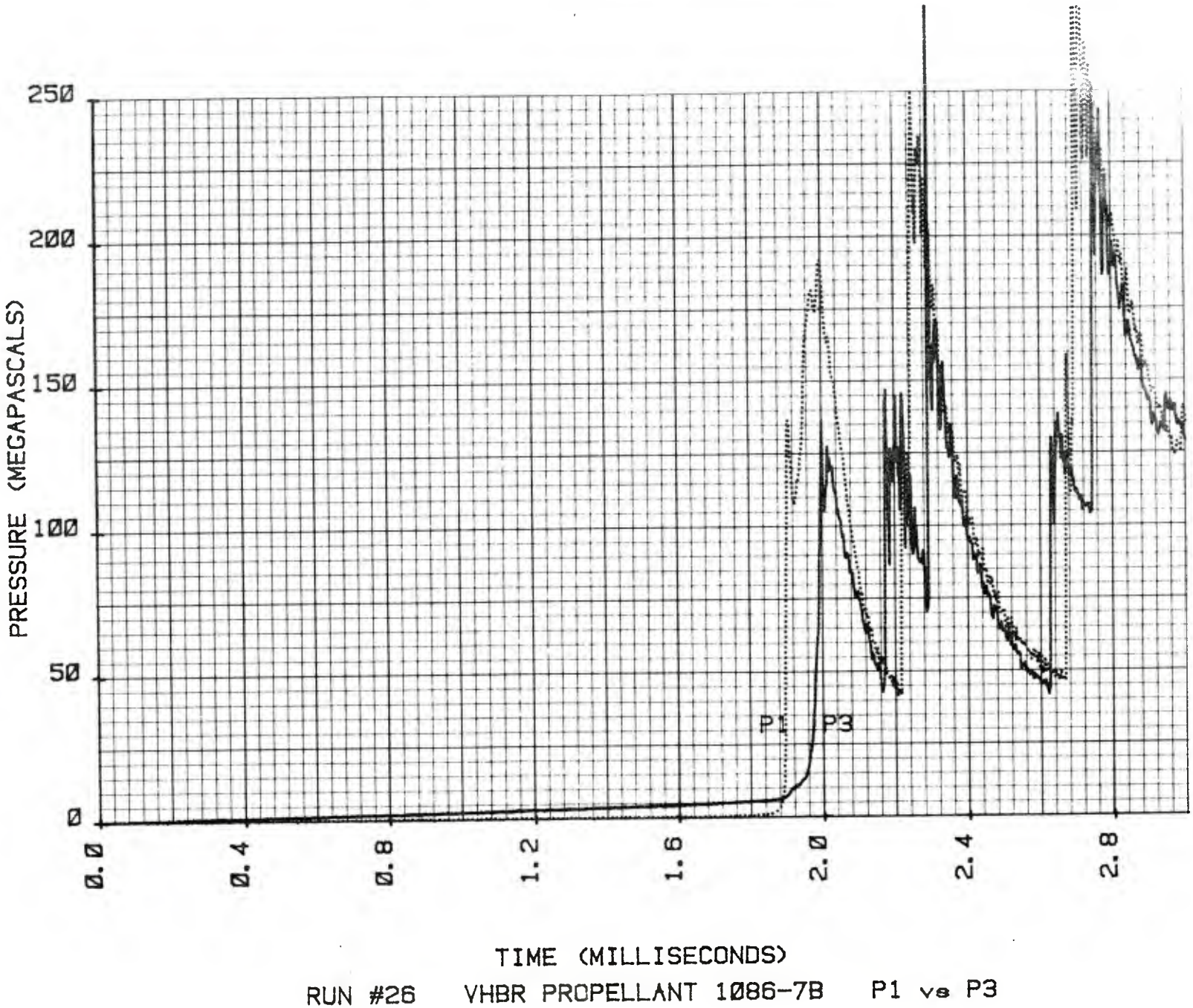

Figure 17a. Pressure History for Two Propellant Samples Coated with Silicone Ablator and Tested at a Loading Density of 0.15 g/cc

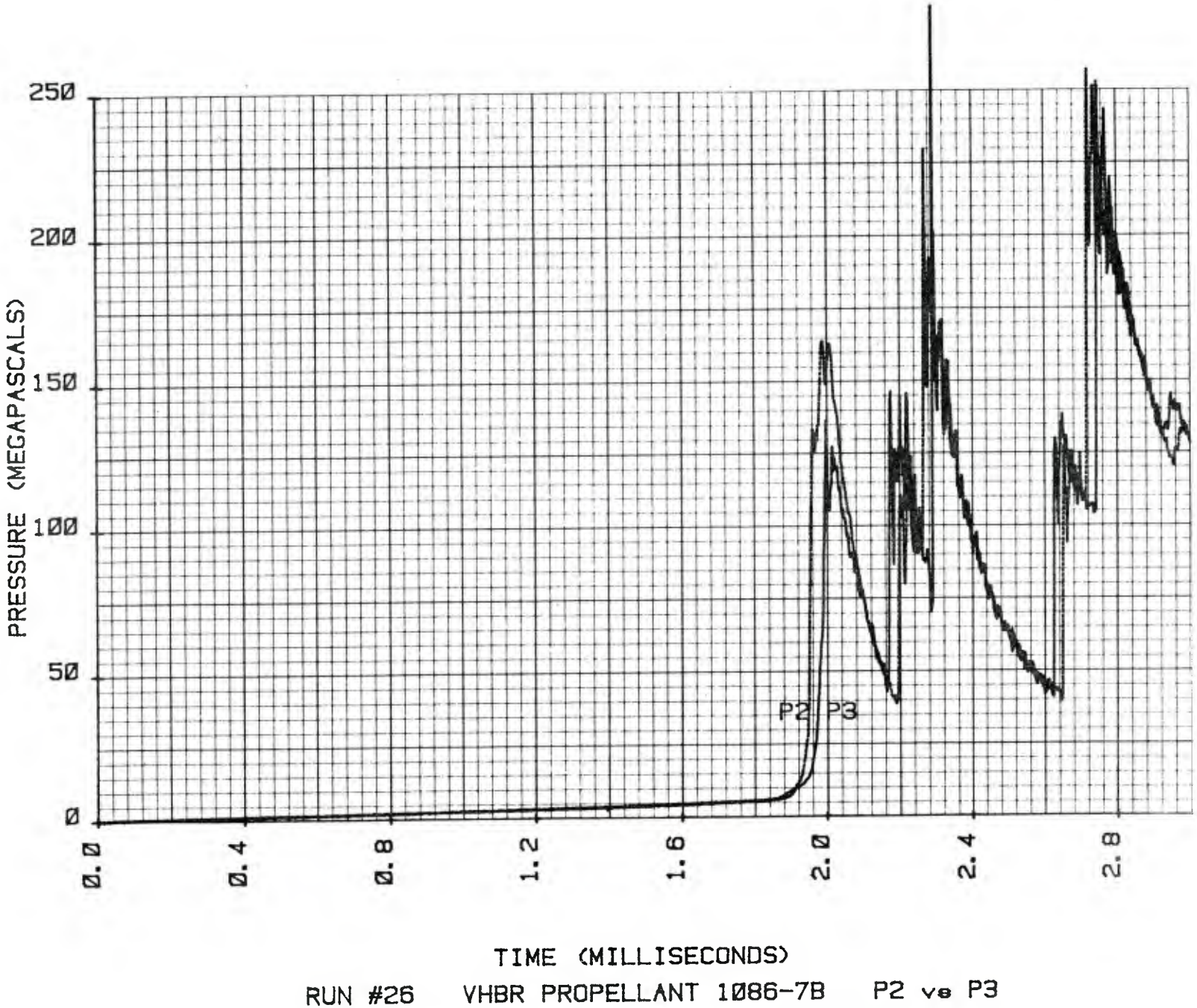

Figure 17b. Pressure History for Two Propellant Samples Coated with Silicone Ablator and Tested at a Loading Density of 0.15 g/cc

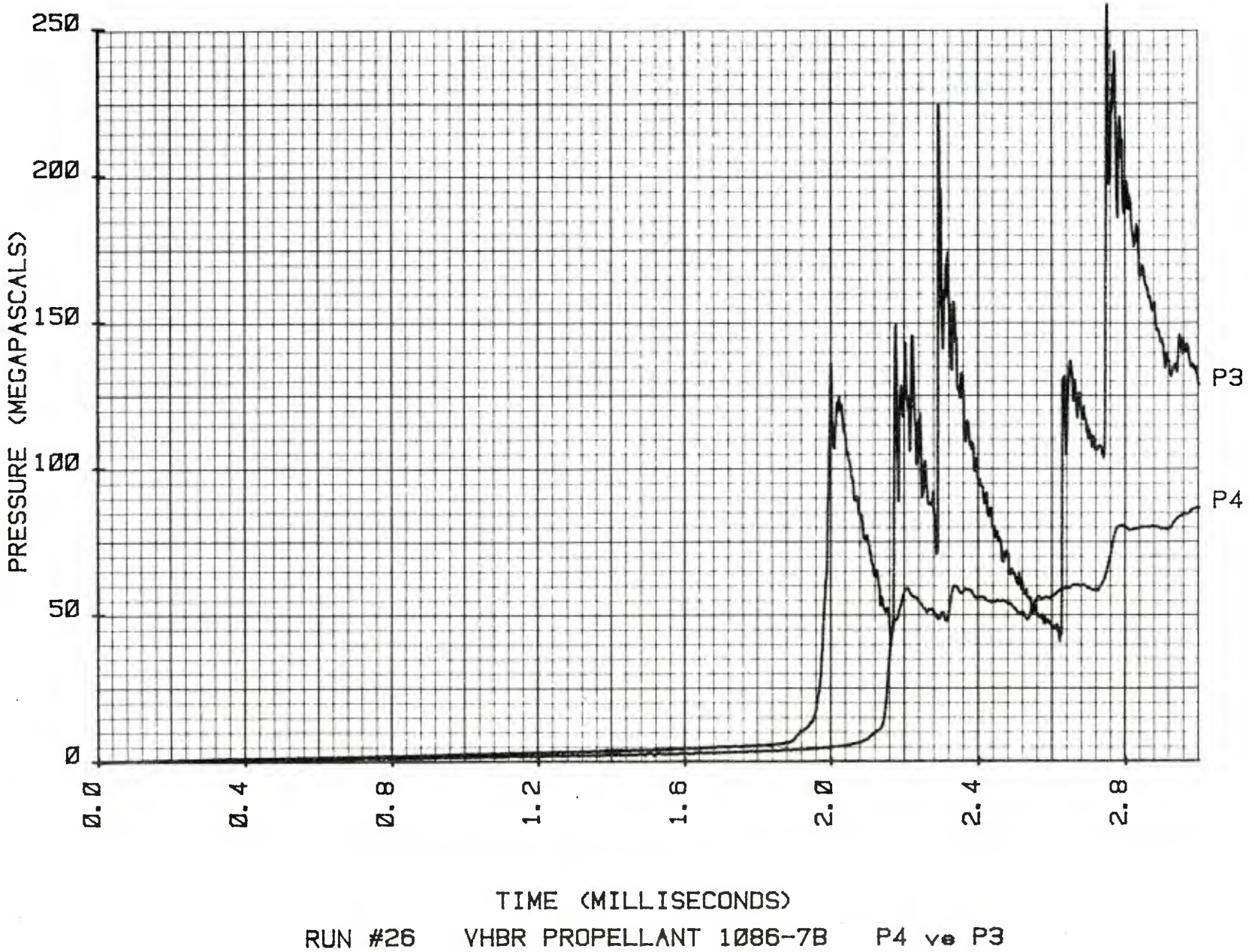

Figure 17c. Pressure History for Two Propellant Samples Coated with Silicone Ablator and Tested at a Loading Density of 0.15 g/cc

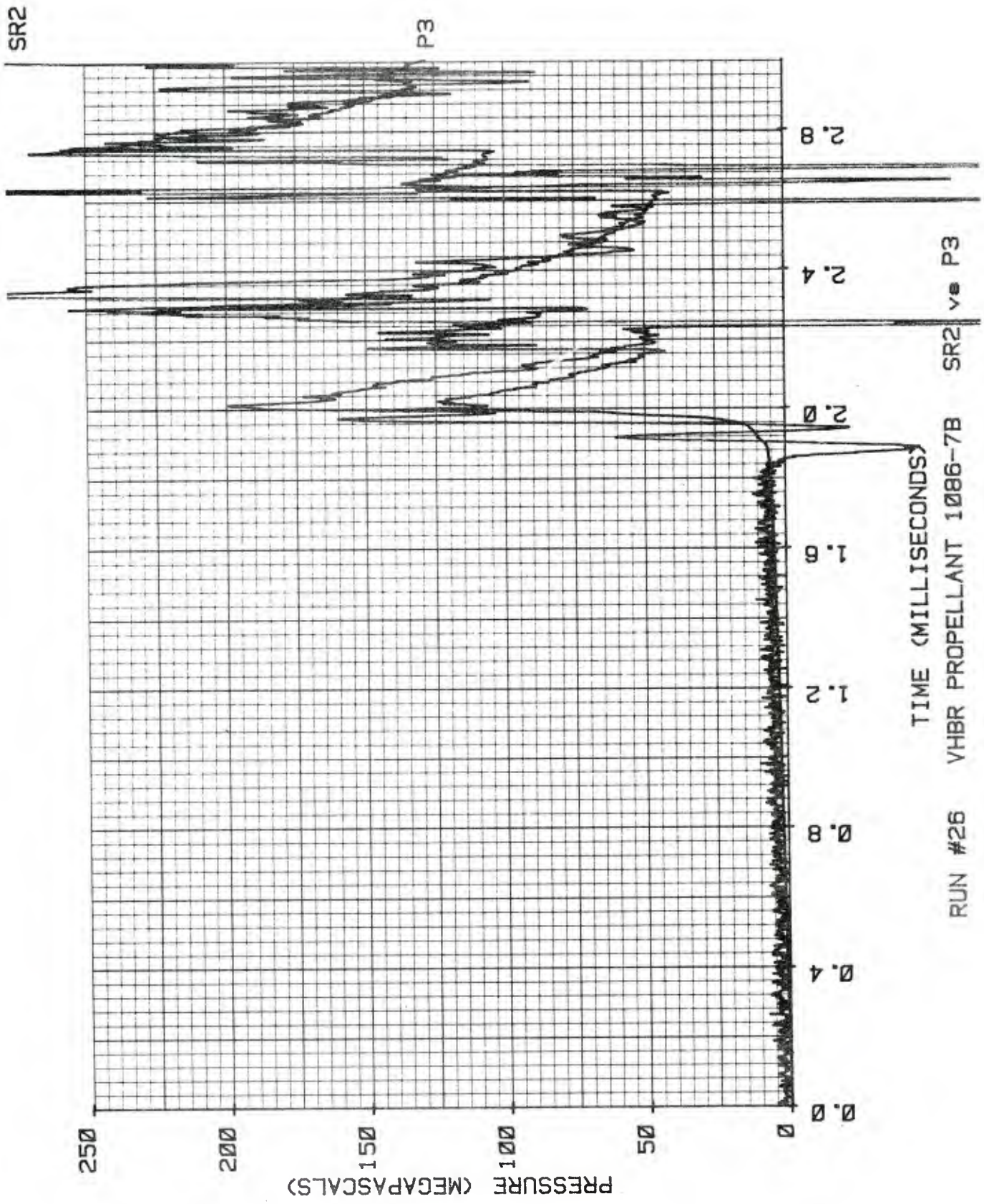

Figure 17d. Pressure History for Two Propellant Samples Coated with Silicone Ablator and Tested at a Loading Density of 0.15 g/cc

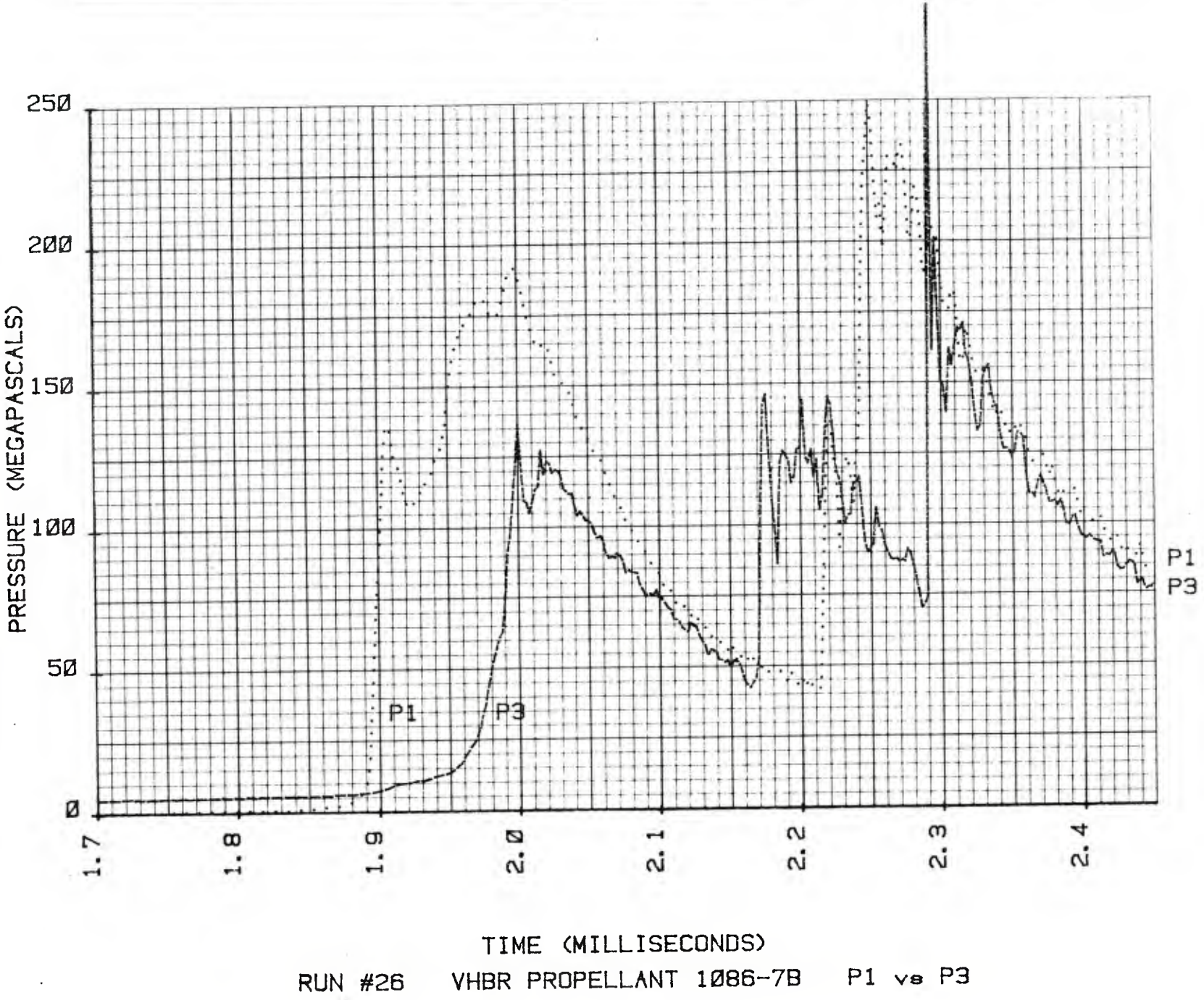

Figure 17e. Pressure History for Two Propellant Samples Coated with Silicone Ablator and Tested at a Loading Density of 0.15 g/cc

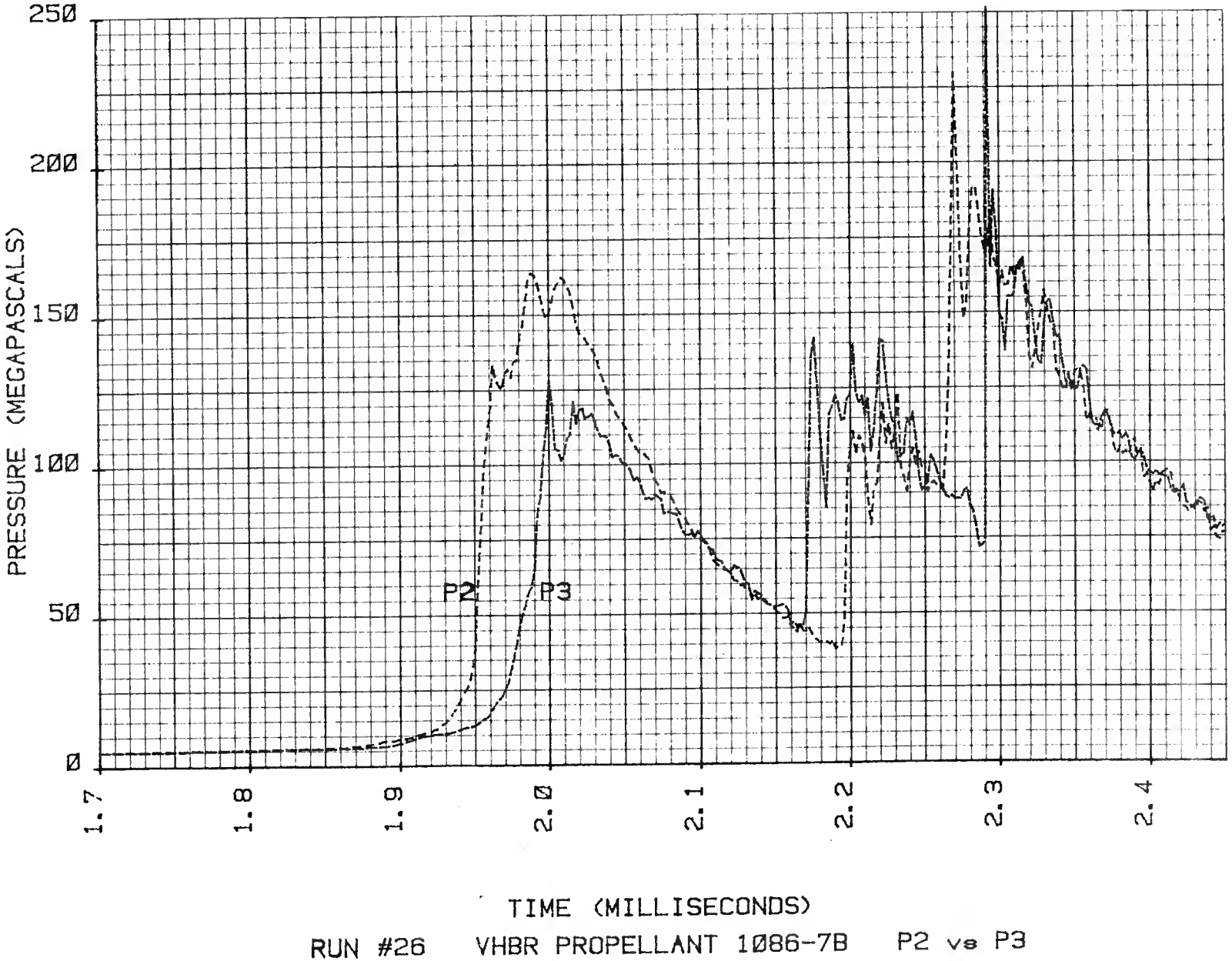

Figure 17f. Pressure History for Two Propellant Samples Coated with Silicone Ablator and Tested at a Loading Density of 0.15 g/cc

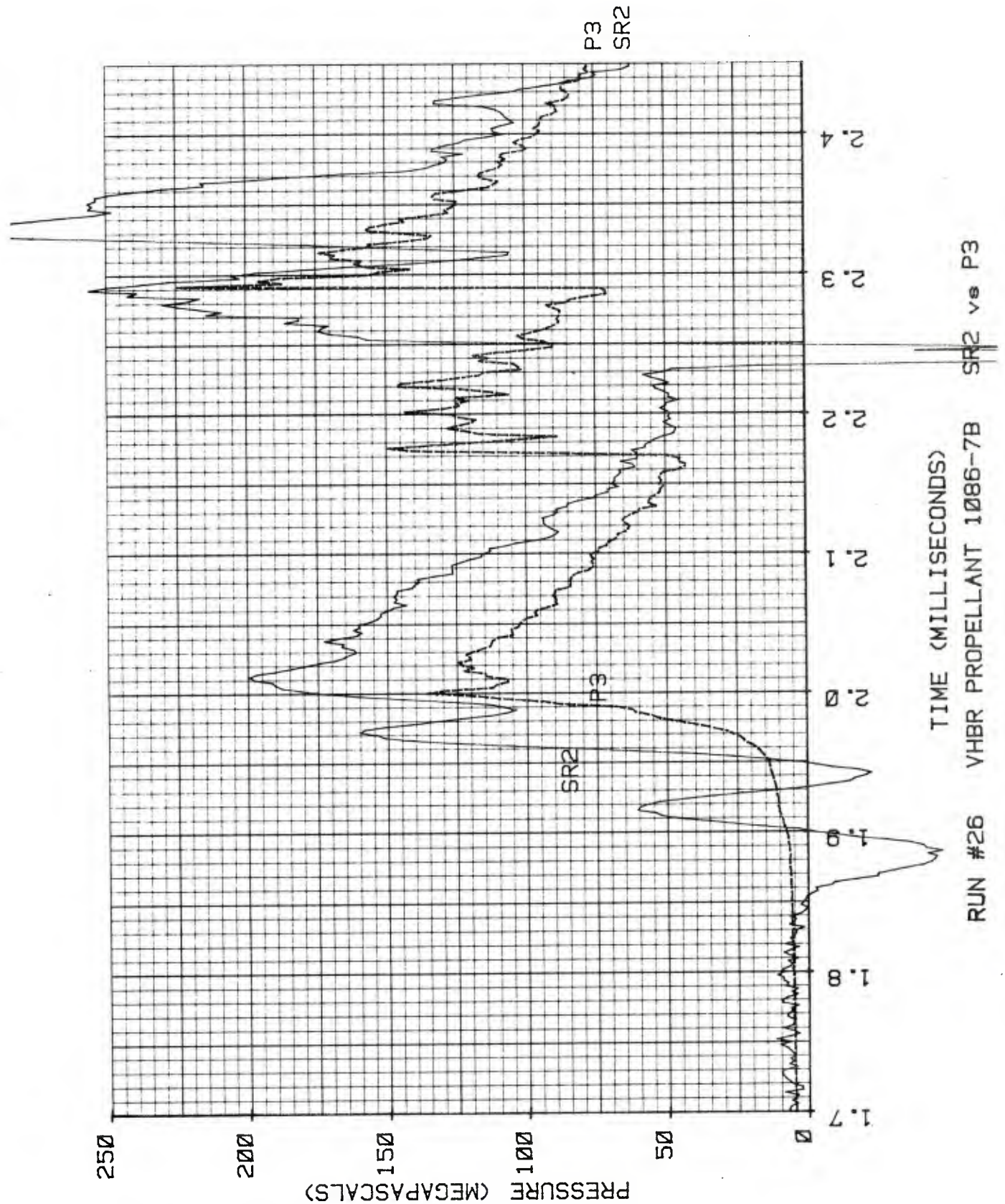

Figure 17g. Pressure History for Two Propellant Samples Coated with Silicone Ablator and Tested at a Loading Density of 0.15 g/cc

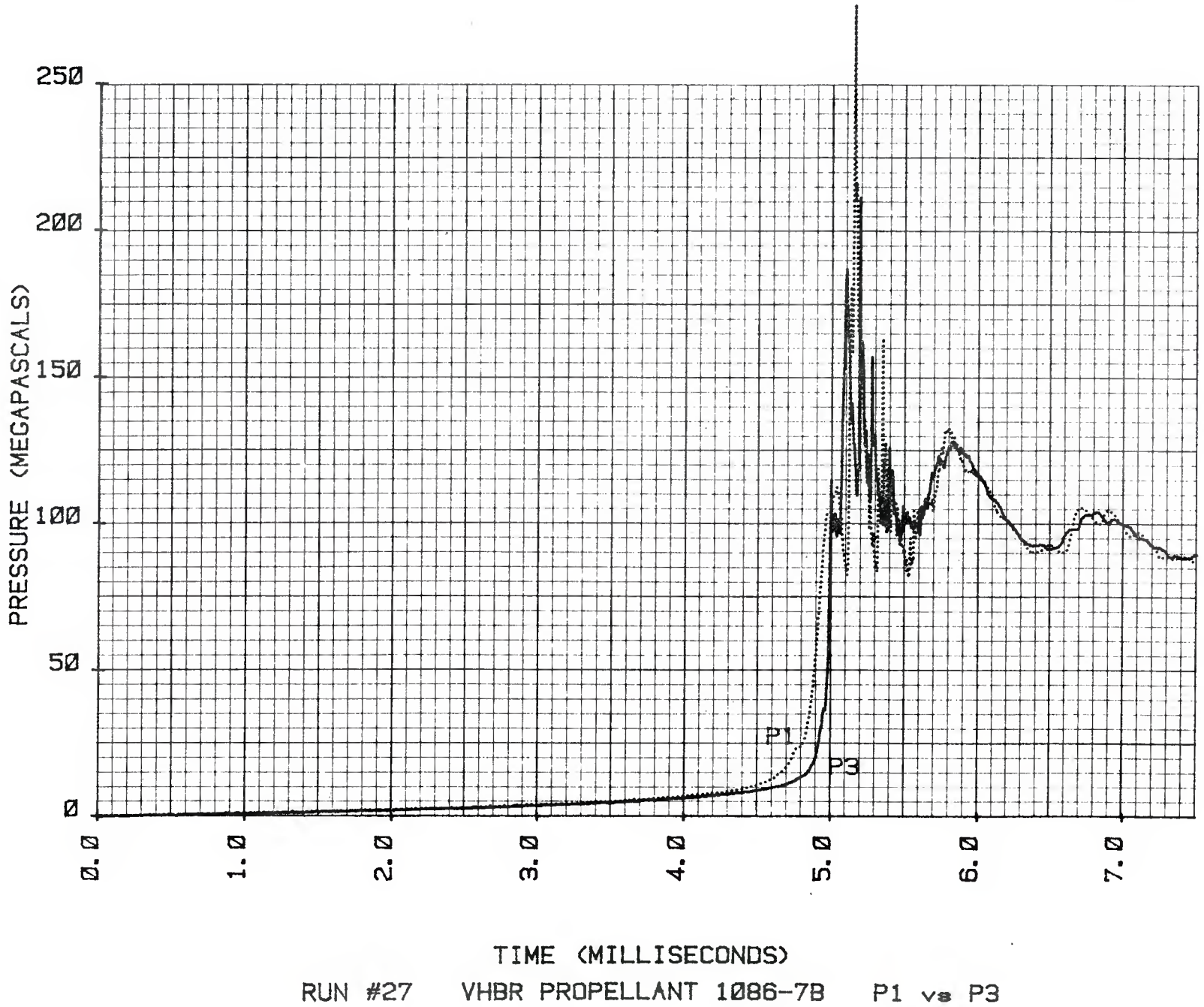

Figure 18a. Pressure History for a Single Propellant Sample Coated with Silicone Ablator and Tested at a Loading Density of 0.147 g/cc

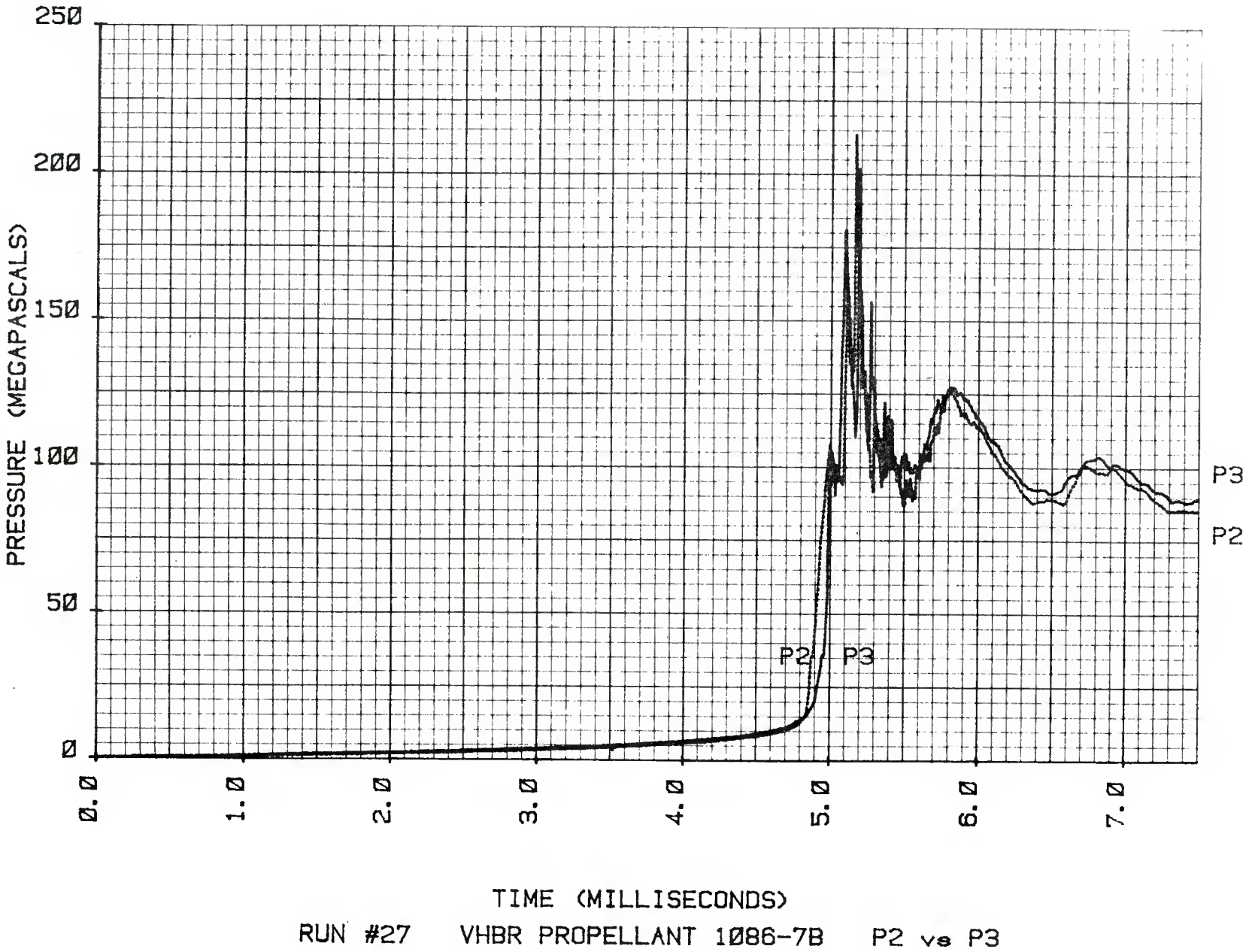

Figure 18b. Pressure History for a Single Propellant Sample Coated with Silicone Ablator and Tested at a Loading Density of 0.147 g/cc

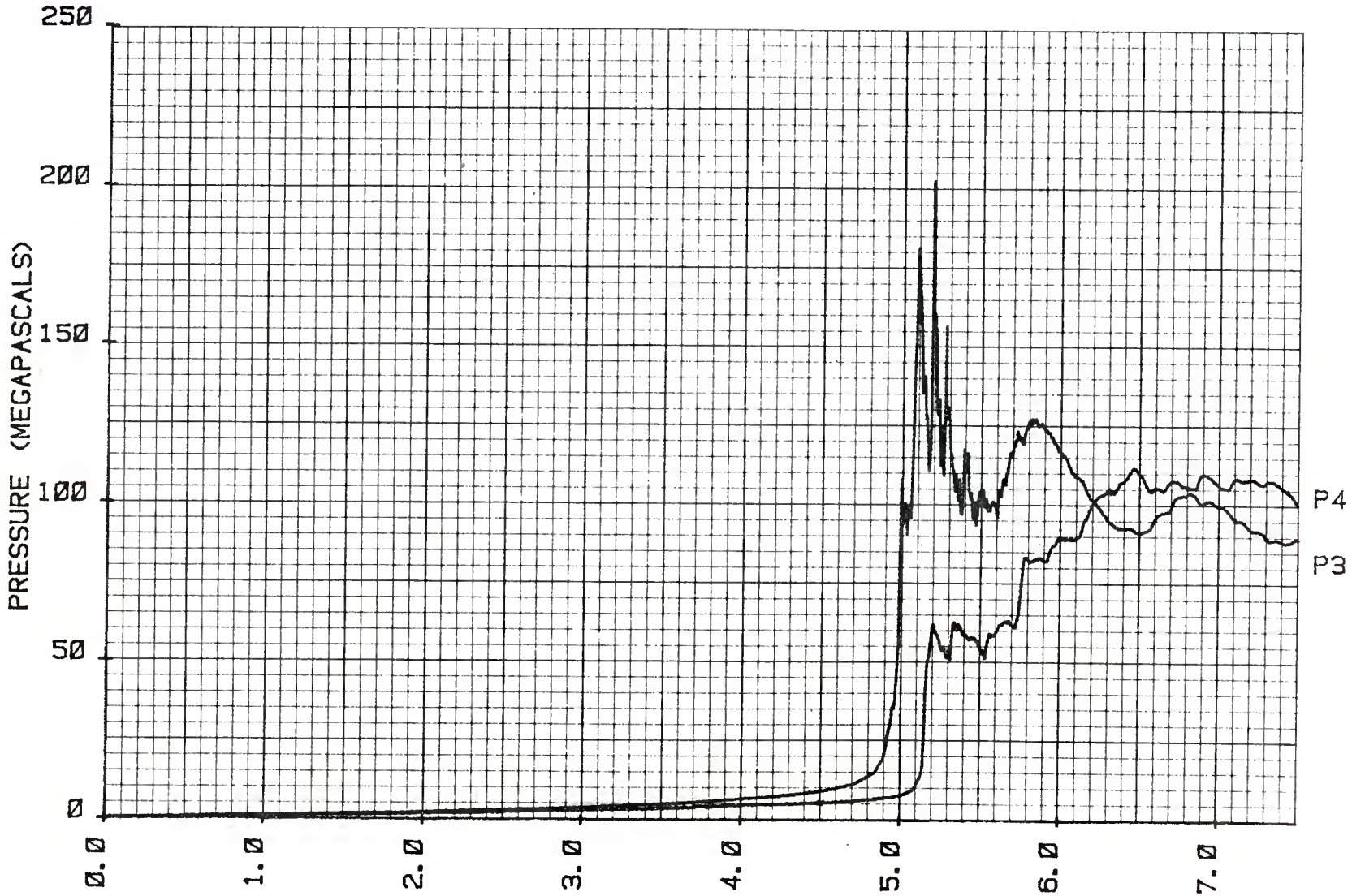

Figure 18c. Pressure History for a Single Propellant Sample Coated with Silicone Ablator and Tested at a Loading Density of 0.147 g/cc

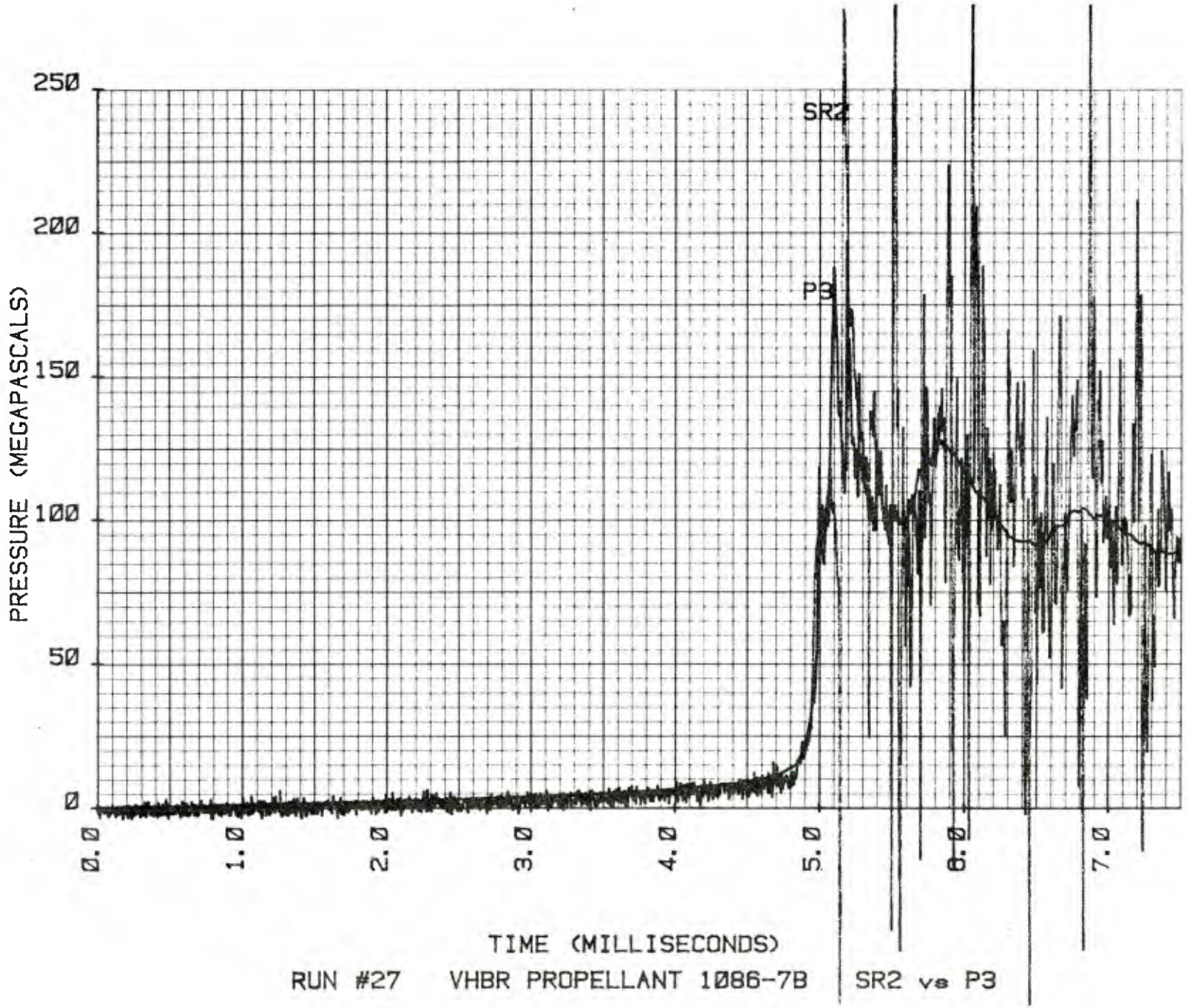

Figure 18d. Pressure History for a Single Propellant Sample Coated with Silicone Ablator and Tested at a Loading Density of 0.147 g/cc

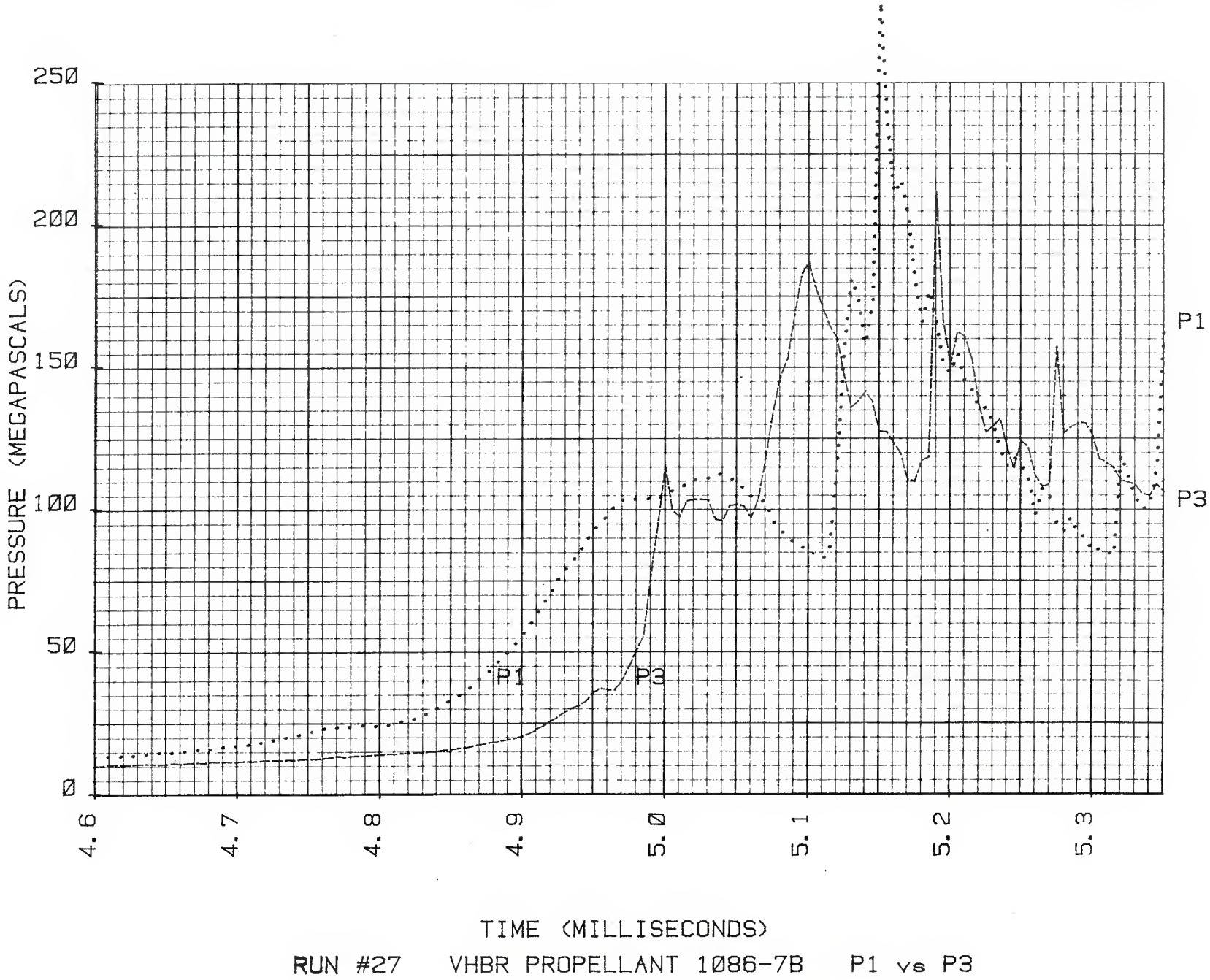

Figure 18e. Pressure History for a Single Propellant Sample Coated with Silicone Ablator and Tested at a Loading Density of 0.147 g/cc

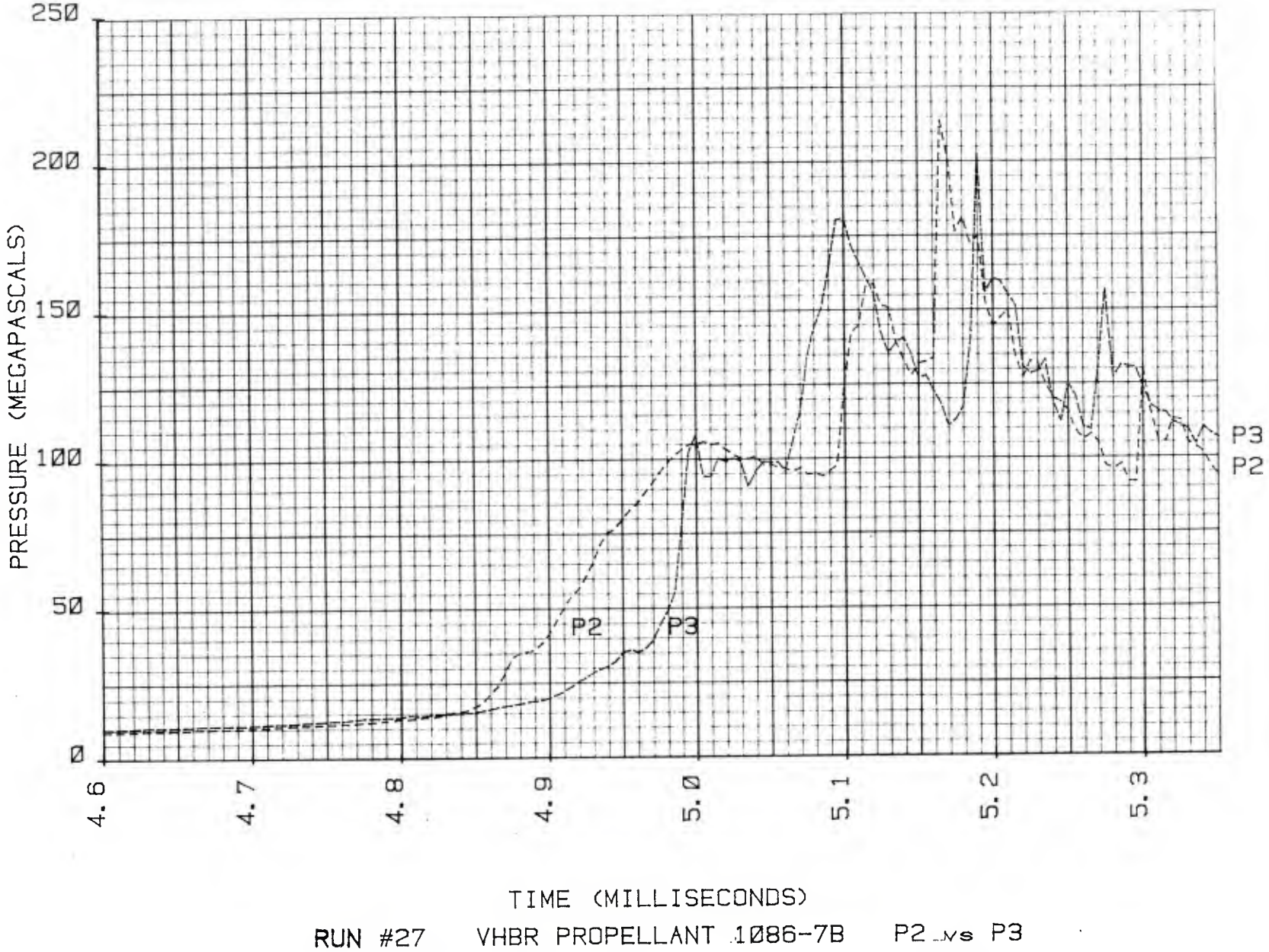

Figure 18f. Pressure History for a Single Propellant Sample Coated with Silicone Ablator and Tested at a Loading Density of 0.147 g/cc

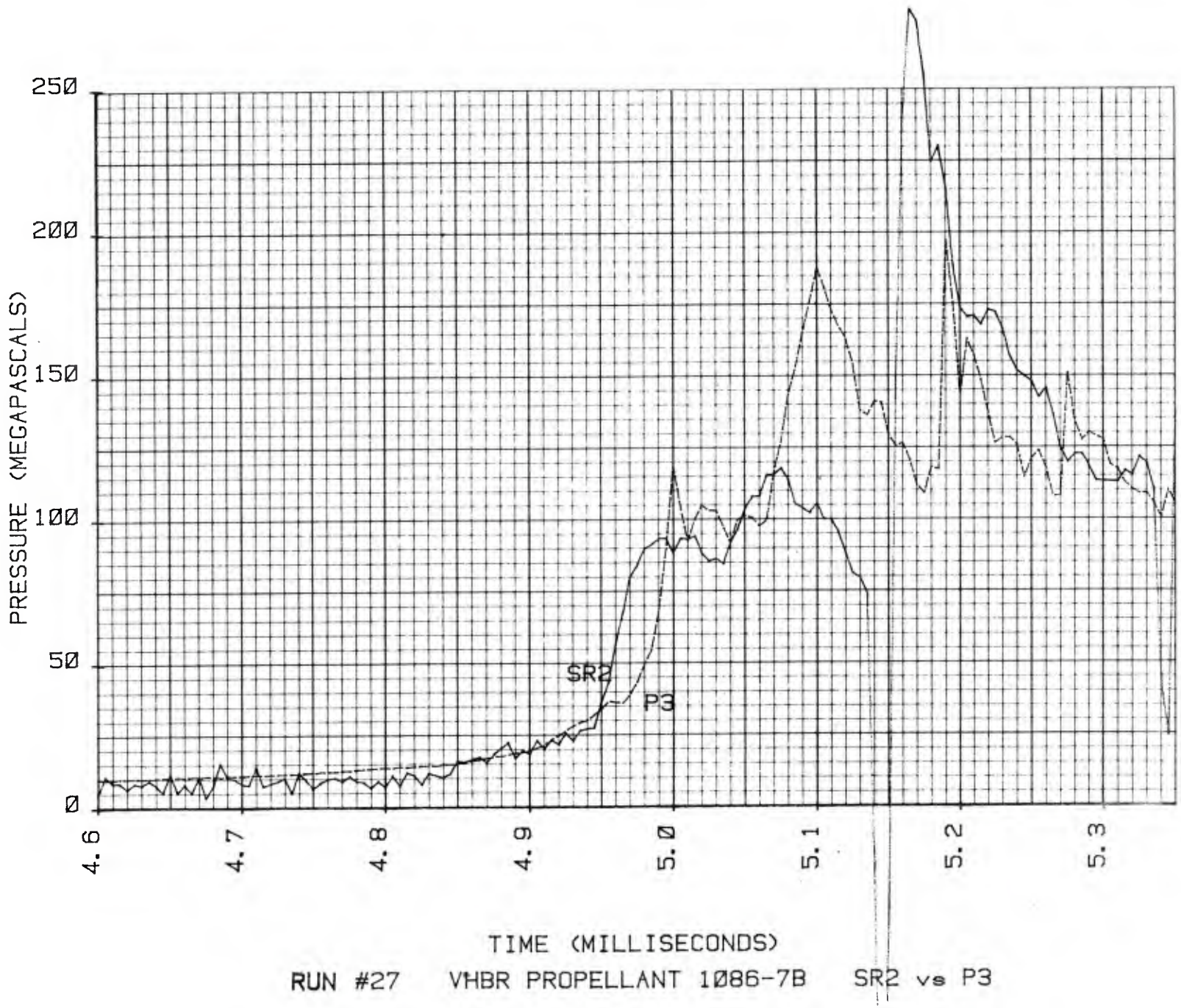

Figure 18g. Pressure History for a Single Propellant Sample Coated with Silicone Ablator and Tested at a Loading Density of 0.147 g/cc

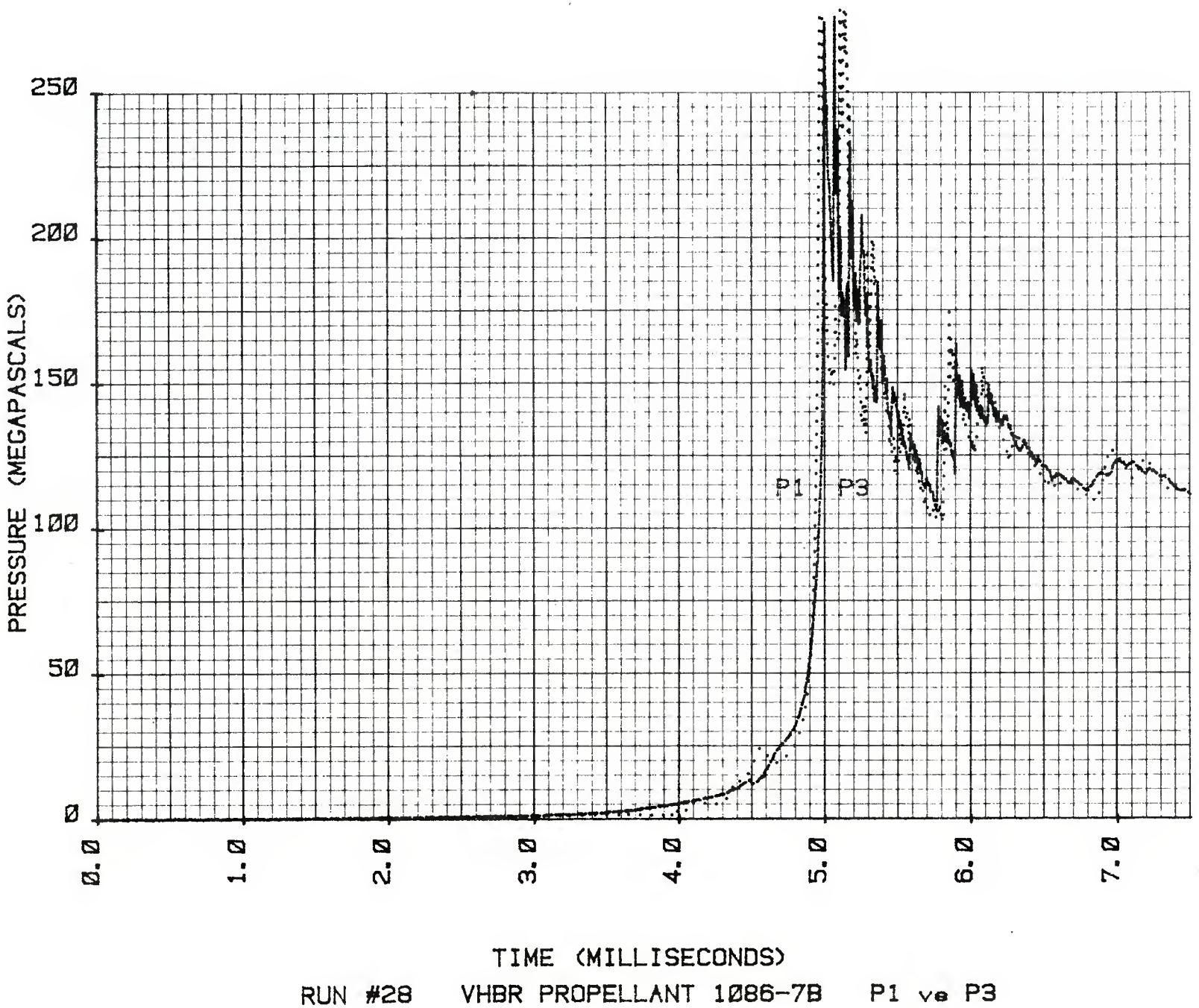

Figure 19a. Pressure History for a Single Uncoated Sample Tested at a Loading Density of 0.147 g/cc

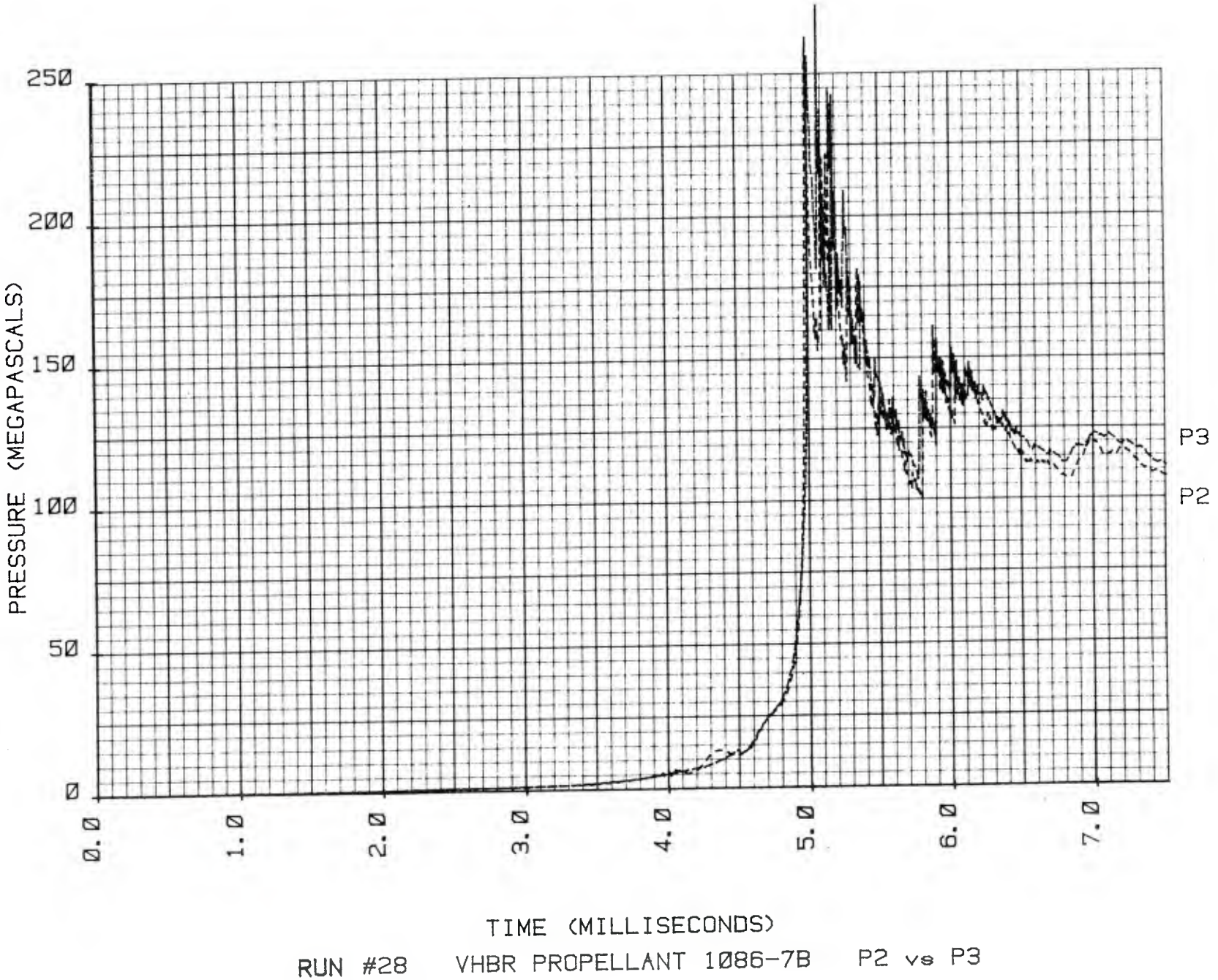

Figure 19b. Pressure History for a Single Uncoated Sample Tested at a Loading Density of 0.147 g/cc

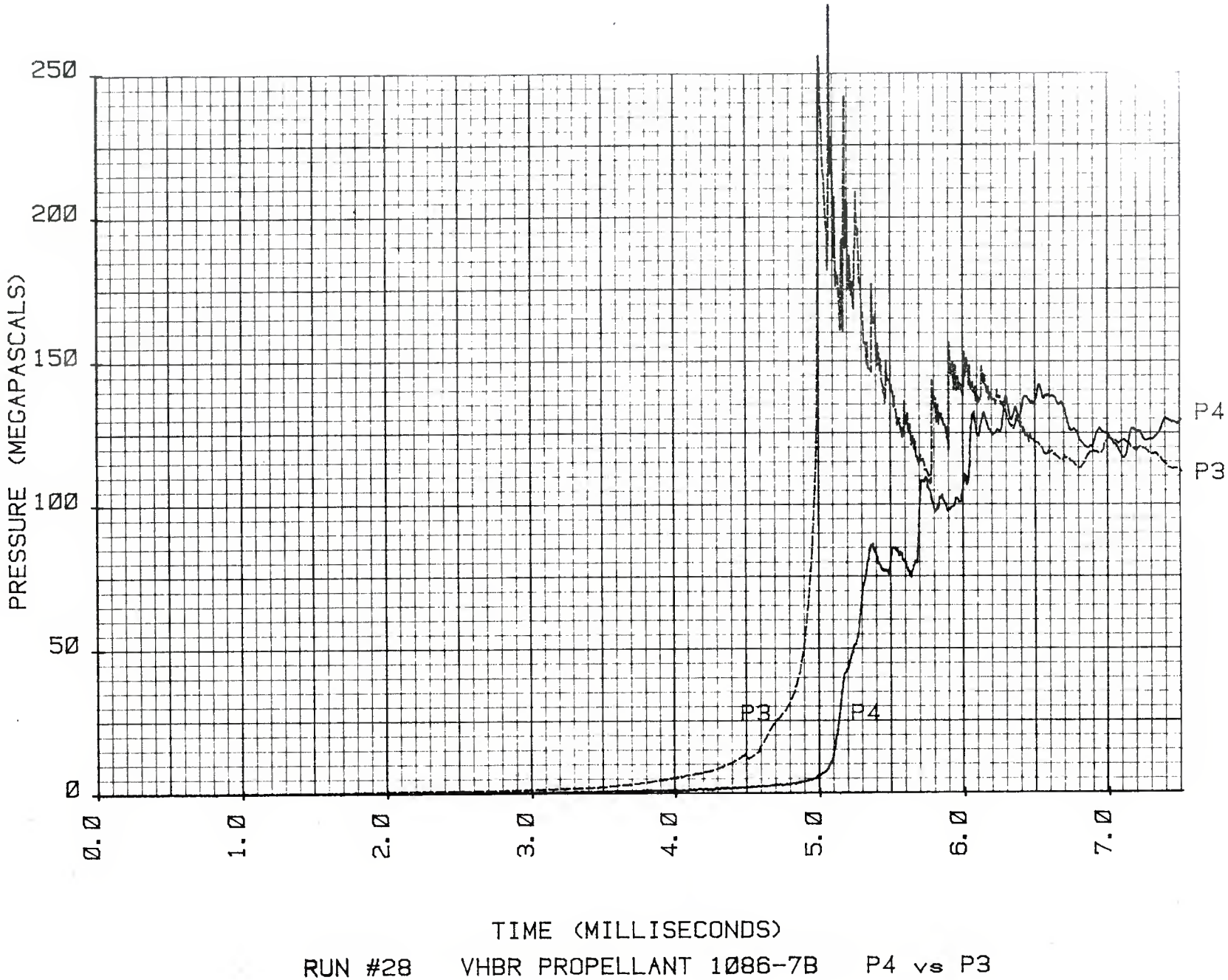

Figure 19c. Pressure History for a Single Uncoated Sample Tested at a Loading Density of 0.147 g/cc

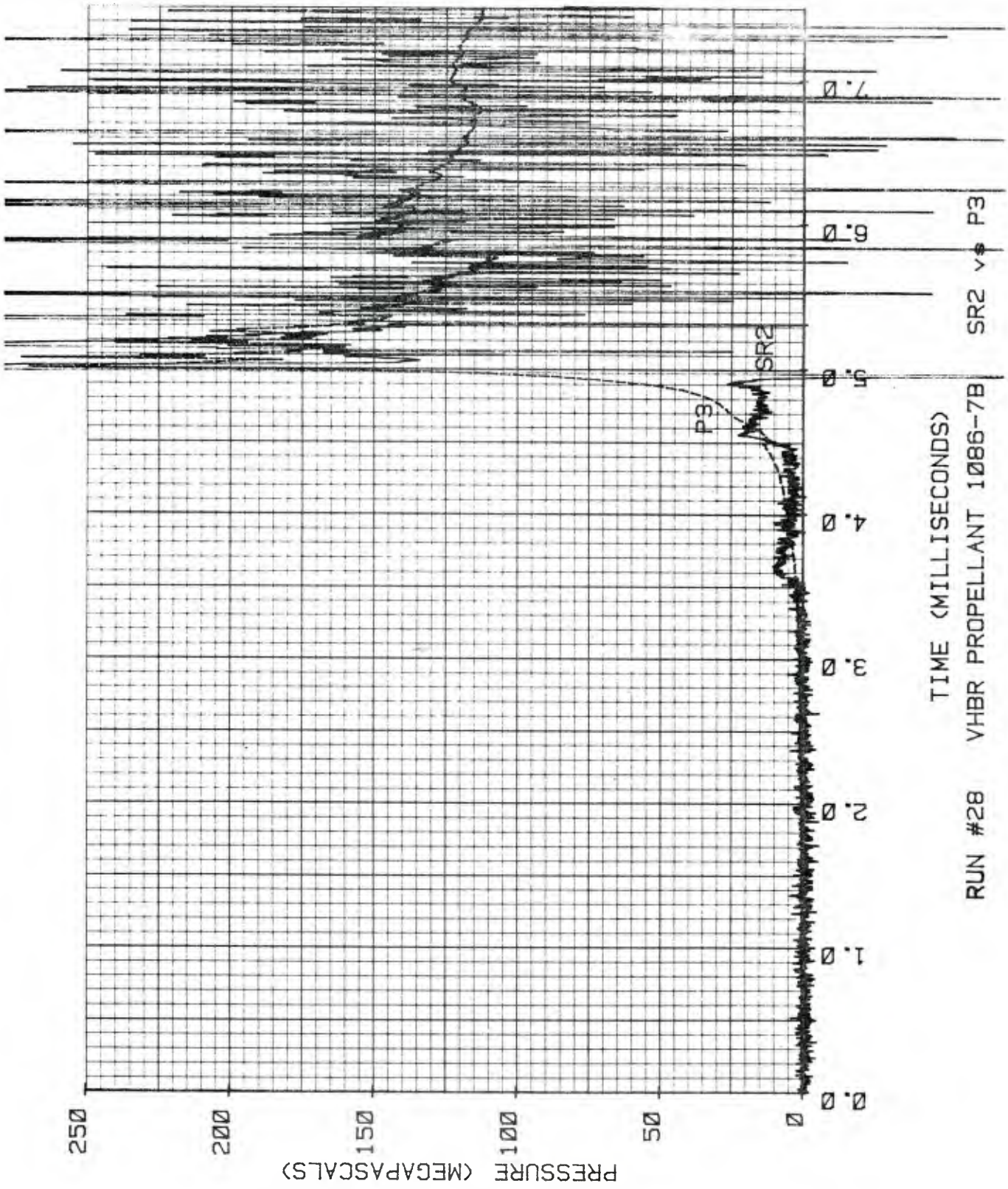

Figure 19d. Pressure History for a Single Uncoated Sample Tested at a Loading Density of 0.147 g/cc

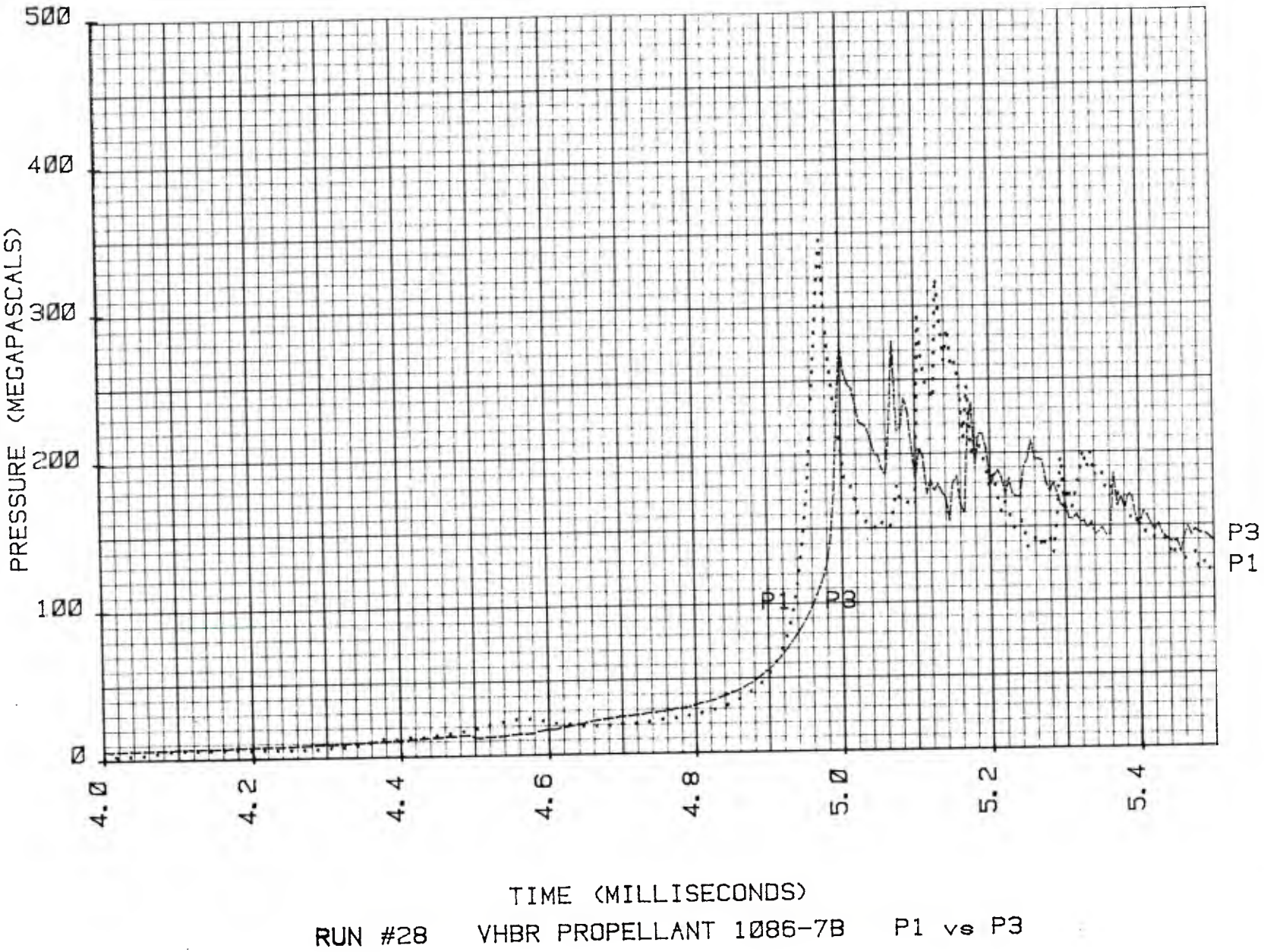

Figure 19e. Pressure History for a Single Uncoated Sample Tested at a Loading Density of 0.147 g/cc

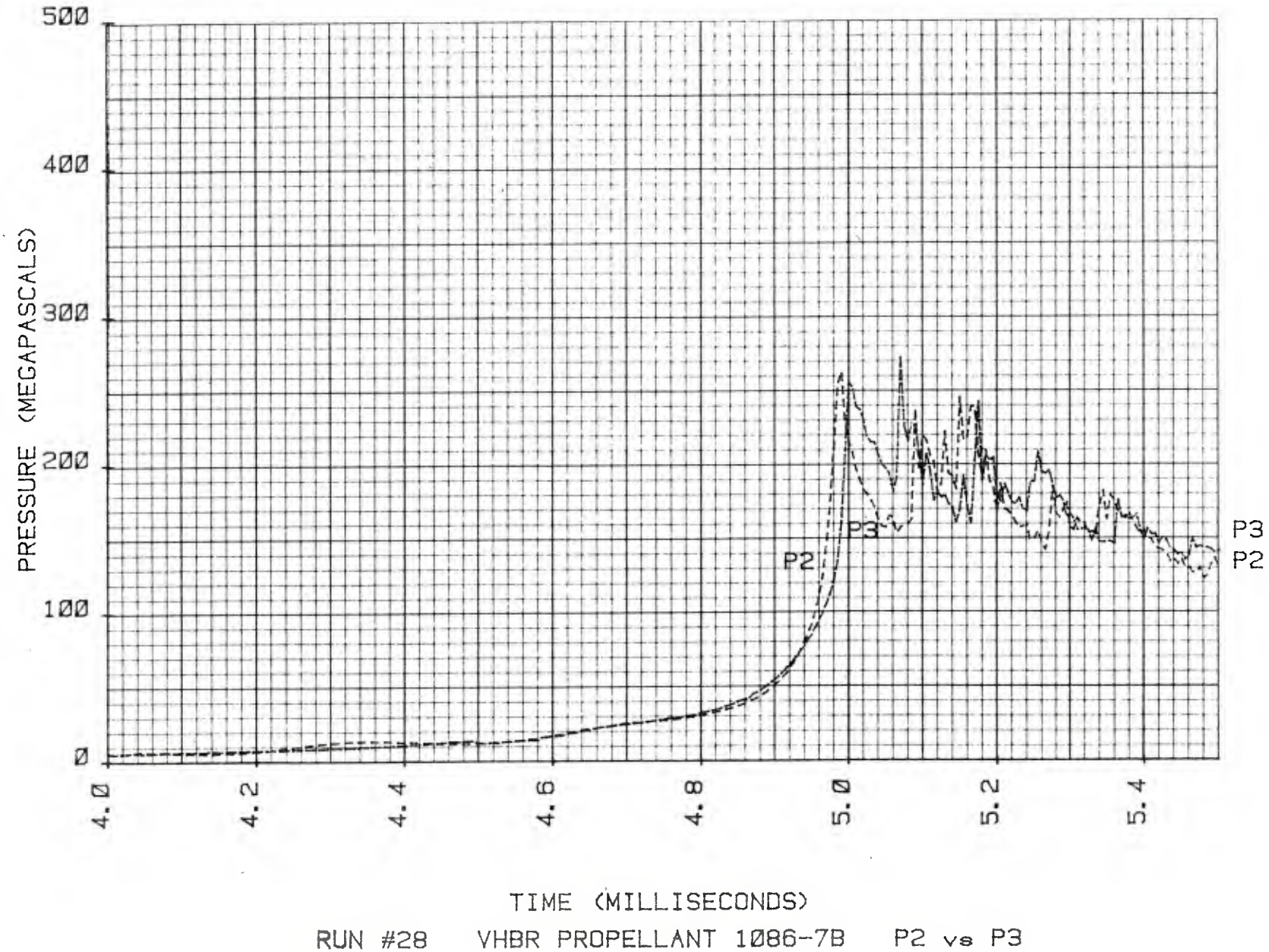

Figure 19f. Pressure History for a Single Uncoated Sample Tested at a Loading Density of 0.147 g/cc

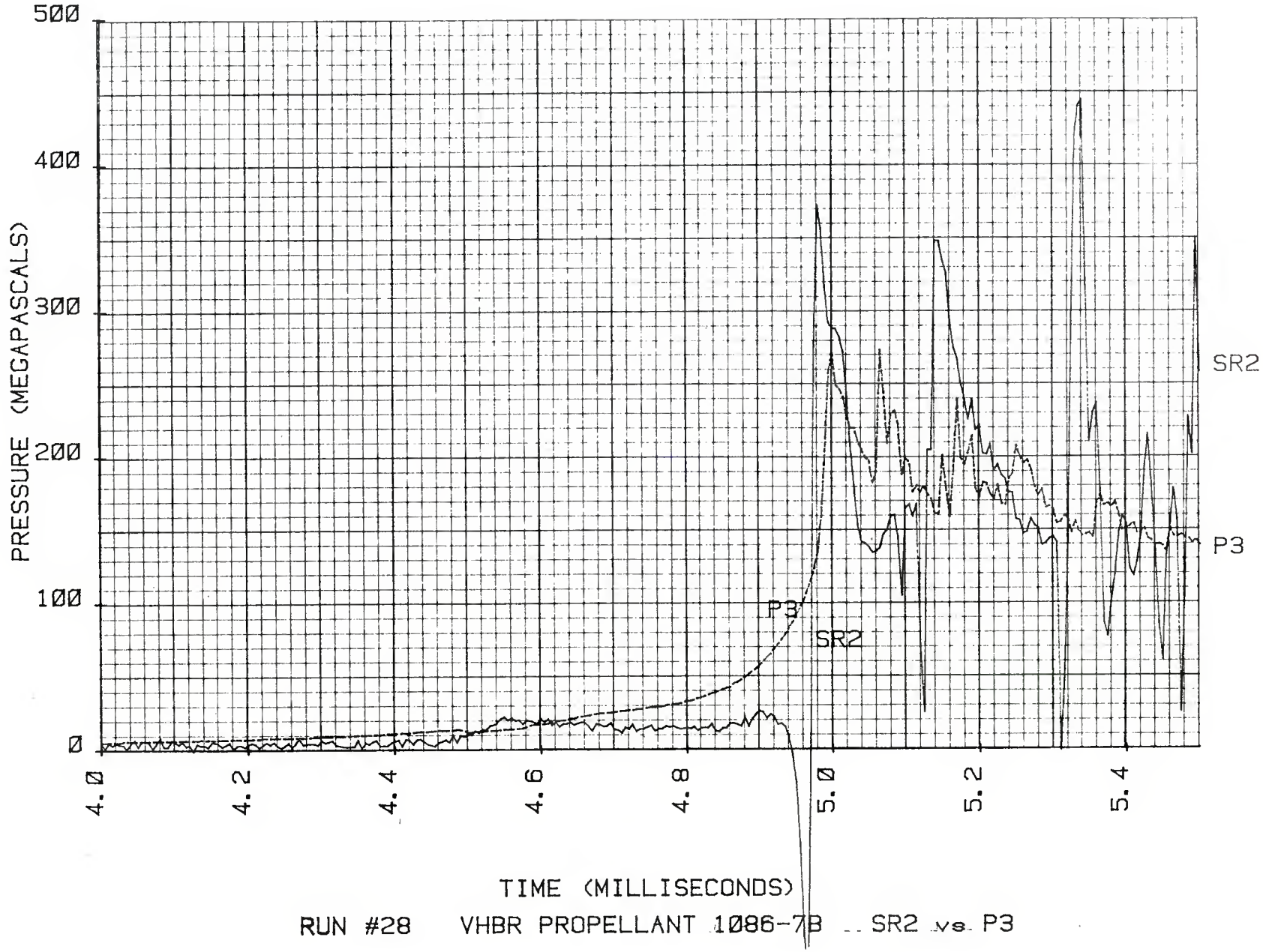

Figure 19g. Pressure History for a Single Uncoated Sample Tested at a Loading Density of 0.147 g/cc

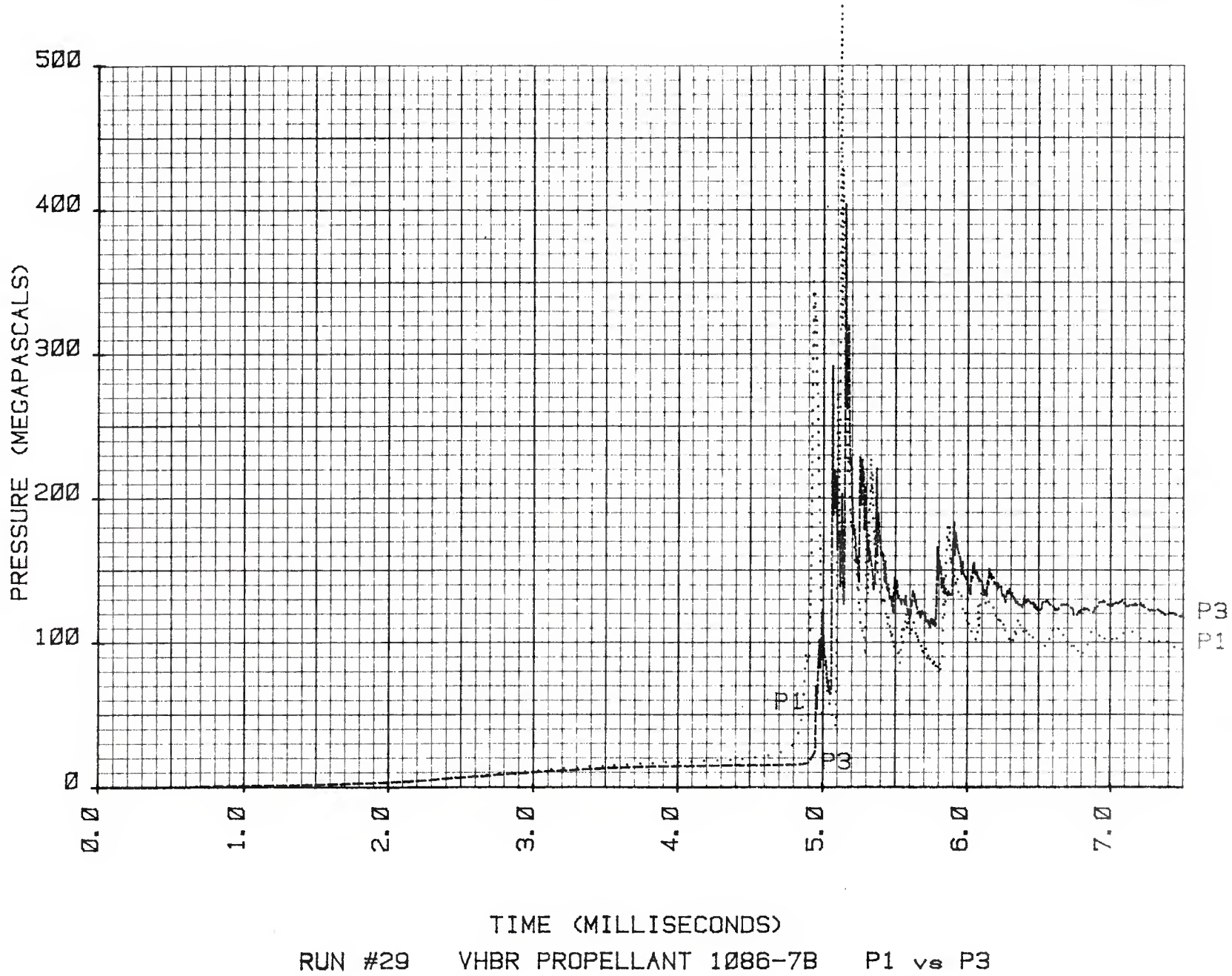

Figure 20a. Pressure History for a Single Sample Coated with Silicone Ablator, Backed with a 0.50 cm Rubber Disc and Tested at a Loading Density of 0.149 g/cc

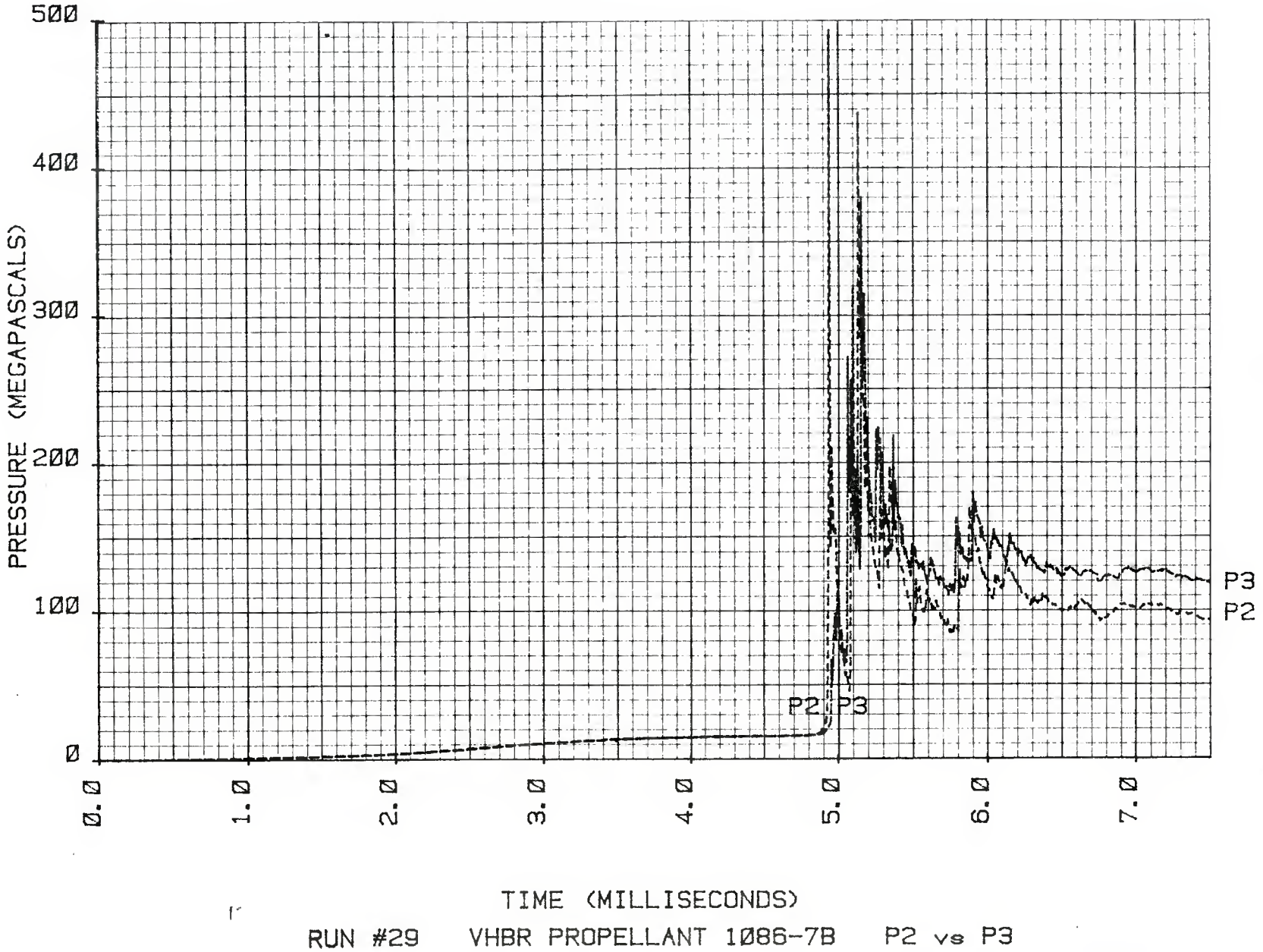

Figure 20b. Pressure History for a Single Sample Coated with Silicone Ablator, Backed with a 0.50 cm Rubber Disc and Tested at a Loading Density of 0.149 g/cc

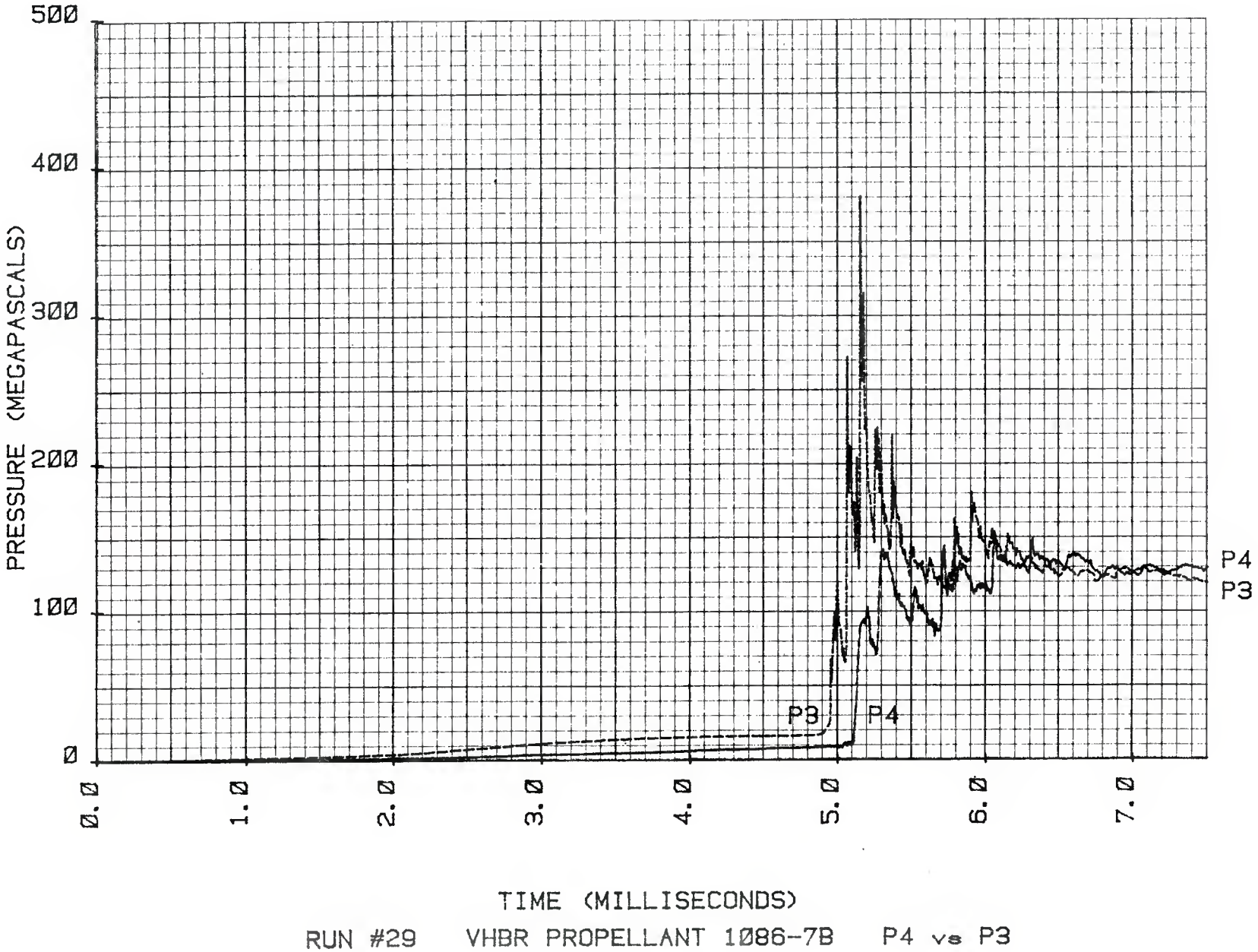

Figure 20c. Pressure History for a Single Sample Coated with Silicone Ablator, Backed with a 0.50 cm Rubber Disc and Tested at a Loading Density of 0.149 g/cc

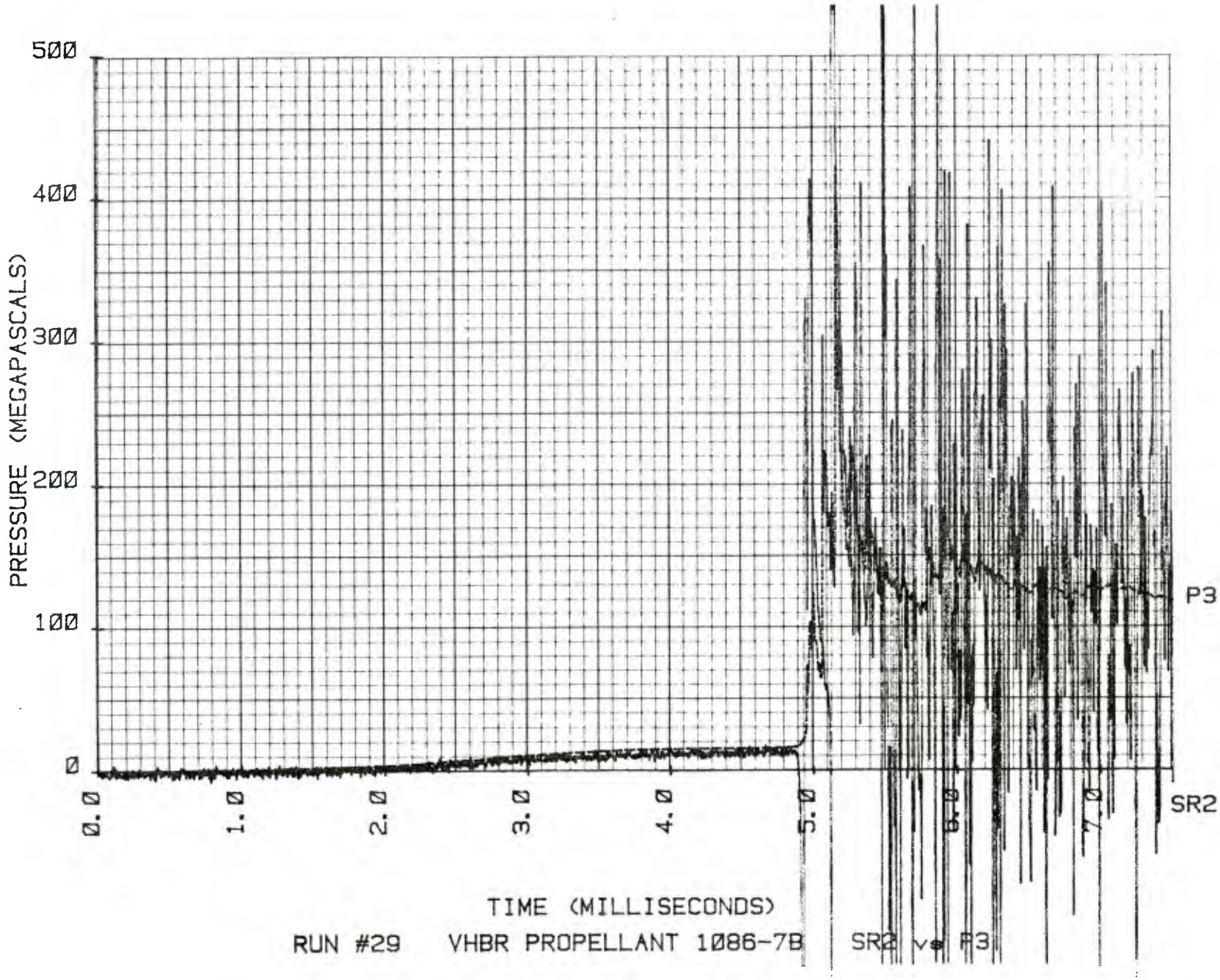

Figure 20d. Pressure History for a Single Sample Coated with Silicone Ablator, Backed with a 0.50 cm Rubber Disc and Tested at a Loading Density of 0.149 g/cc

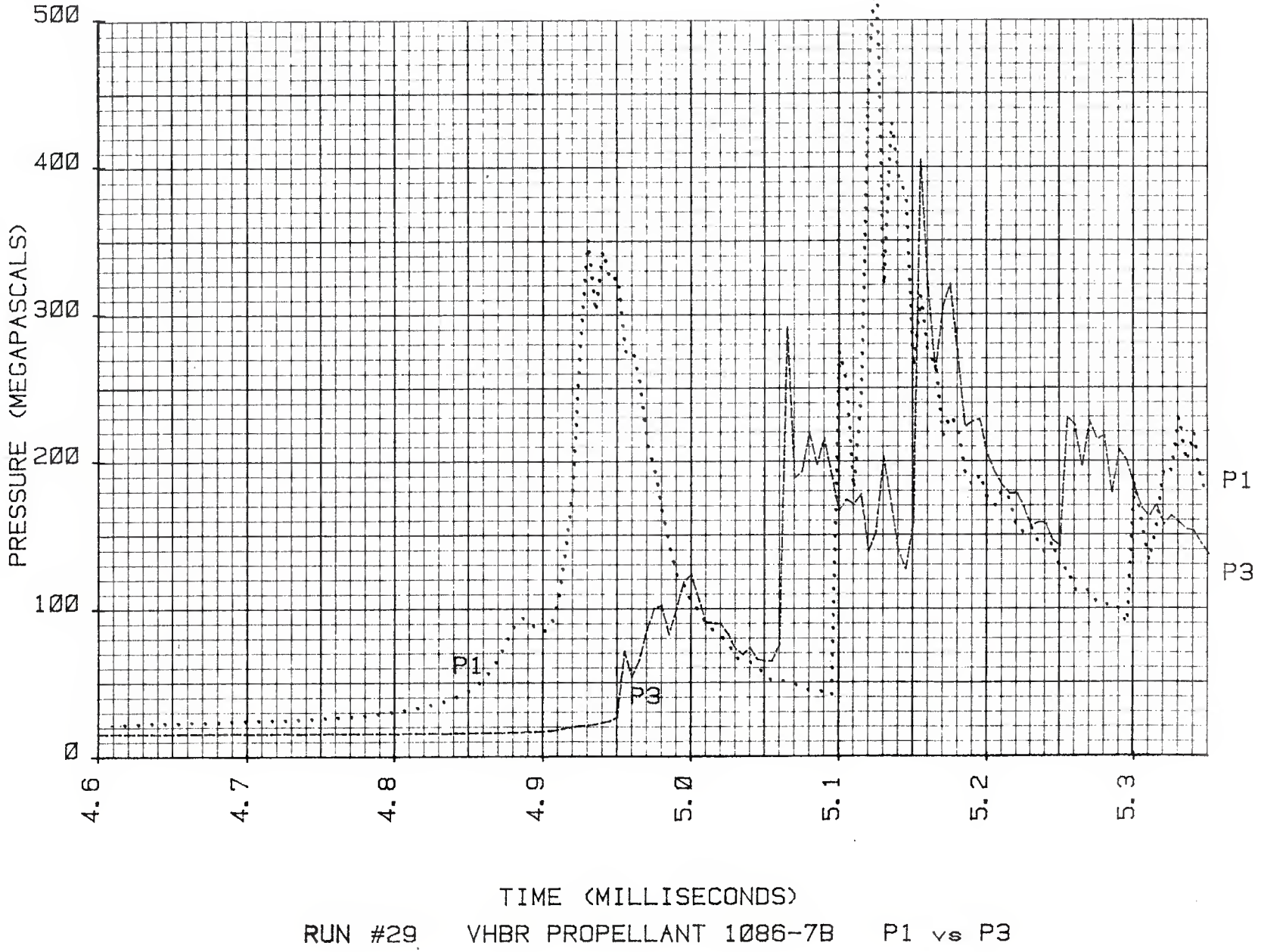

Figure 20e. Pressure History for a Single Sample Coated with Silicone Ablator, Backed with a 0.50 cm Rubber Disc and Tested at a Loading Density of 0.149 g/cc

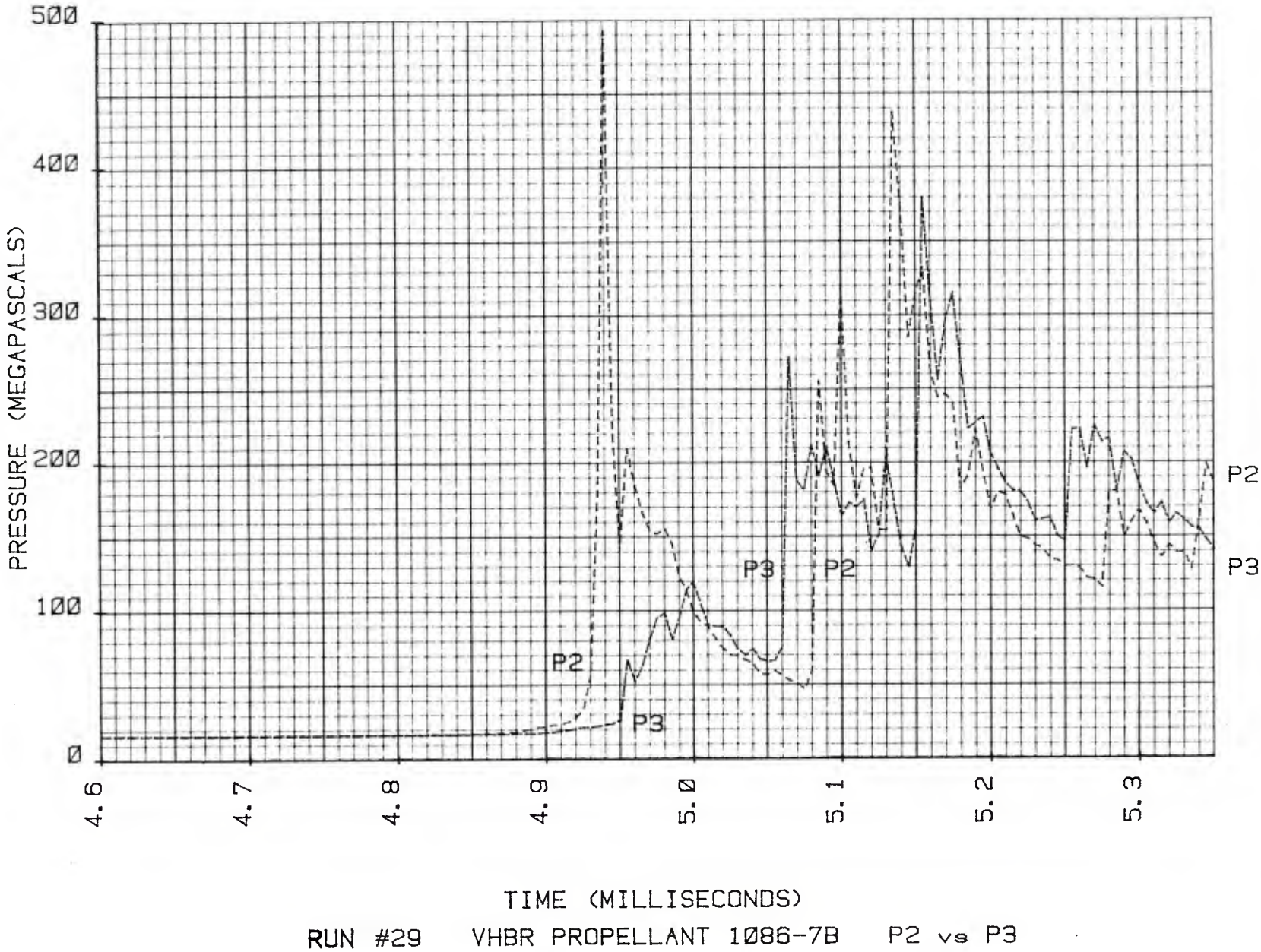

Figure 20f. Pressure History for a Single Sample Coated with Silicone Ablator, Backed with a 0.50 cm Rubber Disc and Tested at a Loading Density of 0.149 g/cc

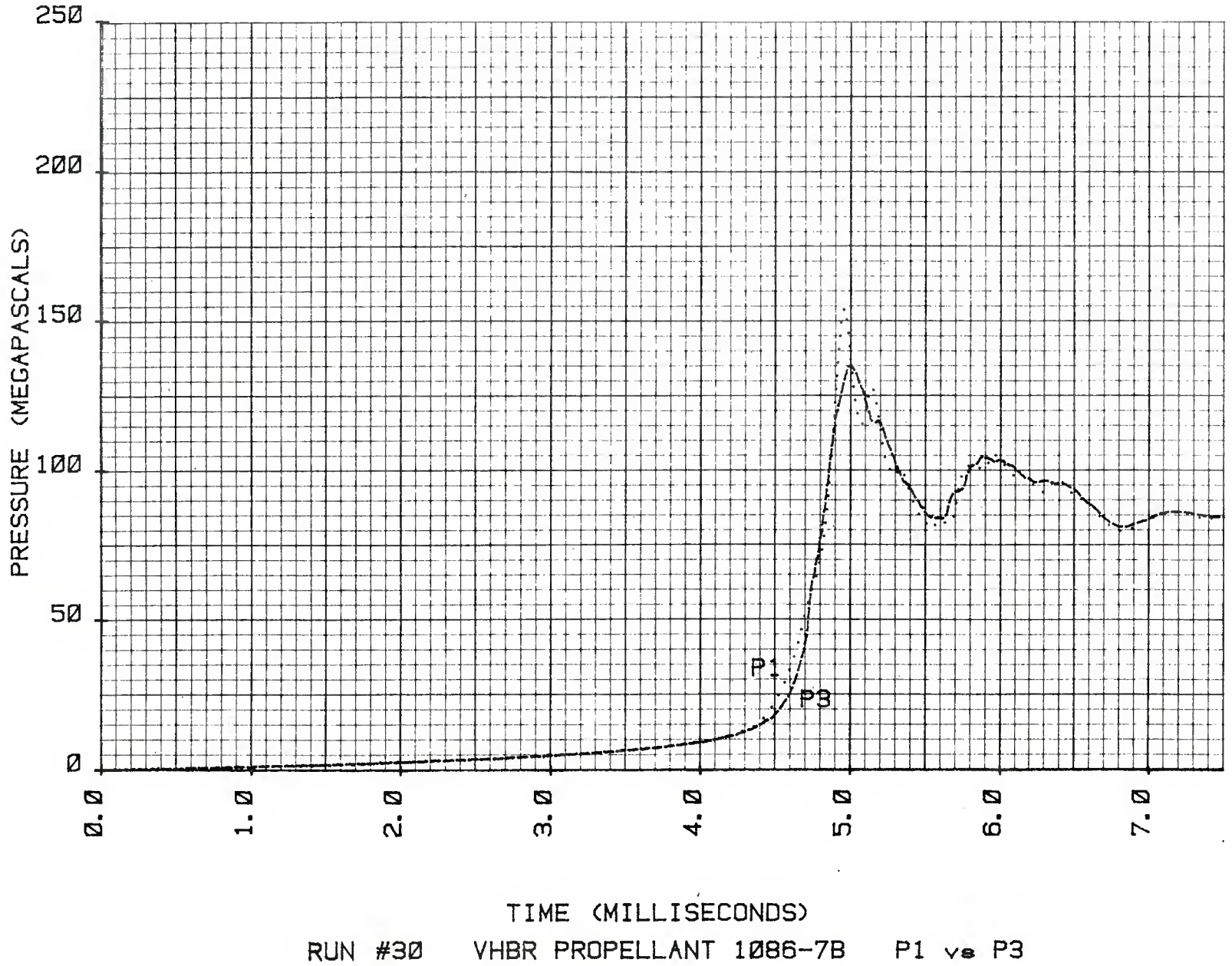

Figure 21a. Pressure History for a Single Sample Coated with Organic Grease and Tested at a Loading Density of 0.107 g/cc

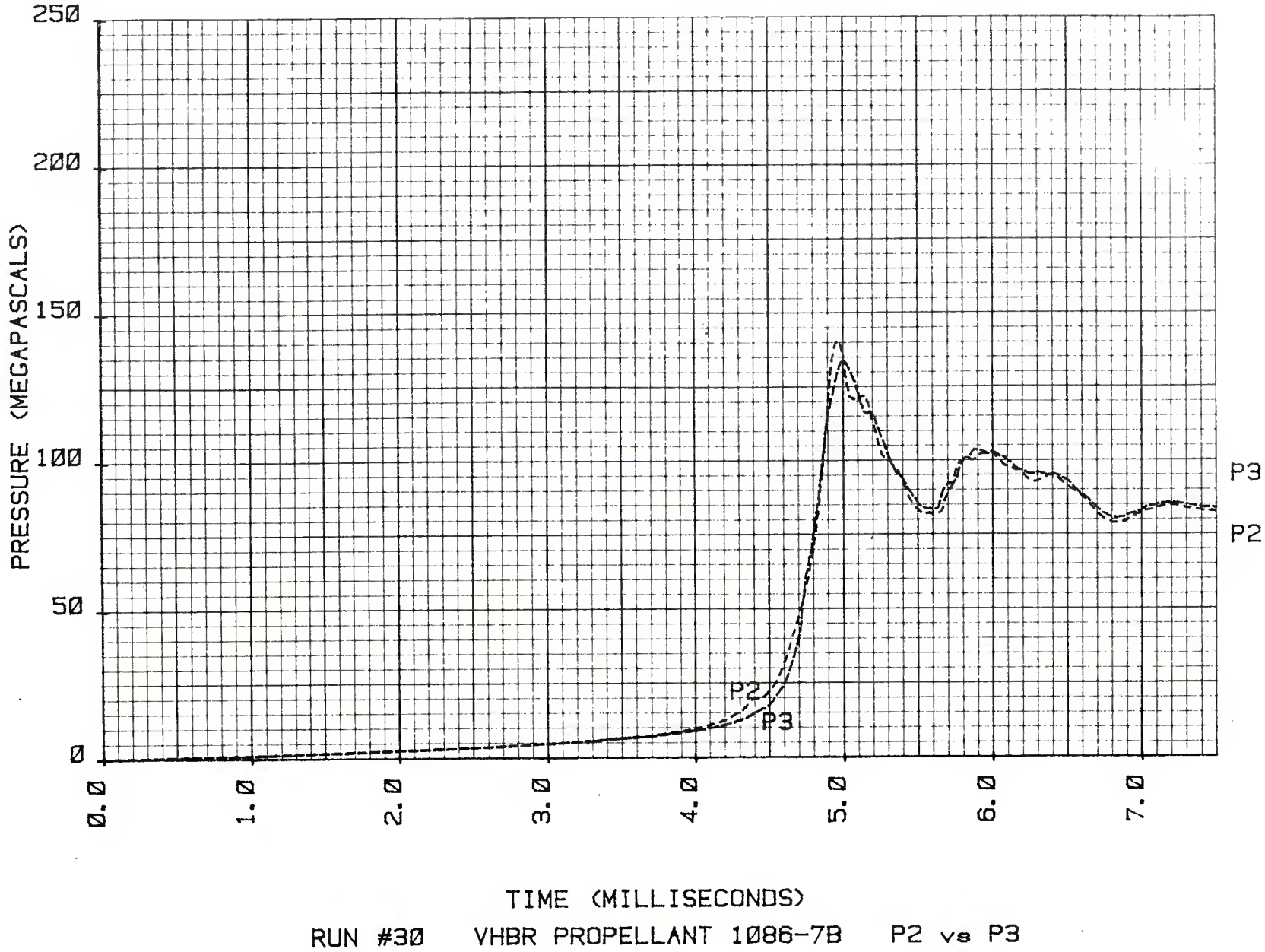

Figure 21b. Pressure History for a Single Sample Coated with Organic Grease and Tested at a Loading Density of 0.147 g/cc

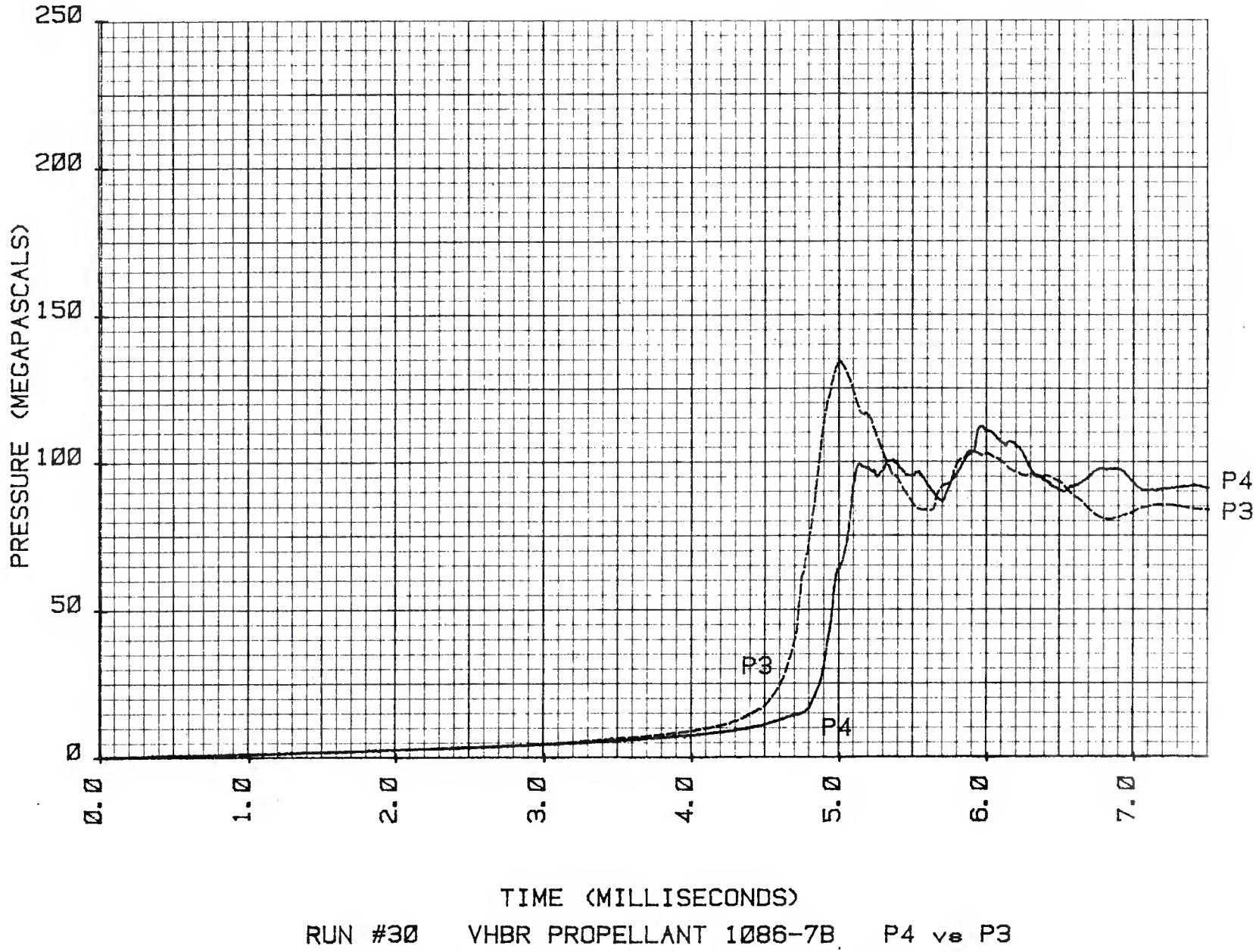

Figure 21c. Pressure History for a Single Sample Coated with Organic Grease and Tested at a Loading Density of 0.107 g/cc

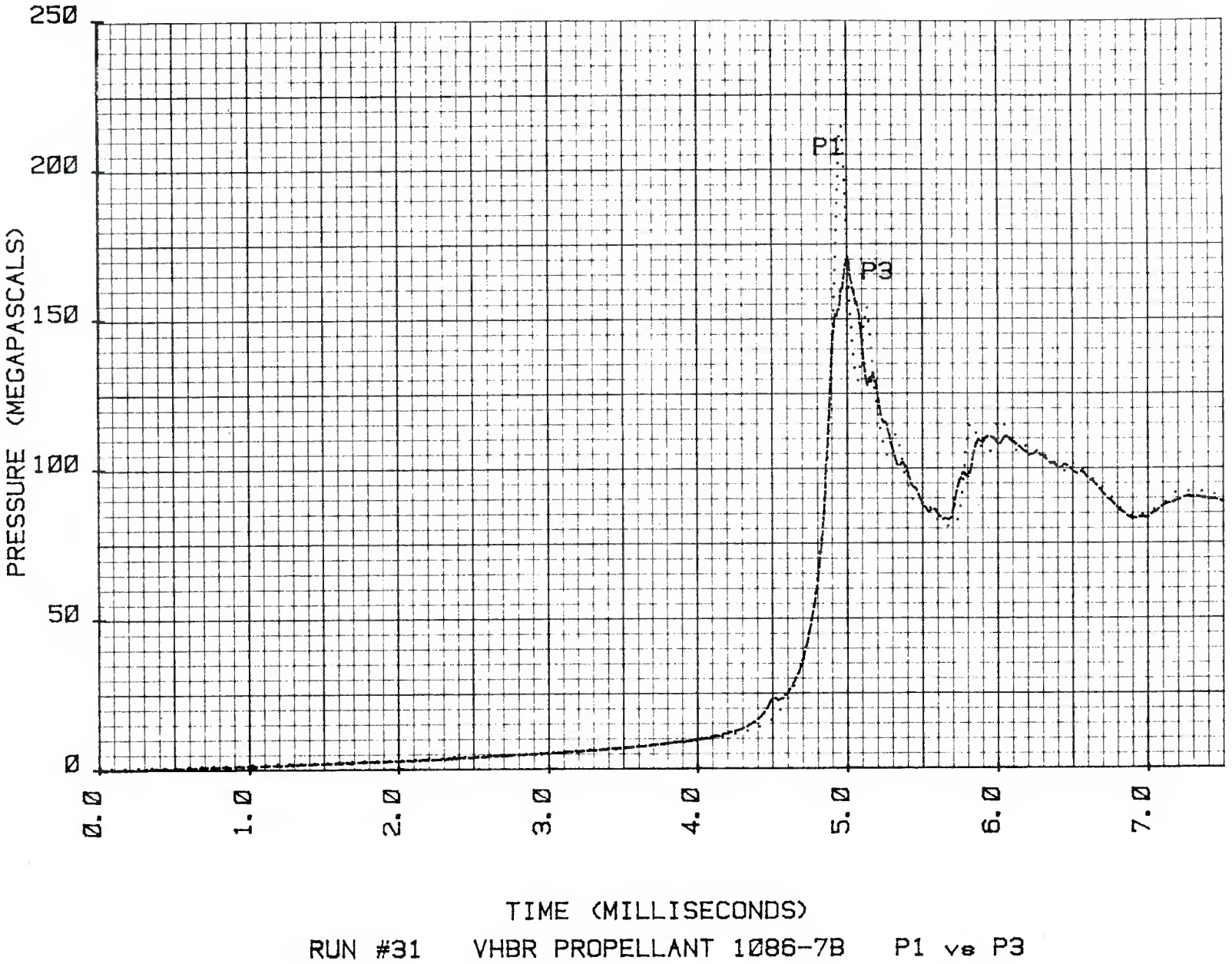

Figure 22a. Pressure History for a Single Sample Coated with Organic Grease and Tested at a Loading Density of 0.147 g/cc

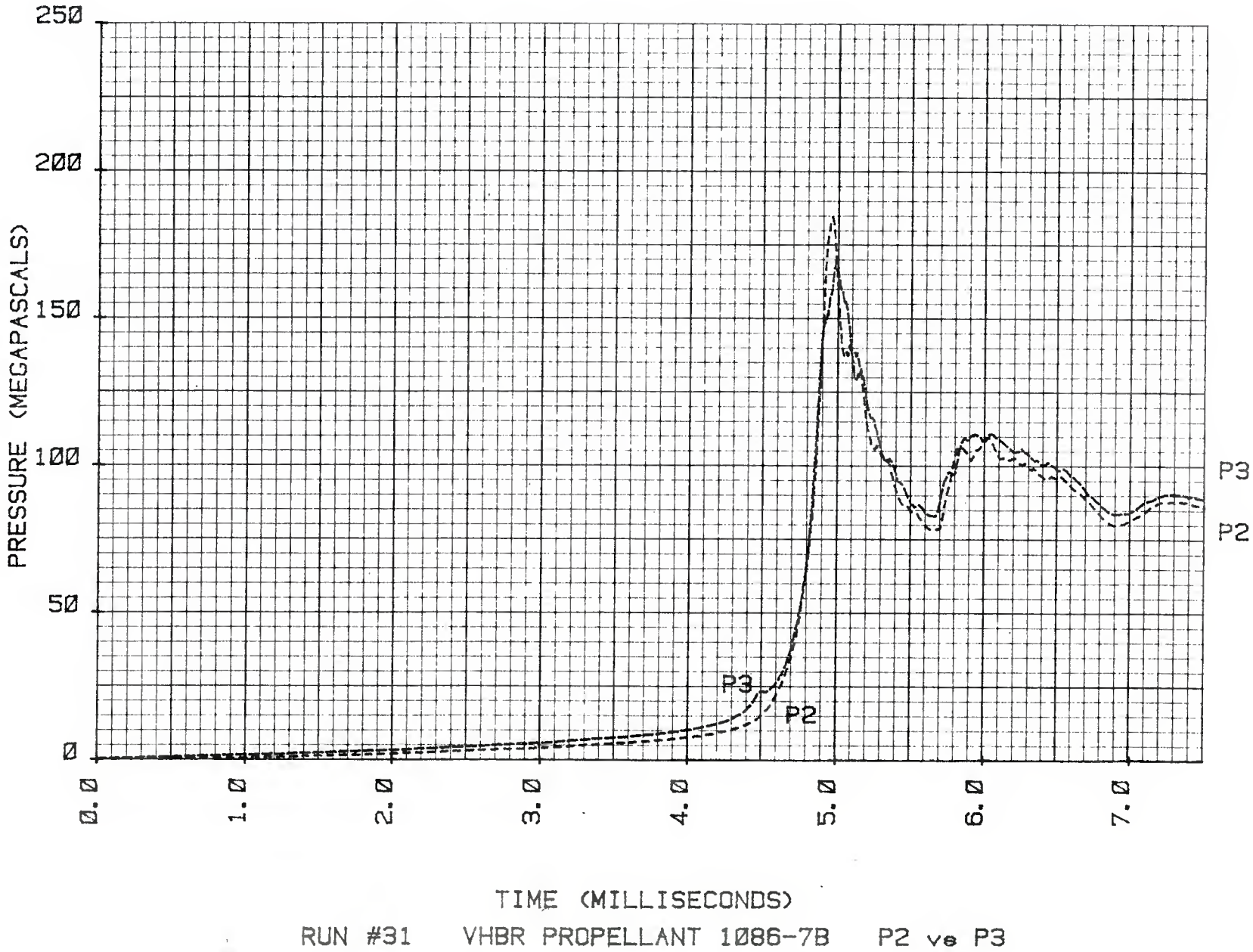

Figure 22b. Pressure History for a Single Sample Coated with Organic Grease and Tested at a Loading Density of 0.147 g/cc

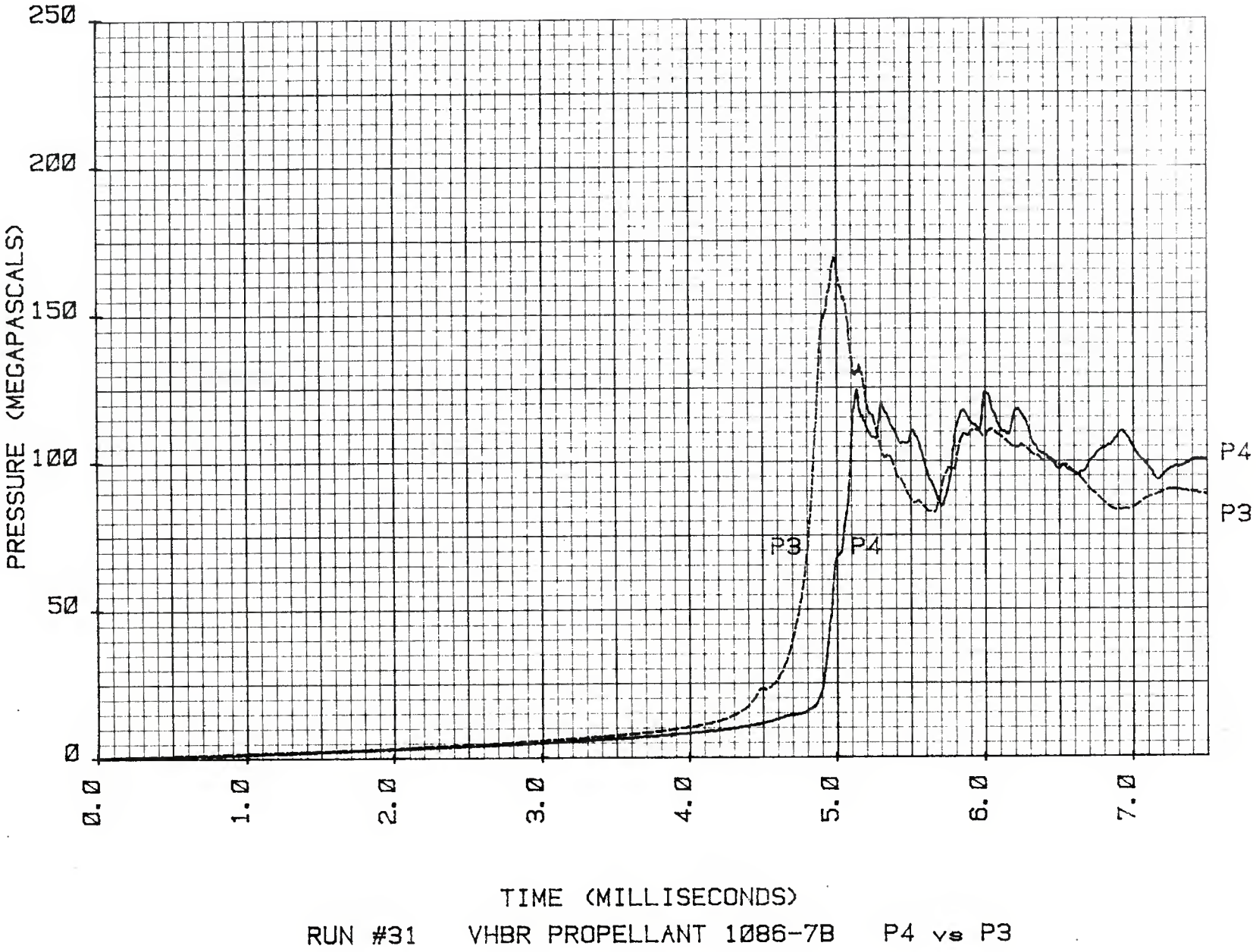

Figure 22c. Pressure History for a Single Sample Coated with Organic Grease and Tested at a Loading Density of 0.147 g/cc

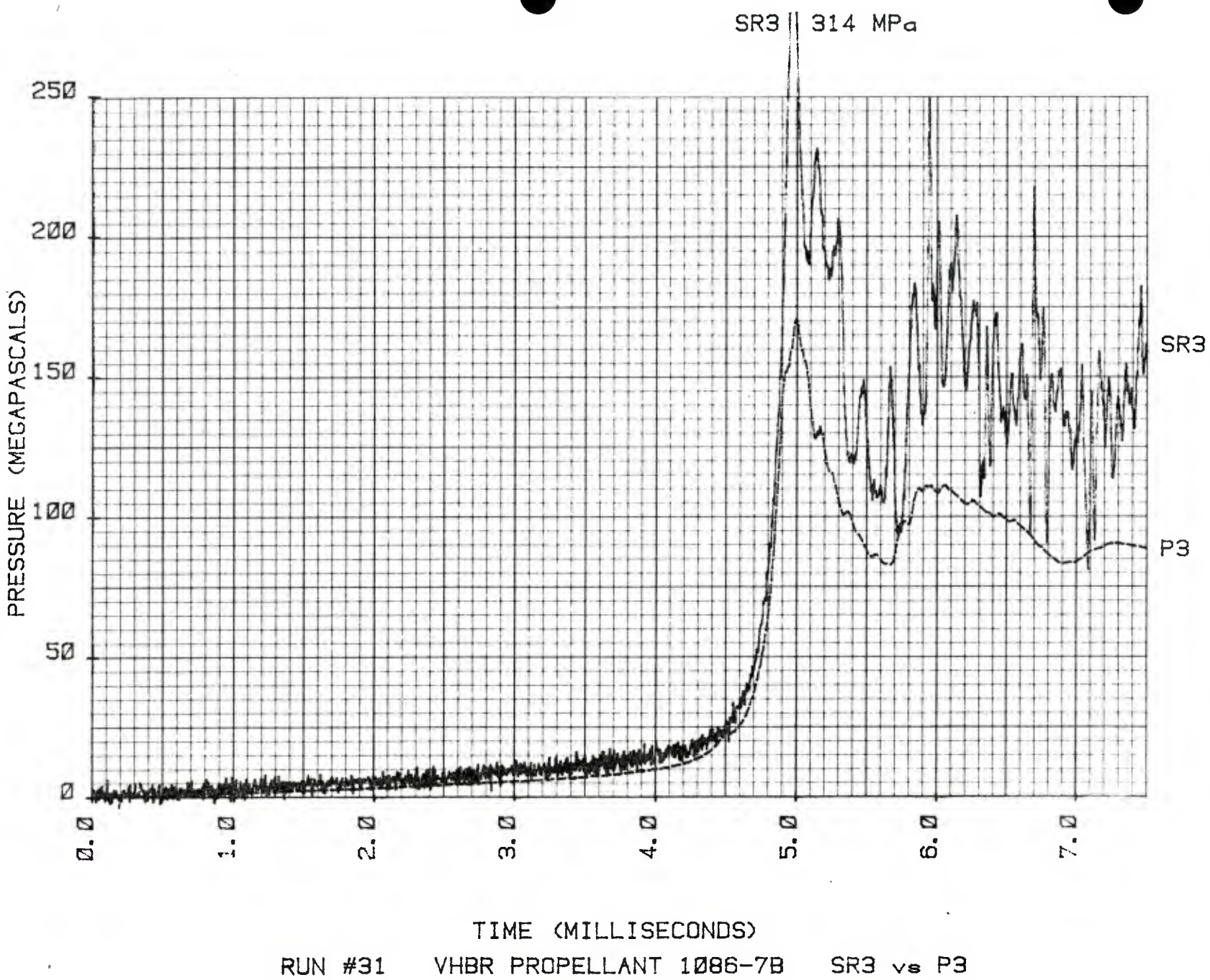

Figure 22d. Pressure History for a Single Sample Coated with Organic Grease and Tested at a Loading Density of 0.147 g/cc

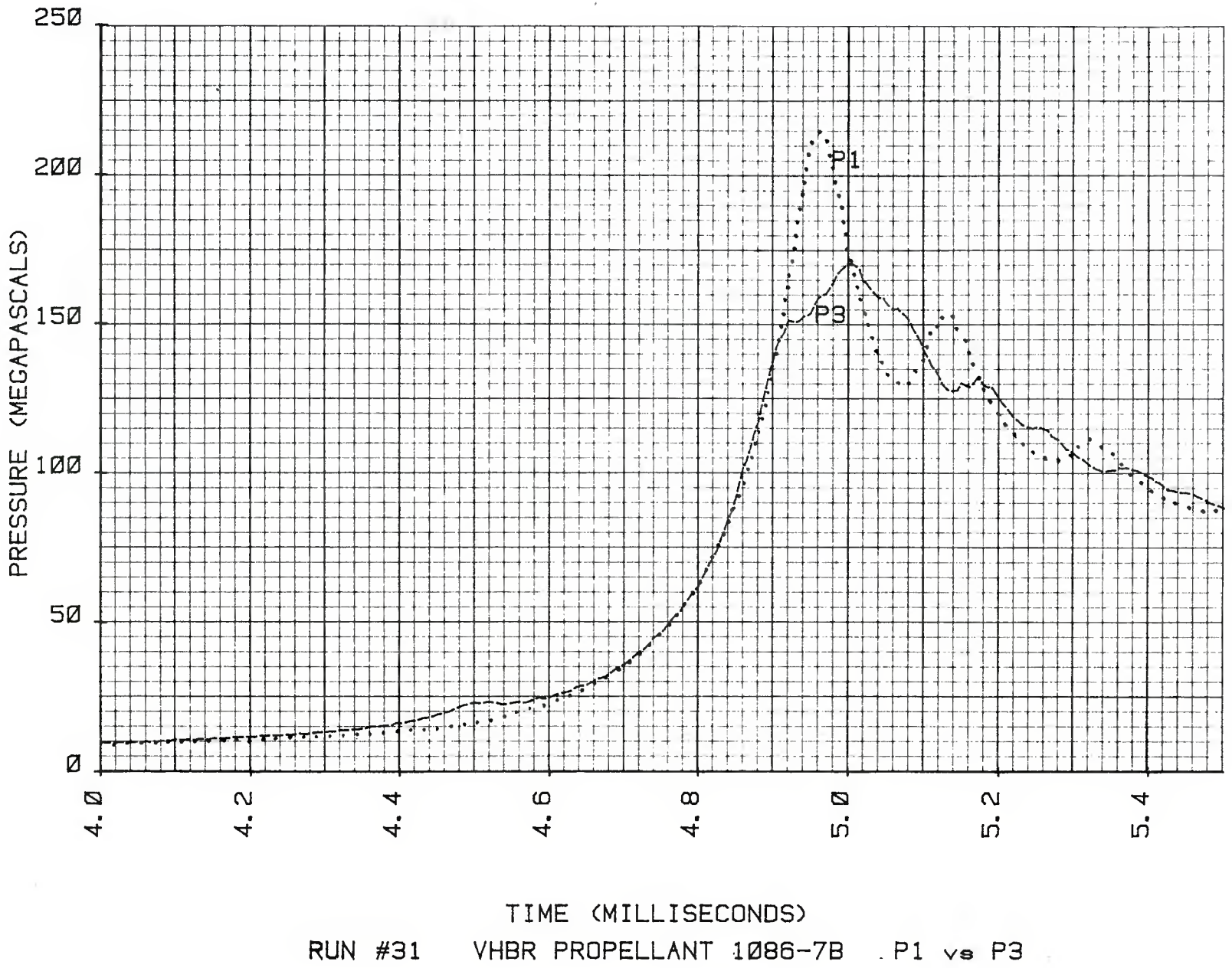

Figure 22e. Pressure History for a Single Sample Coated with Organic Grease and Tested at a Loading Density of 0.147 g/cc

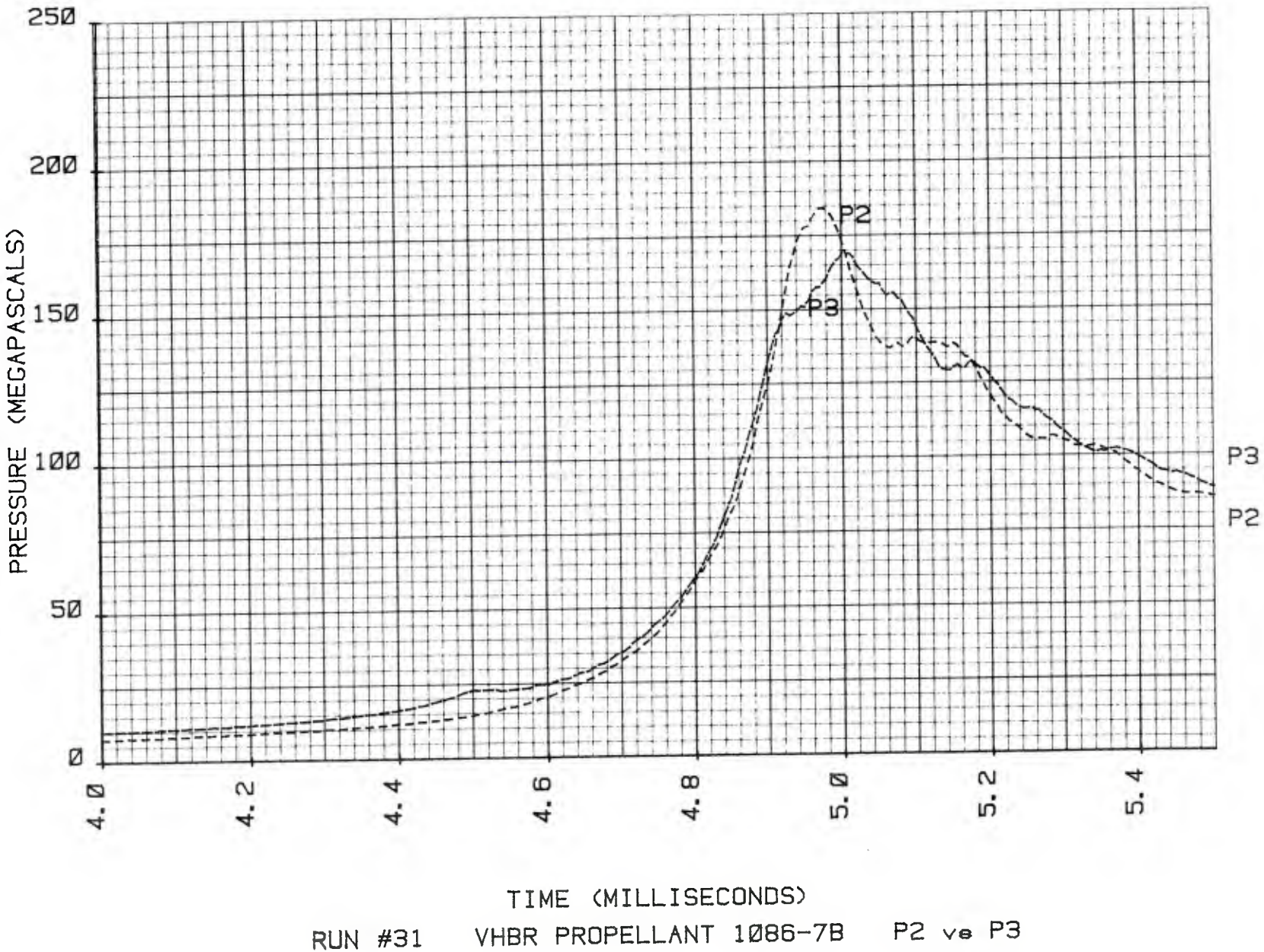

Figure 22f. Pressure History for a Single Sample Coated with Organic Grease and Tested at a Loading Density of 0.147 g/cc

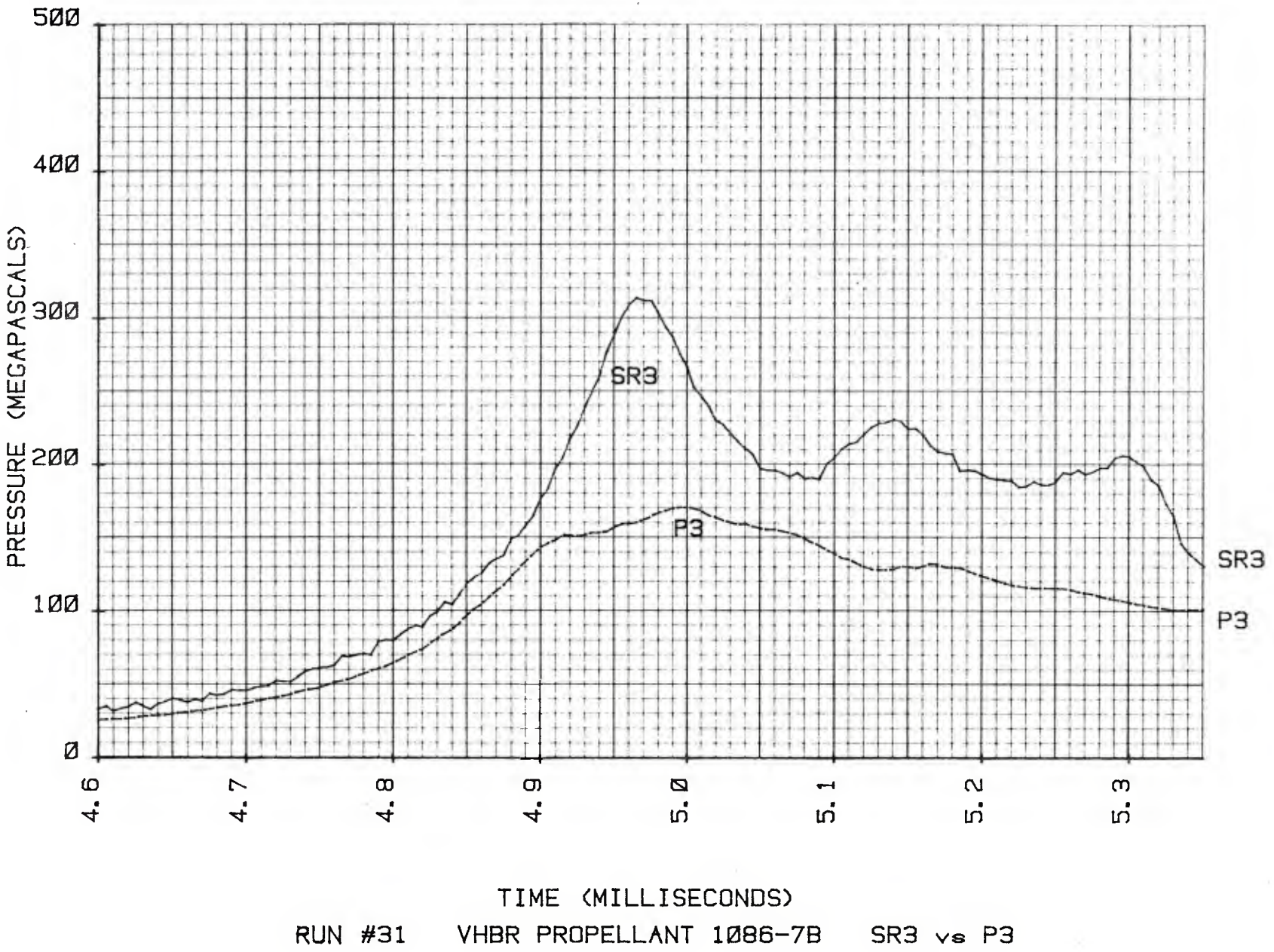

Figure 22g. Pressure History for a Single Sample Coated with Organic Grease and Tested at a Loading Density of 0.147 g/cc

DISTRIBUTION LIST

No. Of Copies	Organization
12	Administrator Defense Technical Info Center ATTN: DTIC-DDA Cameron Station Alexandria, VA 22314
1	Headquarters USAF/RD ATTN: R. Thorkildson Washington, DC 20330-5040
1	HQDA/SAUS-OR, D. Hardison Washington, DC 20301
1	HQDA/DAMA-ZA Washington, DC 20310
1	HQDA, DAMA-CSM, E. Lippi Washington, DC 20310
1	HQDA/SARDA Washington, DC 20310
1	Commandant US Army War College ATTN: Library-FF229 Carlisle Barracks, PA 17013
1	Ballistic Missile Defense Advanced Technology Center P. O. Box 1500 Huntsville, AL 35807
1	Chairman DOD Explosives Safety Board Room 856-C Hoffman Bldg. 1 2461 Eisenhower Avenue Alexandria, VA 22331
1	HQDA DAMA-ART-M Washington, DC 20310
3	Commander US Army Materiel Command ATTN: AMCDRA-ST AMCSF-E, Safety Office AMCDE-DW 5001 Eisenhower Avenue Alexandria, VA 22333
12	Commander US Army AMCCOM, ARDC ATTN: SMCAR-TSS SMCAR-TDC D. Gyorog SMCAR-LCA J. Lannon A. Beardell D. Downs S. Einstein L. Schlosberg S. Westley S. Bernstein P. Kemmey C. Heyman A. Bracuti Dover, NJ 07801
9	US Army AMCCOM, ARDC ATTN: SMCAR-SCA, L. Stiefel B. Brodman SMCAR-LCB-I, D. Spring SMCAR-LCE, R. Walker SMCAR-LCU-CT, E. Barrieres R. Davitt SMCAR-LCU-CV C.Mandala W. Joseph SMCAR-LCM-E, S. Kaplowitz Dover, NJ 07801
1	Commander US Army Development & Employment Agency ATTN: MODE-TED-SAB Fort Lewis, WA 98433

DISTRIBUTION LIST

No. Of Copies	Organization
1	Commander US Army AMCCOM, ARDC ATTN: SMCAR-QAR, J. Rutkowski Dover, NJ 07801
5	Project Manager Cannon Artillery Weapons Systems ATTN: AMCPM-CW, F. Menke AMCPM-CWW H. Noble AMCPM-CWS M. Fisette AMCPM-CWA, R. DeKleine H. Hassmann Dover, NJ 07801
2	Project Manager Munition Production Base Modernization and Expansion ATTN: AMCPM-PBM, A. Siklosi AMCPM-PBM-E, L. Laibson Dover, NJ 07801
3	Project Manager Tank Main Armament System ATTN: AMCPM-TMA, K. Russell AMCPM-TMA-105 AMCPM-TMA-120 Dover, NJ 07801
3	Commander US Army AMCCOM, ARDC ATTN: AMSMC-LCW-A M.Salsbury AMSMC-LCS AMSMC-LC, J. Frasier Dover, NJ 07801
5	Commander US Army Armament Munitions and Chemical Command ATTN: SMCAR-ESP-L, Tech Lib SMCAR-LC, L. Ambrosini SMCAR-IRC, G. Cowan SMCAR-LEM, W. Fortune R. Zastrow Rock Island, IL 61299
2	Director Benet Weapons Laboratory Armament R&D Center US Army AMCCOM ATTN: SMCAR-LCB-TL SMCWV-RD, R. Thierry Watervliet, NY 12189
1	Commander US Army Aviation Research and Development Command ATTN: AMSAV-E 4300 Goodfellow Blvd. St. Louis, MO 63120
1	Commander US Army TSARCOM 4300 Goodfellow Blvd. St. Louis, MO 63120
1	Director US Army Mobility Research And Development Command Ames Research Center Moffett Field, CA 94035
1	Commander US Army Communications-Electronics Command ATTN: AMSEL-ED Fort Monmouth, NJ 07703

DISTRIBUTION LIST

No. Of Copies	Organization
1	Commander US Army Electronics Research and Development Command Technical Support Activity ATTN: DELSD-L Fort Monmouth, NJ 07703-5301
1	Commander US Army Harry Diamond Lab. ATTN: DELHD-TA-L 2800 Powder Mill Road Adelphi, MD 20783
1	Commander US Army Missile Command ATTN: AMSMI-YDL Redstone Arsenal, AL 35898
1	Commander US Army Natick Research and Development Laboratories ATTN: DRDNA-DT D. Sieling Natick, MA 01760
1	Commander US Army Tank Automotive Command ATTN: AMSTA--TSL Warren, MI 48090
1	US Army Tank Automotive Command ATTN: AMSTA-CG Warren, MI 48090
1	Project Manager Improved TOW Vehicle ATTN: AMCPM-ITV US Army Tank Automotive Research & Development Command Warren, MI 48090
1	Project Manager Fighting Vehicle Systems ATTN: AMCPM-FVS Warren, MI 48090
1	Director US Army TRADOC Systems Analysis Activity ATTN: ATAA-SL, Tech Lib White Sands Missile Range, NM 88002
1	Project Manager M-60 Tank Development ATTN: AMCPM-M60TD Warren, MI 48090
1	Commander US Army Training & Doctrine Command ATTN: ATCD-MA/ MAJ Williams Fort Monroe, VA 23651
2	Commander US Army Materials and Mechanics Research Center ATTN: AMXMR-ATL Tech Library Watertown, MA 02172
1	Commander US Army Research Office ATTN: Tech Library P. O. Box 12211 Research Triangle Park, NC 27709 - 2211
1	Commander US Army Belvoir R&D Center ATTN: STRBE-WC Tech Library (Vault), Bldg. 315 Ft. Belvoir, VA 22060-5606

DISTRIBUTION LIST

No. Of Copies	Organization
1	Commandant US Army Infantry School ATTN: ATSH-CD-CSO-OR Fort Benning, GA 31905
1	US Army Armor & Engineer Board ATTN: STEBB-AD-S Fort Knox, KY 40121
1	Commandant US Army Aviation School ATTN: Aviation Agency Fort Rucker, AL 36360
1	Commandant Command and General Staff College Fort Leavenworth, KS 66027
1	Commandant US Army Special Warfare School ATTN: Rev & Tng Lit Div Fort Bragg, NC 28307
1	Commander US Army Logistics Mgmt Ctr Defense Logistics Studies Fort Lee, VA 23801
1	Commander US Army Foreign Science & Technology Center ATTN: AMXST-MC-3 220 Seventh Street, NE Charlottesville, VA 22901
1	President US Army Artillery Board Ft. Sill, OK 73503
2	Commandant US Army Field Artillery School ATTN: ATSF-CO-MW, B. Willis Ft. Sill, OK 73503
3	Commandant US Army Armor School ATTN: ATZK-CD-MS/ M. Falkovitch Armor Agency Fort Knox, KY 40121
1	Commander US Army Missile Command ATTN: AMSMI-R Redstone Arsenal, AL 35898
1	Office of Naval Research ATTN: Code 473, R. S. Miller 800 N. Quincy Street Arlington, VA 22217
1	Commander Naval Sea Systems Command ATTN: SEA-62R2, R. Beauregard National Center, Bldg. 2 Room 6E08 Washington, DC 20362
1	Commander Naval Air Systems Command ATTN: NAIR-954-Tech Lib Washington, DC 20360
2	Program Manager M1 Abrams Tank System ATTN: AMCPM-GCM-SA T. Dean Warren, MI 48090
1	Assistant Secretary of the Navy (R, E, and S) ATTN: R. Reichenbach Room 5E787 Pentagon Bldg. Washington, DC 20350
1	Naval Research Lab Tech Library Washington, DC 20375

DISTRIBUTION LIST

No. Of Copies	Organization
5	Commander Naval Surface Weapons Center ATTN: Code G33, J. L. East W. Burrell J. Johndrow Code G23, D. McClure Code DX-21 Tech Lib Dahlgren, VA 22448
2	Commander US Naval Surface Weapons Center ATTN: J. P. Consaga C. Gotzmer Indian Head, MD 20640
4	Commander Naval Surface Weapons Center ATTN: S. Jacobs/Code 240 Code 730 K. Kim/Code R-13 R. Bernecker Silver Spring, MD 20910
2	Commanding Officer Naval Underwater Systems Center Energy Conversion Dept. ATTN: CODE 5B331, R. S. Lazar Tech Lib Newport, RI 02840
4	Commander Naval Weapons Center ATTN: Code 388, R. L. Derr C. F. Price T. Boggs Info. Sci. Div. China Lake, CA 93555
2	Superintendent Naval Postgraduate School Dept. of Mechanical Engineering ATTN: A. E. Fuhs Code 1424 Library Monterey, CA 93940
6	Commander Naval Ordnance Station ATTN: P. L. Stang J. Birkett S. Mitchell C. Christensen D. Brooks Tech Library Indian Head, MD 20640
1	AFSC/SDOA Andrews AFB, MD 20334
1	Program Manager AFOSR Directorate of Aerospace Sciences ATTN: L. H. Caveny Bolling AFB, DC 20332
5	AFRPL (DYSC) ATTN: D. George J. N. Levine D. Thrasher N. Vander Hyde Tech Library Edwards AFB, CA 93523
1	AFFTC AFRPL/LKCG ATTN: SSD-Tech LIb Edwards AFB, CA 93523
1	AFATL/DLYV Eglin AFB, FL 32542-5000
1	Air Force Armament Laboratory ATTN: AFATL/DLODL Eglin AFB, FL 32542-5000
1	AFFDL ATTN: TST-Lib Wright-Patterson AFB, OH 45433

DISTRIBUTION LIST

No. Of Copies	Organization
1	Lawrence Livermore Laboratory ATTN: M.S. L-355, A. Buckingham P.O. Box 808 Livermore, CA 94550
1	Lawrence Livermore Laboratory ATTN: M.S. L-355, M. Finger P.O. Box 808 Livermore, CA 94550
1	Foster Miller Associates ATTN: A. Erickson 135 Second Avenue Waltham, MA 02154
1	Aerodyne Research, Inc. Bedford Research Park ATTN: V. Yousefian Bedford, MA 01730
1	Aerojet Solid Propulsion Co. ATTN: P. Micheli Sacramento, CA 95813
1	Atlantic Research Corporation ATTN: M. K. King 5390 Cherokee Avenue Alexandria, VA 22314
1	AVCO Everett Rsch Lab ATTN: D. Stickler 2385 Revere Beach Parkway Everett, MA 02149
2	Calspan Corporation ATTN: C. Morphy P.O. Box 400 Buffalo, NY 14225
1	General Applied Science Labs ATTN: J. Erdos Merrick & Stewart Avenues Westbury, NY 11590
1	General Electric Armament & Electrical Systems ATTN: M.J. Bulman Lakeside Avenue Burlington, VT 05401
1	Hercules, Inc. Allegany Ballistics Laboratory ATTN: R. B. Miller P. O. Box 210 Cumberland, MD 21501
1	Hercules, Inc Bacchus Works ATTN: K. P. McCarty P. O. Box 98 Magna, UT 84044
1	Hercules, Inc. Eglin Operations AFATL DLDL ATTN: R. L. Simmons Eglin AFB, FL 32542
1	IITRI ATTN: M. J. Klein 10 W. 35th Street Chicago, IL 60616

DISTRIBUTION LIST

No. Of Copies	Organization
1	Olin Corporation Badger Army Ammunition Plant ATTN: R. J. Thiede Baraboo, WI 53913
1	Olin Corporation Smokeless Powder Operations ATTN: R. L. Cook P. O. Box 222 St. Marks, FL 32355
1	Paul Gough Associates, Inc. ATTN: P. S. Gough P. O. Box 1614 Portsmouth, NH 03801
1	Physics International 2700 Merced Street San Leandro, CA 94577
1	Princeton Combustion Research Lab., Inc. ATTN: M. Summerfield 475 US Highway One North Monmouth Junction, NJ 08852
1	Scientific Rsch Assoc., Inc. ATTN: H. McDonald P.O. Box 498 Glastonbury, CT 06033
2	Rockwell International Rocketdyne Division ATTN: BA08 J. E. Flanagan J. Gray 6633 Canoga Avenue Canoga Park, CA 91304
1	Science Applications, Inc. ATTN: R. B. Edelman 23146 Cumorah Crest Woodland Hills, CA 91364
1	Teldyne McCormick Selph ATTN: C. Leveritt 3601 Union Road Hollister, CA 95023
3	Thiokol Corporation Huntsville Division ATTN: D. Flanagan R. Glick Tech Library Huntsville, AL 35807
2	Thiokol Corporation Wasatch Division ATTN: J. Peterson Tech Library P. O. Box 524 Brigham City, UT 84302
2	Thiokol Corporation Elkton Division ATTN: R. Biddle Tech Lib. P. O. Box 241 Elkton, MD 21921
2	United Technologies Chemical Systems Division ATTN: R. Brown Tech Library P. O. Box 358 Sunnyvale, CA 94086
1	Universal Propulsion Company ATTN: H. J. McSpadden Black Canyon Stage 1 Box 1140 Phoenix, AZ 85029
1	Veritay Technology, Inc. ATTN: E. B. Fisher Propulsion Department P.O. Box 22 Bowmansville, NY 14026

DISTRIBUTION LIST

No. Of Copies	Organization
1	Pennsylvania State University Dept of Mechanical Engineering ATTN: K. Kuo University Park, PA 16802
1	Battelle Memorial Institute ATTN: Tech Library 505 King Avenue Columbus, OH 43201
1	Brigham Young University Dept. of Chemical Engineering ATTN: M. Beckstead Provo, UT 84601
1	California Institute of Tech 204 Karman Lab Main Stop 301-46 ATTN: F. E. C. Culick 1201 E. California Pasadena, CA 91109
1	University of Minnesota Dept. of Mechanical Engineering ATTN: E. Fletcher Minneapolis, MN 55455
1	Professor Herman Krier Dept of Mech/Indust Engr. Univ. of Illinois 144 MEB; 1206 W. Green St. Urbana, IL 61801
1	University of Massachusetts Dept. of Mechanical Engineering ATTN: K. Jakus Amherst, MA 01002
1	Case Western Reserve University Division of Aerospace Sciences ATTN: J. Tien Cleveland, OH 44135
3	Georgia Institute of Tech School of Aerospace Eng. ATTN: B. T. Zinn E. Price W. C. Strahle Atlanta, GA 30332
1	Institute of Gas Technology ATTN: D. Gidaspow 3424 S. State Street Chicago, IL 60616
1	Johns Hopkins University Applied Physics Laboratory Chemical Proplsion Information Agency ATTN: T. Christian Johns Hopkins Road Laurel, MD 20707
1	Charles Stark Draper Lab. Div. Massachusetts Inst. of Tech. 68 Albany Street ATTN: T. Toong Cambridge, MA 02139
1	Pennsylvania State University Applied Research Lab ATTN: G. M. Faeth P. O. Box 30 State College, PA 16801

DISTRIBUTION LIST

No. Of Copies	Organization
1	Purdue University School of Mechanical Engineering ATTN: J. R. Osborn TSPC Chaffee Hall West Lafayette, IN 47906
1	Rensselaer Polytechnic Inst. Department of Mathematics Troy, NY 12181
1	Rutgers University Dept. of Mechanical and Aerospace Engineering ATTN: S. Temkin University Heights Campus New Brunswick, NJ 08903
1	SRI International Propulsion Sciences Division ATTN: Tech Library 333 Ravenswood Avenue Menlo Park, CA 94025
1	Stevens Institute of Tech Davidson Laboratory Castle Point Station ATTN: R. McAlevy, III Hoboken, NJ 07030
2	Los Alamos Scientific Lab ATTN: T3, D. Butler M. Division, B. Craig P. O. Box 1663 Los Alamos, NM 87544
1	University of Southern California Mechanical Engineering Dept. ATTN: OHE200, M. Gerstein Los Angeles, CA 90007
2	University of Utah Dept. of Chemical Engineering ATTN: A. Baer G. Flandro Salt Lake City, UT 84112
1	University of Princeton AMES Department ATTN: F. Williams Princeton, NJ 08540
1	Washington State University Dept. of Mechanical Engineering ATTN: C. T. Crowe Pullman, WA 9916
1	AFWL/SUL Kirtland AFB, NM 87117

Aberdeen Proving Ground

Dir, USAMSAA
ATTN: AMXSY-D
AMXSY-MP, H. Cohen

Cdr, USATECOM
ATTN: AMSTE-TO-F

Cdr, CSTA
ATTN: STECS-AA-W
D. Lacey
C. Herud

Dir, HEL
ATTN: J. Weisz

Cdr, CRDC, AMCCOM
ATTN: SMCCR-RSP-A
SMCCR-MU
SMCCR-SPS-IL

USER EVALUATION SHEET/CHANGE OF ADDRESS

This Laboratory undertakes a continuing effort to improve the quality of the reports it publishes. Your comments/answers to the items/questions below will aid us in our efforts.

1. BRL Report Number _____ Date of Report _____

2. Date Report Received _____

3. Does this report satisfy a need? (Comment on purpose, related project, or other area of interest for which the report will be used.) _____

_____

_____

4. How specifically, is the report being used? (Information source, design data, procedure, source of ideas, etc.) _____

_____

_____

5. Has the information in this report led to any quantitative savings as far as man-hours or dollars saved, operating costs avoided or efficiencies achieved, etc? If so, please elaborate. _____

_____

_____

6. General Comments. What do you think should be changed to improve future reports? (Indicate changes to organization, technical content, format, etc.)

_____

_____

_____

CURRENT ADDRESS

_____
Name

_____
Organization

_____
Address

_____
City, State, Zip

7. If indicating a Change of Address or Address Correction, please provide the New or Correct Address in Block 6 above and the Old or Incorrect address below.

OLD ADDRESS

_____
Name

_____
Organization

_____
Address

_____
City, State, Zip

(Remove this sheet along the perforation, fold as indicated, staple or tape closed, and mail.)